Random heterogeneous media: Microstructure and improved bounds on effective properties

S Torquato

Department of Mechanical and Aerospace Engineering and Department of Chemical Engineering, North Carolina State University, Raleigh NC 27695-7910

The purpose of the present article is to review recent advances made in the determination and calculation of improved bounds on the effective properties of random heterogeneous media that depend upon the microstructure via n-point correlation functions. New breakthroughs made in the quantitative characterization of the microstructure of heterogeneous materials are also reviewed. The following four different effective properties shall be studied: (i) effective conductivity tensor (which includes, by mathematical analogy, the dielectric constant, magnetic permeability, and diffusion coefficient); (ii) effective stiffness tensor; (iii) diffusion-controlled trapping constant; and (iv) fluid permeability tensor. It shall be demonstrated that improved upper and lower bounds can provide a relatively sharp estimate of the effective property even when the bounds diverge from one another. Although this article reviews state-of-the-art advances in the field, an attempt will be made to elucidate methods and principles for the nonexpert.

CONTENTS

1. INTRODUCTION

In the most general sense, a heterogeneous material consists of domains of different materials (phases) or the same material in different states. This article focuses attention on the many instances in which the "microscopic" length scale (eg, the average domain size) is much larger than the molecular dimensions (so that the domains possess macroscopic properties) but much smaller than the characteristic length of the macroscopic sample. In such circumstances, the heterogeneous material can be viewed as a continuum on the microscopic scale (thus is subject to classical analysis) and macroscopic or "effective" properties can be ascribed to it. Such heterogeneous media abound in nature and in man-made situations: Examples include aligned and chopped fiber composites, porous and cracked media, polycrystals, polymer blends, foams, fluidized beds, photographic emulsions, cermets, soils, rocks, blood, and animal and plant tissue.

In light of the manifest technological importance of determining the effective properties of heterogeneous media, a vast body of literature has evolved based upon direct measurement (either experimentally or computationally), semiempirical relations, and theoretical techniques (see Refs 1–12 and references therein for general reviews of the field). The time and cost to attack this problem by performing measurements on each material sample for all possible phase properties and microstructures is clearly prohibitive. Successful empirical relations tend to be more useful for correlating data rather than predicting them. Inasmuch as the effective property depends not only on the phase properties but is sensitive to the details of the microstructure (ie, phase volume fractions; orientations, sizes, shapes, and spatial distribution of the domains; connectivity of the phases, etc), it is natural to take the broader

Transmitted by Associate Editor George J Dvorak.

approach of predicting the effective property from a knowledge of the microstructure. One can then relate changes in the microstructure quantitatively to changes in the macroscopic property. This program, if successful, has important practical implications such as providing a cost-effective means of optimally designing composite materials for a particular application and of determining the effective properties of real materials from cross-sectional images of the sample.

Unfortunately, in most situations, the details of the microstructure are not completely known. This naturally leads one to attempt to estimate the effective properties from partial statistical information on the sample in the form of correlation functions and, in particular, to establish the range of possible values the effective properties can take given such limited morphological information, that is, to determine rigorous upper and lower bounds on the properties.

In this article advances made largely in the last 5 years on the determination and calculation of "improved" bounds on effective properties of *two-phase random* heterogeneous media shall be reviewed. Improved bounds are by definition bounds that depend *nontrivially* upon two-point and higher-order correlation functions. They therefore contain information beyond that embodied in the volume fractions. In the instances of the conductivity and elastic moduli of isotropic two-phase media, for example, improved bounds are those that are more stringent than the well-known Hashin–Shtrikman bounds [13,14]. Although some improved bounds have been in existence for almost 30 years, they were not evaluated until recently because of the difficulty involved in ascertaining the statistical correlation functions. Significant advances have been made recently in the quantitative characterization of the microstructure of two-phase disordered media, enabling investigators to compute rigorous bounds on the effective properties for the first time for nontrivial models and real materials. These new breakthroughs in the description of the morphology of heterogeneous media are also reviewed. Although this article reviews state-of-the-art advances in the field, an attempt will be made to elucidate methods and principles for the nonexpert.

A variety of phenomena governed by linear partial differential equations that are self-adjoint shall be considered. Specifically, improved bounds on the following effective properties will be studied:

Effective conductivity tensor, $\boldsymbol{\sigma}_e$
Effective stiffness tensor, $\mathbf{C}_e$
Diffusion-controlled trapping constant, γ
Fluid permeability tensor, $\mathbf{k}$

Knowledge of the effective thermal (or electrical) conductivity tensor $\boldsymbol{\sigma}_e$ (and mathematically analogous properties described in the ensuing section) and/or the effective stiffness tensor $\mathbf{C}_e$ is of importance for a host of composites and porous media (eg, polymer composites, insulation, advanced reentry vehicles, fiber-reinforced materials, geologic media, etc). The trapping constant γ is proportional to the rate at which a diffusing species gets trapped by static sinks (traps) when the process is diffusion-controlled. Diffusion-controlled processes play an important role in combustion, polymer chain growth kinetics, heterogeneous catalysis, radiation damage, and cell metabolism. The flow of a fluid through a porous medium arises in a variety of technological problems such as oil and gas recovery, hydrology, gel chromatography, filtration, and biological membranes, to mention but a few examples. A key macroscopic property for describing slow viscous flow through such media is the fluid permeability tensor $\mathbf{k}$.

Although previous reviews have discussed bounds to varying degrees [2–5,7,8,10,12], heretofore none have been written which focus exclusively on improved bounds and microstructure characterization, and which deal with the wide variety of effective properties described above. Indeed, a unified treatment of these various problems (which are not mathematically identical) will be emphasized throughout this article.

For these classes of problems, the random microstructures are static, that is, do not evolve in time. Nonetheless, many of the methods described here can be generalized to dynamical situations (eg, flow of suspensions). Perfect bonding will be assumed across the two-phase interface. Again many of the techniques reviewed here can be extended to treat imperfect bonding. The limitation to two-phase media is also not restrictive since similar methods can be employed to study heterogeneous media with three or more phases. This does preclude any discussion of polycrystals, however, which can be considered to be a composite with an infinite number of anisotropic phases, each phase being defined by the crystallographic orientation of the individual grains. The reader is referred to the work of Avellaneda et al [15] and of Avellaneda and Milton [16] and references therein for a description of recent developments in the study of bounds on the effective properties of polycrystals. It should also be noted that variational principles, similar to ones described below, may be employed to study the problem of wave propagation in random media (see the review of Willis [8]).

Bounds which incorporate microstructural information up to the n-point level shall be referred to as "n-point" bounds. It will be demonstrated that improved n-point upper and lower bounds can be quite sharp and provide significant improvement over volume-fraction dependent bounds for an appreciable range of phase properties and volume fractions. For a certain range of parameters the bound widths can be very large and, as a result, have been deemed by some to have no utility under such conditions. To the contrary, it will be shown that one of the bounds can yield a good and sometimes excellent estimate of the effective property, even when the reciprocal bound diverges from it. This last point has yet to be fully appreciated.

Whenever possible, theoretical results will be compared to available experimental and computer-simulation data. In general, d-dimensional media shall be considered ($d = 2$ and $d = 3$ being the cases of greatest physical interest). The instance $d = 2$ models media whose phase boundaries are cylindrical surfaces, with generators parallel to one axis. Examples of such media include long, oriented fibers (such as glass, carbon, graphite, and boron) in a polymer matrix. This classification also includes thin films [17].

Although this review focusses on the study of the microstructure and improved property bounds for heterogeneous media, it should be mentioned that there are now available efficient means of computing "exactly" effective properties for nontrivial model microstructures. For example, in the cases of diffusion in random media (eg, conductivity and trapping problems), Brownian motion simulation techniques which make use of first-passage time analysis are clearly superior to standard finite-difference or finite-element techniques in terms of computational speed and accuracy [see, for example, Torquato and Kim [18] and references therein]. Indeed, such "computer experiments" will be employed in section 5 to access the accuracy of the rigorous bounds of the effective diffusion properties.

2. LOCAL AND AVERAGED EQUATIONS

The random medium is a domain of space $\mathcal{V}(\omega) \in \mathcal{R}^d$ (where the realization ω is taken from some probability space) of volume V which is composed of two regions: the phase 1 region $\mathcal{V}_1$ of volume fraction ϕ_1 and the phase 2 region $\mathcal{V}_2$ of volume fraction ϕ_2. Let $\partial\mathcal{V}$ denote the surface between $\mathcal{V}_1$ and $\mathcal{V}_2$. The medium is assumed to be statistically homogeneous, ie, stationary. It is useful to introduce the characteristic function $I(\mathbf{x};\omega)$ of phase 1 defined by

$$I(\mathbf{x};\omega) = \begin{cases} 1, & \mathbf{x} \in \mathcal{V}_1(\omega), \\ 0, & \mathbf{x} \in \mathcal{V}_2(\omega). \end{cases} \tag{2.1}$$

The local governing equations and the average constitutive relations associated with the conduction, elasticity, trapping, and flow problems are now described.

2.1. Conductivity

Let phases 1 and 2 have isotropic thermal conductivities σ_1 and σ_2, respectively. The equations governing steady-state heat conduction at some local position $\mathbf{x}$ in the sample are the following:

Local differential equation:

$$\nabla \cdot \mathbf{Q}(\mathbf{x}) = 0 \qquad \text{in } \mathcal{V}_i \qquad (i = 1, 2), \tag{2.2}$$

$$Q_n \text{ and } T \text{ continuous across } \partial\mathcal{V}. \tag{2.3}$$

Local constitutive relation:

$$\mathbf{Q}(\mathbf{x}) = -\sigma(\mathbf{x})\nabla T(\mathbf{x}), \tag{2.4}$$

where

$$\sigma(\mathbf{x}) = \sigma_1 I(\mathbf{x}) + \sigma_2(1 - I(\mathbf{x})). \tag{2.5}$$

Here $\mathbf{Q}(\mathbf{x})$ is the local heat flux vector, Q_n is the normal component of $\mathbf{Q}$ at the interface, $T(\mathbf{x})$ is local the temperature field, and $\sigma(\mathbf{x})$ is the local conductivity.

The following ensemble-averaged constitutive relation defines the symmetric, second-rank effective conductivity tensor $\boldsymbol{\sigma}_e$ [2]:

Averaged constitutive relation:

$$< \mathbf{Q}(\mathbf{x}) > = -\boldsymbol{\sigma}_e \cdot < \nabla T(\mathbf{x}) > . \tag{2.6}$$

Angular brackets denote an *ensemble* average. This refers to an average over an ensemble, that is, a collection of a large number of systems which are identical in their macroscopic details but are different in their microscopic details. (See section 4.1 for a quantitative definition of an ensemble average for particulate systems.) Relation (2.6) has been derived using a two-scale method of homogenization by, among others, Papanicolaou and Varadhan [19]. The tensor $\boldsymbol{\sigma}_e$ describes the macroscopic behavior of the system in the limit as the ratio of the microscopic length scale to the macroscopic length scale tends to zero. Macroscopic anisotropy (ie, the tensor nature of the effective conductivity) can arise out of asymmetry in the microstructure, ie, due to statistical anisotropy (eg, a distribution of oriented, nonspherical inclusions in a matrix, layered media such as sandstones and laminates, etc) [20]. Definition (2.6) applies also to instances in which the composite possesses anisotropic phases. As noted above, however, the present discussion treats isotropic phases only.

It is well known that, for reasons of mathematical analogy, the general results given here for the effective thermal conductivity translate immediately into equivalent results for the electrical conductivity, dielectric constant, magnetic permeability, and diffusion coefficient. This class of problems is summarized in Table 1 along with the three other classes of problems examined here.

2.2. Elastic Moduli

Let phases 1 and 2 be isotropic with moduli K_1, G_1 and K_2, G_2, respectively, where K_i is the bulk modulus of phase i and G_i is the shear modulus of phase i. The equations governing the elastic behavior of linear composite materials at some position $\mathbf{x}$ are the basic relations of elastostatics:

Local differential equation:

$$\nabla \cdot \boldsymbol{\tau}(\mathbf{x}) = 0 \qquad \text{in } \mathcal{V}_i \qquad (i = 1, 2), \tag{2.7}$$

Table 1. The four different classes of effective media problems considered here.[a]

Class	General effective property $\mathbf{K}^*$	Generalized averaged (or applied) gradient $< \mathbf{G} >$	Generalized averaged flux $< \mathbf{F} >$
A	thermal conductivity	temperature gradient	heat flux
	electrical conductivity	electric field	electric current
	dielectric constant	electric field	electric displacement
	magnetic permeability	magnetic field	magnetic induction
	diffusion coefficient	concentration gradient	mass flux
B	elastic moduli	strain field	stress field
C	inverse trapping constant	species production rate	concentration field
D	fluid permeability	applied pressure gradient	velocity field

[a] $< \mathbf{F} > = \mathbf{K}^* < \mathbf{G} >$, where $\mathbf{K}^*$ is the general effective property, $< \mathbf{G} >$ is the averaged generalized gradient, and $< \mathbf{F} >$ is the averaged generalized flux. Class A and B problems share many common features and hence may be attacked using similar techniques. Class C and D problems are similarly related to one another.

$$\mathbf{T} \text{ and } \mathbf{u} \text{ continuous across } \partial\mathcal{V}. \tag{2.8}$$

Local constitutive relation:

$$\boldsymbol{\tau}(\mathbf{x}) = \lambda(\mathbf{x})\mathrm{tr}[\boldsymbol{\epsilon}(\mathbf{x})]\mathbf{U} + 2G(\mathbf{x})\boldsymbol{\epsilon}(\mathbf{x}), \tag{2.9}$$

where

$$\boldsymbol{\epsilon}(\mathbf{x}) = \tfrac{1}{2}[\nabla\mathbf{u}(\mathbf{x}) + (\nabla\mathbf{u}(\mathbf{x}))^T], \tag{2.10}$$

$$\lambda(\mathbf{x}) = \lambda_1 I(\mathbf{x}) + \lambda_2(1 - I(\mathbf{x})), \tag{2.11}$$

$$G(\mathbf{x}) = G_1 I(\mathbf{x}) + G_2(1 - I(\mathbf{x})). \tag{2.12}$$

Here the $\boldsymbol{\tau}(\mathbf{x})$ is the symmetric, second-rank local stress tensor, $\mathbf{T}$ is the interface traction, $\boldsymbol{\epsilon}(\mathbf{x})$ is the symmetric, second-rank local strain tensor, $\mathbf{u}(\mathbf{x})$ is the local displacement, $\lambda(\mathbf{x})$ and $G(\mathbf{x})$ are the local Lamé constants ($K = \lambda + 2G/d$), where d is the space dimension), and $\mathbf{U}$ is the unit dyadic.

The following averaged equation defines the symmetric, fourth-rank effective stiffness tensor $\mathbf{C}_e$:

Averaged constitutive relation:

$$< \boldsymbol{\tau}(\mathbf{x}) > = \mathbf{C}_e : < \boldsymbol{\epsilon}(\mathbf{x}) > . \tag{2.13}$$

Relation (2.13) has also been derived using the homogenization method; see, for example, the work of Sanchez-Palencia [21]. As in the conduction problem, $\mathbf{C}_e$ describes the macroscopic behavior of the system in the limit that the *scaled* microscopic length tends to zero. For macroscopically isotropic media, $\mathbf{C}_e$ is expressible in terms of two independent effective parameters, namely, λ_e and G_e, that is,

$$< \boldsymbol{\tau} > = \lambda_e \, \mathrm{tr} < \boldsymbol{\epsilon} > \mathbf{U} + 2G_e < \boldsymbol{\epsilon} >, \tag{2.14}$$

with

$$K_e = \lambda_e + \frac{2}{d}G_e. \tag{2.15}$$

For transversely isotropic fiber-reinforced two-phase materials, Hill [22] showed that it is only necessary to determine three of the five effective elastic moduli that characterize the composite since the other two can then be easily calculated. Here the effective transverse bulk modulus k_e, transverse shear modulus G_e, and axial shear modulus μ_e shall be considered. Hashin [23] demonstrated that the problem of determining μ_e is mathematically equivalent to determining the effective transverse thermal conductivity.

It is noteworthy that the equations governing the slow viscous flow of an incompressible fluid are identical to those governing the

elastic behavior of an incompressible material [7]. Thus, the determination of the *effective viscosity* of a suspension of perfectly rigid particles in an incompressible fluid (under creeping flow conditions) is equivalent to the determination of the effective shear modulus of a composite composed of the same perfectly rigid particles in an incompressible matrix for a *specified* arrangement of particles. However, in the flow problem at nondilute conditions (ie, when interparticle interactions are nonnegligible), the particle arrangement changes with time and is not known in advance; thus, the effective viscosity and shear modulus generally will not be the same [24]. In the fluid suspension instance, the bulk motion will greatly affect the spatial arrangement of particles, whereas in the elastic composite case the infinitesimal strain has a negligible effect on the particle distribution. Nonetheless, the determination of the effective shear modulus for such a suspension can serve as a good approximation of the effective viscosity of the fluid suspension at all particle concentrations [25]. At dilute conditions, the effective behavior is necessarily isotropic and independent of particle arrangement, and hence the effective viscosity and effective shear modulus are identical.

2.3. Trapping constant

Let phase 2 be the trap (sink) region and phase 1 be the trap-free region through which reactive particles may diffuse. The reactant diffuses with diffusion coefficient D in the trap-free region but is instantly absorbed on contact with any trap (concentration field $c = 0$ on $\partial\mathcal{V}$). At steady state, the rate of production s of the reactant (per unit trap-free volume), is exactly compensated by its removal by the traps. The equations governing this diffusion-controlled process at some local position $\mathbf{x}$ in the sample are the following:

Local differential equation:

$$\Delta u(\mathbf{x}) = -1 \qquad \text{in} \quad \mathcal{V}_1, \tag{2.16}$$

$$u = 0 \qquad \text{on} \quad \partial\mathcal{V}. \tag{2.17}$$

Δ denotes the Laplacian operator. Note that $u(\mathbf{x})$ is a scaled concentration field [see Eq. (2.19)]. It is important to emphasize that, unlike the previous two problems of conduction and elasticity, there is no local constitutive relation for the trapping problem. This is also true of the fluid permeability described below. Thus, the trapping and permeability problems are fundamentally different than the conduction and elasticity problems.

Rubinstein and Torquato [26] have used a two-scale homogenization method to derive the ensemble-averaged equation for the trapping constant γ:

Averaged constitutive relation:

$$s = \gamma D < c(\mathbf{x})I(\mathbf{x}) >, \tag{2.18}$$

where

$$c = D^{-1}su. \tag{2.19}$$

The trapping constant γ is proportional to the *average rate of trapping* which is equal to $\gamma D\phi_1$. Note that γ is a scalar quantity even for statistically anisotropic media [27]. The trapping constant γ, unlike σ_e or $\mathbf{C}_e$, describes the macroscopic behavior of the concentration field *divided by* the second power of scaled microscopic length scale (ratio of microscopic to macroscopic length scales) in the limit that the scaled microscopic length scale tends to zero [26].

2.4. Fluid permeability

Let phase 2 be the impermeable solid region and phase 1 be the pore or void region through which the slow viscous, incompressible fluid with viscosity μ flows. The fluid motion satisfies the tensor Stokes equations [28]:

Local differential equations:

$$\Delta\mathbf{w}(\mathbf{x}) = \nabla\mathbf{p}(\mathbf{x}) - \mathbf{U} \qquad \text{in} \quad \mathcal{V}_1, \tag{2.20}$$

$$\nabla \cdot \mathbf{w}(\mathbf{x}) = 0 \qquad \text{in} \quad \mathcal{V}_1, \tag{2.21}$$

$$\mathbf{w}(\mathbf{x}) = 0 \qquad \text{on} \quad \partial\mathcal{V}. \tag{2.22}$$

Here $\mathbf{w} = [w_{ij}]$ is the ith component of the velocity field due to a unit pressure gradient in the jth direction, equal to the null tensor in $\mathcal{V}_2$, and $\mathbf{p}$ is the associated scaled vector pressure field. Again note that a local constitutive relation does not exist in the permeability problem.

There have been many derivations of Darcy's law for the fluid permeability [29–31]. Rubinstein and Torquato [28] gave another derivation based upon an ensemble-average approach. They related the symmetric fluid permeability tensor $\mathbf{k}$ to the tensor $\mathbf{w}$ as follows:

$$\mathbf{V} = \frac{-\mathbf{k}}{\mu} \cdot \nabla p_0, \tag{2.23}$$

where

$$\mathbf{k} = < \mathbf{w}(\mathbf{x})I(\mathbf{x}) >. \tag{2.24}$$

Here $\mathbf{V}$ is the average velocity and ∇p_0 is the applied pressure gradient. Macroscopic anisotropy (ie, the tensor nature of the permeability) again arises from statistical anisotropy of the microstructure. The fluid permeability tensor $\mathbf{k}$, similar to γ, describes the macroscopic behavior of the velocity field divided by the second power of the microscopic length scale in the limit that the length scale of the fine structure tends to zero [28–30].

2.5. Relationship between trapping constant and fluid permeability

The problems of diffusion-controlled reactions among perfectly absorbing traps and of slow viscous flow through beds of particles share a common feature: Screening effects, at small solid volume fractions, lead to expansions for γ and k which are nonanalytic in the solid volume fraction ϕ_2 [32–35]. No one ever considered investigating the possibility of a deeper relationship between these two different physical parameters. Torquato [27] has very recently proved a theorem regarding a rigorous relation between γ and the permeability tensor k.

Theorem: *For an anisotropic porous medium of general topology having a fluid or trap-free region of porosity* ϕ_1 [27],

$$\mathbf{k}^{-1} \geq \gamma\mathbf{U}. \tag{2.25}$$

In other words, the inverse permeability tensor $\mathbf{k}^{-1}$ (or fluid "resistance" tensor) minus the rotationally invariant trapping constant tensor $\gamma\mathbf{U}$ is positive-semidefinite. Thus, for isotropic media, $k^{-1} \geq \gamma$, where $\mathbf{k} = k\mathbf{U}$. [Note that according to definitions (2.18) and (2.24), both k and γ^{-1} have dimensions of (length)^2 .]

Inequality (2.25) should prove to be a useful relation since in some cases one property may be easier to measure or predict than the other. How sharp is the inequality? It has been shown [27] that there is a certain class of microgeometries in which the difference $\mathbf{k}^{-1} - \gamma\mathbf{U}$ can have a zero eigenvalue, that is, the equality of (2.25) is achieved for one of the eigenvalues. Assume, without loss of generality, that the coordinate frame is aligned with the principal axes of the medium. An equal eigenvalue is achieved for transport in parallel channels (in the x_3-direction) of constant cross section dispersed throughout a solid or trap region with porosity ϕ_1. For example, for identical channels of arbitrary cross-sectional shape in three dimensions, it is easily shown that $k_{33} = \gamma^{-1} = \phi_1^3/cs^2$, where c is a shape-dependent constant (eg, $c = 2$ for circles, $c =$

5/3 for equilateral triangles, and $c = 1.78$ for squares), and s is the specific surface (interface area per unit volume). The part of the above expression relating k_{33} to ϕ_1 and s is the well-known Kozeny equation which for flow in real *isotropic* porous media is a useful empirical relation ($c = 5$ models many porous media well) [1,6]. However, this relation is new in the context of the trapping problem primarily because previous investigators usually considered modeling a dispersed or disconnected trap phase. Note that since there is no flow in the other principal directions for this anisotropic geometry, that is, $k_{11}^{-1} = k_{22}^{-1} = \infty$, the bound of (2.25) is clearly satisfied for these eigenvalues. The observation that there are microstructures that achieve the equality of (2.25) for one of the eigenvalues is new and may have important implications for simulating flow through porous media [27].

Apparently, for porous media in which the solid phase is composed of *distributions of particles*, the sharper bound

$$k_o/k \geq \gamma/\gamma_o \tag{2.26}$$

exists [27, 36], where k_o and γ_o are the infinitely dilute limits of k and γ, respectively. Torquato [36] has conjectured the inequality (2.26) based upon a number of known results for the flow and trapping problems. It was shown in Ref 36 that bound (2.26) can be quite sharp for low to moderate values of ϕ_2.

2.6. Remarks

In order to determine the effective conductivity tensor $\boldsymbol{\sigma}_e$, effective stiffness tensor $\mathbf{C}_e$, trapping constant γ and fluid permeability tensor $\mathbf{k}$, one must evaluate ensemble averages of the local fields as defined by relations (2.6), (2.13), (2.18), and (2.23), respectively. Except for a few special idealized random microstructures, such evaluations require knowledge of an infinite set of statistical correlation functions, which is generally never known and thus an exact analytical solution for the effective property for random media is generally not possible.

In order to underscore this last point it is useful to briefly review some analytical studies for the simplest of the problems considered here, i.e., the case of conduction. Brown [37], in a pioneering paper, showed the precise connection between the effective conductivity of any macroscopically *isotropic* three-dimensional ($d = 3$) two-phase medium (ie, $\boldsymbol{\sigma}_e = \sigma_e \mathbf{U}$) and the details of the microstructure by developing an exact series representation for the former explicitly in terms of functionals of the set of n-point probability functions $S_n^{(i)}(\mathbf{x}_1, \ldots, \mathbf{x}_n)$. The latter quantity gives the probability of finding n points at positions $\mathbf{x}_1, \ldots \mathbf{x}_n$ in phase i. The $S_n^{(i)}$ are described in full detail in Section 5. Thirty years later, Torquato [38] generalized this formalism for d-dimensional isotropic media. More recently, Sen and Torquato [20] obtained corresponding series representations of the effective conductivity tensor for d-dimensional anisotropic media of arbitrary topology. It is useful to present some of their results [20] for this discussion and for later use; they found

$$(\beta_{ij}\phi_i)^2[\boldsymbol{\sigma}_{ij} - \sigma_j \mathbf{U}]^{-1}[\boldsymbol{\sigma}_e + (d-1)\sigma_j \mathbf{U}] = \phi_i \beta_{ij} \mathbf{U} - \sum_{n=2}^{\infty} \mathbf{A}_n^{(i)} \beta_{ij}^n, \qquad i \neq j, \tag{2.27}$$

where

$$\beta_{ij} = \frac{\sigma_i - \sigma_j}{\sigma_i + (d-1)\sigma_j}, \qquad i \neq j, \tag{2.28}$$

and the symmetric, second-rank tensor coefficients $\mathbf{A}_n^{(i)}$ (which generally do not possess common principal axes) are multidimensional integrals over the set of n-point probability functions $S_1^{(i)}, \ldots, S_n^{(i)}$. (Note that the indices of (2.28) do *not* imply β_{ij} is a tensor quantity; β_{ij} is a scalar quantity involving the phase conductivities σ_i.) Using a shorthand notation,

$$\mathbf{A}_n^{(i)} = \mathbf{A}_n^{(i)}[S_1^{(i)}, \ldots, S_n^{(i)}]. \tag{2.29}$$

The explicit version of (2.29) is given in Ref 20. The coefficient $\mathbf{A}_2^{(i)}$ is given explicitly in section 3.1.2. (For macroscopically isotropic media, $\mathbf{A}_2^{(i)} = \mathbf{0}$, thus $\mathbf{A}_3^{(i)}$ is the first *nonzero* parameter in such instances. Consequently, the lowest level of anisotropic information enters through the two-point parameter $\mathbf{A}_2^{(i)}$.) The methodology leading to the n-point tensor integrals $\mathbf{A}_n^{(i)}$ of (2.29) is free of the well-known conditional-convergence problems which arise in related perturbation expansions [2,8].

For the subsequent discussion of bounds, it is useful to expand $\boldsymbol{\sigma}_e$ in powers of the scalar

$$\delta_{ij} = \frac{(\sigma_i - \sigma_j)}{\sigma_j}, \qquad i \neq j \tag{2.30}$$

so that

$$\frac{\boldsymbol{\sigma}_e}{\sigma_j} = \mathbf{U} + \phi_i \mathbf{U} \delta_{ij} + \sum_{n=2}^{\infty} \mathbf{a}_n^{(i)} \delta_{ij}^n, \qquad i \neq j \tag{2.31}$$

Sen and Torquato [20] used (2.27) to relate the $\mathbf{A}_n^{(i)}$ to the $\mathbf{a}_n^{(i)}$. The expression explicitly relating $\mathbf{A}_2^{(i)}$ to $\mathbf{a}_2^{(i)}$ is given in section 3.1.2.

It is worth noting in passing other expansion techniques for $\boldsymbol{\sigma}_e$ and expansion techniques for the three other properties examined here. When one of the phases consists of well-defined inclusions (eg, spheres, ellipsoids, cylinders, etc), one may obtain so-called "cluster" expansions for $\boldsymbol{\sigma}_e$ in which successive terms take into account interactions between successively larger clusters of particles [39–42]. The coefficients of this expansion are integrals over the solution to the n-particle heat conduction boundary-value problem weighted with the n-particle probability density function ρ_n (defined in section 4). Since the analytical solutions for the conduction and structure problem are already not easily obtainable at the two-particle level, cluster expansions can only yield information about dilute systems. For the elastic moduli of random composites, perturbation expansions [2,8,43] of the type (2.27) and cluster expansions [3,7,8,24] have been obtained. In the cases of the trapping constant and fluid permeability, expansions like (2.27) of course do not exist, but low-density expansions for transport around beds of random particles have been derived [32–35].

The remarks made above enable one to draw two important general conclusions about any effective parameter:

1. The effective property is indeed sensitive to the details of the microstructure by virtue of its dependence on an infinite set of statistical correlation functions.

2. An exact solution for the effective property of a random medium is generally unobtainable since presently available knowledge and technology can not generally yield five-point and higher-order correlation functions (see discussions of sections 4 and 5).

However, as shall be shown in the subsequent sections, bounds provide a rigorous as well as practical means of estimating the effective properties by utilizing limited but nontrivial statistical information on the heterogeneous medium.

3. BOUNDING PRINCIPLES AND IMPROVED BOUNDS

Inspection of the local and averaged equations for the conduction and elasticity problems reveals the close mathematical similarities between the two problems. Thus, the same techniques can be used to derive bounds on the effective conductivity tensor $\boldsymbol{\sigma}_e$ and the effective stiffness tensor $\mathbf{C}_e$. Several methods have been developed to derive bounds on these effective parameters. The oldest and most well-known technique is the use of variational principles and

was largely developed by Hashin and Shtrikman [13,14], Prager [44], and Beran [45]. There are two types of variational principles: classical variational principles (ie, energy minimization principles) [2,44,45] and Hashin–Shtrikman principles [13, 14]. The variational method, described in detail below, has been employed by numerous investigators [23,46–64]. The analytic method, initiated by Bergman [65,66] for σ_e and by Kantor and Bergman [67] for $\mathbf{C}_e$, exploits the analytic properties of these effective properties as a function of the phase properties; it has also been applied by others [68–71]. One of the advantages of the analytic method is that it is easily extended to produce bounds on σ_e when σ_1 and σ_2 are complex [66,68–70]. The method of Padé approximants developed by Milton and Golden [72] is closely related to the analytic method as a consequence of the fact that the conductivity tensor σ_e is a Stieltjes function. The translation method and closely related compensated-compactness technique has been initiated by Tartar and Murat [73–75] and by Lurie and Cherkaev [76,77] to bound σ_e and $\mathbf{C}_e$. This method was subsequently applied by Francfort and Murat [78], Milton [64], Kohn and Milton [59], and others. Finally, the field equation recursion method was developed by Milton [79]. The reader is referred to Milton [64,80,81] for a detailed review of the last few methods.

For the trapping and flow problems only variational principles are available to derive bounds on the trapping constant γ and fluid permeability tensor $\mathbf{k}$. Prager and his co-workers [82–84] pioneered the use of variational principles to bound these properties. Since these initial papers, variational principles have been applied to those problems by a number of investigators [26,28,85–89]. In all cases the bounds are obtained from *energy minimization principles.*

In light of the fact that variational principles, specifically, energy minimization principles, represent the only method which can be utilized to derive bounds on all four properties studied here, energy minimization principles are described in some detail below. In each case, various specific *improved* bounds which have been obtained are explicitly stated.

3.1. Conductivity

The classical variational principles for the effective conductivity tensor σ_e are as follows:

Minimum potential energy:

$$< \nabla T > \cdot \sigma_e \cdot < \nabla T > \leq < \mathbf{E} \cdot \sigma \mathbf{E} >, \qquad \forall \mathbf{E} \in A_U, \quad (3.1)$$

$$A_U = \{ \text{stationary } \phi(\mathbf{x}); \nabla \times \mathbf{E} = 0, \ < \mathbf{E} >= < \nabla T > \}. \quad (3.2)$$

In words, the trial field $\mathbf{E}$ must be irrotational and the ensemble average of $\mathbf{E}$ must equal the ensemble average of the actual temperature gradient ∇T [cf. (2.2)–(2.4)]. Thus, any $\mathbf{E}$ satisfying these admissibility conditions gives an upper bound on σ_e when substituted into the right-hand side of (3.1).

Minimum complementary energy:

$$< \mathbf{Q} > \cdot \sigma_e^{-1} \cdot < \mathbf{Q} > \geq < \mathbf{J} \cdot \sigma^{-1} \mathbf{J} >, \qquad \forall \mathbf{J} \in A_L, \quad (3.3)$$

$$A_L = \{ \text{stationary } \mathbf{J}(\mathbf{x}); \nabla \cdot \mathbf{J} = 0, \ < \mathbf{J} >= < \mathbf{Q} > \}. \quad (3.4)$$

Here as in (3.1), $\sigma(\mathbf{x})$ is the local conductivity defined by (2.4). The variational principle (3.3) yields a lower bound on σ_e when the trial heat flux vector $\mathbf{J}$ meets the admissiblity conditions of (3.4). These variational principles are quite old; see, for example, Beran [2] and references therein. The proofs of (3.1) and (3.3) have been given by Milton and McPhedran [90] among others.

3.1.1. Macroscopically isotropic media

The first and one of the simplest conductivity bounds were obtained by Weiner [91], showing that σ_e always lies between the weighted arithmetic and harmonic means of the phases, that is, $< \sigma^{-1} >^{-1} \leq \sigma_e \leq < \sigma >$. These one-point bounds are easily generated from the variational principles (3.1) and (3.3) by taking the admissible temperature gradient and heat flux to be constant vectors and correspond exactly to the eigenvalues of anisotropic composites composed of alternating slabs parallel or perpendicular to the applied field. Using variational principles which involve the *polarization* fields, Hashin and Shtrikman [13] and Hashin [23] obtained the best possible bounds on σ_e for the cases $d = 3$ and $d = 2$, respectively, given only volume-fraction information (ϕ_i). These bounds actually depend upon the two-point probability function $S_2^{(i)}$ in a trivial manner and thus are two-point bounds. They are exact through second-order in the difference $(\sigma_i - \sigma_j)$, that is, they give the coefficients $\mathbf{a}_1^{(i)}$ and $\mathbf{a}_2^{(i)}$ of (2.31). These bounds are the best possible bounds given ϕ_i since they are exactly realized for certain space-filling composite-sphere (cylinder) assemblages described below. Since the Hashin–Shtrikman and Hashin bounds are special cases of three-point bounds about to be described they are not given here explicitly.

Using trial fields based upon the first few terms of the perturbation expansion of the fields and the principles (3.1) and (3.3), Beran [45] derived three-point bounds on σ_e for $d = 3$ which are exact through third-order in $(\sigma_i - \sigma_j)$. Torquato [92] and Milton [93] independently showed that the three-point Beran bounds, which involve sixfold integrals of certain three-point correlation functions, can be expressed terms of volume fractions ϕ_i and a single three-fold integral over $S_3^{(i)}$ defined below (see also Torquato and Stell [94]). Silnutzer [53] obtained two-dimensional analogs of the Beran bounds for transversely isotropic fiber-reinforced materials which Schulgasser [95] and Milton [96] simplified in a similar fashion. For $d = 2$ and 3, these three-point bounds are given by

$$\sigma_L^{(3)} \leq \sigma_e \leq \sigma_U^{(3)}, \quad (3.5)$$

$$\frac{\sigma_L^{(3)}}{\sigma_1} = \frac{1+[(d-1)(1+\phi_2)-\zeta_2]\beta_{21}+(d-1)[(d-1)\phi_2-\zeta_2]\beta_{21}^2}{1-[(\phi_2+\zeta_2)-(d-1)]\beta_{21}+\{[\phi_2-(d-1)\phi_1]\zeta_2-(d-1)\phi_2\}\beta_{21}^2}, \quad (3.6)$$

$$\frac{\sigma_U^{(3)}}{\sigma_2} = \frac{1+[(d-1)(\phi_1+\zeta_1)-1]\beta_{12}+(d-1)\{[(d-1)\phi_1-\phi_2]\zeta_1-\phi_1\}\beta_{12}^2}{1-[1+\phi_1-(d-1)\zeta_1]\beta_{12}+[\phi_1-(d-1)\zeta_1]\beta_{12}^2}, \quad (3.7)$$

where β_{ij} depends only on the phase conductivities as given by (2.28). Note that (3.5) depends not only on ϕ_i but on a three-point microstructural parameter $\zeta_2 = 1 - \zeta_1$, which is an integral over the n-point probability functions $S_1^{(2)}, S_2^{(2)}$ and $S_3^{(2)}$ defined in section 2.6. For statistically homogeneous media, the $S_n^{(i)}$ are functions of the relative positions of the n points and so, for example, $S_1^{(i)} = \phi_i$. The three-point parameter ζ_2 in two and three dimensions is respectively given by

$$\zeta_2 = \frac{4}{\pi\phi_1\phi_2}\int_0^\infty \frac{dr}{r}\int_0^\infty \frac{ds}{s} \times \int_0^\pi d\theta \ \cos(2\theta)\left[S_3^{(2)}(r,s,t) - \frac{S_2^{(2)}(r)S_2^{(2)}(s)}{\phi_2}\right], \quad (3.8)$$

and

$$\zeta_2 = \frac{9}{2\phi_1\phi_2}\int_0^\infty \frac{dr}{r}\int_0^\infty \frac{ds}{s} \times \int_{-1}^1 d(\cos\theta)P_2(\cos\theta)\left[S_3^{(2)}(r,s,t) - \frac{S_2^{(2)}(r)S_2^{(2)}(s)}{\phi_2}\right], \quad (3.9)$$

where P_2 is the Legendre polynomial of order 2 and θ is the angle opposite the side of the triangle of length t. For isotropic media, the $S_n^{(i)}$ depend upon the relative distances of the n points. Specifically, $S_3^{(2)}(r, s, t)$ is the probability of finding in phase 2 the vertices of a triangle with sides of lengths r, s, and t, when randomly thrown into the sample. $S_2^{(2)}(r)$ is the probability of finding in phase 2 the endpoints of a line segment of length r. That ζ_1 must lie in the closed interval [0,1] implies that the bounds (3.5) always improve upon the two-point Hashin–Shtrikman or Hashin bounds. When $\zeta_2 = 0$, the bounds (3.5) coincide and equal the two-point Hashin–Shtrikman or Hashin lower bound (for $\sigma_2 \geq \sigma_1$). When $\zeta_2 = 1$, the bounds (3.5) coincide the equal the aforementioned two-point upper bound (for $\sigma_2 \geq \sigma_1$). It is important to emphasize that the three-point bounds (3.5) are valid for *any* isotropic microgeometry.

In cases in which one of the phases is composed of well-defined inclusions, it is desired to derive bounds from (3.1) and (3.3) that incorporate such specific microstructural information. The so-called *nth-order* "cluster" bounds of Torquato [58] accomplish this by utilizing admissible fields which exactly account for interactions between n inclusions. (This class of bounds is now sometimes referred to as "multiple-scattering" bounds—see discussion below on bounds on the trapping constant and fluid permeability.) Such bounds are therefore exact through nth-order in the inclusion volume fraction. Weissberg [49] actually was the first to employ cluster or multiple-scattering bounds and, in particular, derived such bounds for a system of perfectly insulating ($\sigma_2/\sigma_1 = 0$), *fully penetrable spheres* of equal radius. Fully penetrable spheres refers to a distribution of spheres in which sphere centers are randomly centered (ie, Poisson distributed) and thus completely uncorrelated. (This model is discussed fully in section 4.) DeVera and Strieder [55] extended Weissberg's results for this model to the entire range of σ_2/σ_1. All of these bounds are special cases of the general first-order multiple-scattering bound derived by Torquato [58] for distributions of equi-sized spheres with an *arbitrary* degree of impenetrability (see section 4) and in compact notation are given by

$$\sigma_L^{(3)}[\sigma_1, \sigma_2, \phi_2, G_2, G_3] \leq \sigma_e \leq \sigma_U^{(3)}[\sigma_1, \sigma_2, \phi_2, G_2, G_3], \quad (3.10)$$

where the point/q-particle function $G_n(\mathbf{x}; \mathbf{r}^q)$ is the $(n = 1 + q)$ correlation associated with finding a point at $\mathbf{x}$exterior to the spheres and a configuration of q spheres with centers at $\mathbf{r}^q \equiv \mathbf{r}_1, \ldots, \mathbf{r}_q$. (Note that Ref 58 uses slightly different notation for G_n.) The first-order cluster bounds (3.10) are clearly three-point bounds as they involve G_3. In general, nth-order cluster bounds are $(n + 2)$-point bounds. Interestingly, Beasley and Torquato [97] showed that for the instance of totally impenetrable spheres, the multiple-scattering bound (3.10) is identical to the three-point Beran bounds (3.5). As described in section 5, the multiple-scattering bound (3.10) is of a functional form which is easier to calculate from Monte Carlo computer simulations from than the Beran bounds.

Milton [98] has derived a three-point lower bound on σ_e, for the case $d = 3$ and $\sigma_2 \geq \sigma_1$, which improves upon the Beran lower bound:

$$\frac{\sigma_L^{(3)}}{\sigma_1} = \frac{1 + (1 + 2\phi_2)\beta_{21} - 2(\phi_1\zeta_2 - \phi_2)\beta_{21}^2}{1 + \phi_1\beta_{21} - (2\phi_1\zeta_2 + \phi_2)\beta_{21}^2}. \quad (3.11)$$

This actually is the best possible lower bound on σ_e given ϕ_i and ζ_2 since it is exactly realized for space-filling doubly-coated composite spheres (see Fig 1 for a two-dimensional analog).

Milton [69] has formally derived n-point bounds on σ_e for $d = 2$ and $d = 3$ which are exact through nth-order in $(\sigma_i - \sigma_j)$. For even values of n, the n-point bounds of Milton are exactly realized for space-filling multicoated cylinders (disks in two dimensions) where each multicoated cylinder (disk) has $n/2$ coatings and is similar, within a scale factor, to any other multicoated cylinder in the composite. Since the coated cylinders fill all space, there is a distribution in their sizes ranging to the infinitesimally small. In the case of $n = 4$, explicit representations of these bounds may be written for $\sigma_2 \geq \sigma_1$ in the following form [38]:

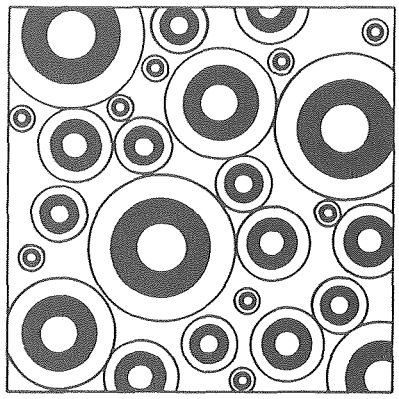

FIG 1. The double-coated cylinder geometry associated with the four-point Milton [69] lower bound (3.13) for $\sigma_2 > \sigma_1$. Here phases 1 and 2 are the white and black phases, respectively. The ratio of the core volume to the core plus inner shell is $\phi_1\zeta_2$. The analogous sphere geometry ($d = 3$) corresponds to the three-point Milton [69] lower bound (3.11). The reciprocal four-point upper bound (3.14) for $d = 2$ and $\sigma_2 > \sigma_1$ is realized for this geometry with the phases interchanged.

$$\sigma_L^{(4)} \leq \sigma_e \leq \sigma_U^{(4)}, \quad (3.12)$$

$$\frac{\sigma_L^{(4)}}{\sigma_1} = \frac{1 - [(d-1)\phi_2 - \gamma_2/\zeta_2]\beta_{21} + (1-d)[\phi_1\zeta_2 + \phi_2\gamma_2/\zeta_2]\beta_{21}^2}{1 - [\phi_2 + \gamma_2/\zeta_2]\beta_{21} + [\phi_1(1-d)\zeta_2 + \phi_2\gamma_2/\zeta_2]\beta_{21}^2}, \quad (3.13)$$

$$\frac{\sigma_U^{(4)}}{\sigma_2} = \frac{1 - [(d-1)\phi_1 - \gamma_1/\zeta_1]\beta_{12} + (1-d)[\phi_2\zeta_1 + \phi_1\gamma_1/\zeta_1]\beta_{12}^2}{1 - [\phi_1 + \gamma_1/\zeta_1]\beta_{12} + [\phi_2(1-d)\zeta_1 + \phi_1\gamma_1/\zeta_1]\beta_{12}^2}, \quad (3.14)$$

and

$$\gamma_1 - \gamma_2 = (d-2)(\zeta_2 - \zeta_1). \quad (3.15)$$

Note that the four-point bounds (3.12) depend upon ϕ_i, ζ_i, and a four-point parameter γ_i [defined in Ref 38 and related to $\mathbf{A}_4^{(i)}$ of (2.29)], which depends upon $S_1^{(i)}$, $S_2^{(i)}$, $S_3^{(i)}$, and $S_4^{(i)}$. The geometries corresponding to the four-point bounds are depicted in Fig 1 for the case $d = 2$. When the radius of the inner cylinder goes to zero, $\zeta_i \to 0$ $(i = 1,2)$, and one recovers the singly-coated cylinder assemblages corresponding to the Hashin [70] two-point bounds. Elsewhere Milton [99] has shown that any effective conductivity tensor function for $d = 2$ is realized by some sequentially layered laminate material and by some hierarchical elliptical cylinder assemblage.

Keller [100], Dykhne [100], and Mendelson [102] proved that the effective conductivity $\sigma_e = \sigma_e(\sigma_1, \sigma_2)$ for $d = 2$ has the following property:

$$\sigma_e(\sigma_1, \sigma_2)\sigma_e(\sigma_2, \sigma_1) = \sigma_1\sigma_2. \quad (3.16)$$

Milton employed (3.16) to show that all even-order coefficients of the expansion of σ_e in powers of $\sigma_i - \sigma_j (i \neq j)$ could be expressed in terms of all lower-order coefficients for the case $d = 2$. This has been shown to imply that $\gamma_i = 0$ for $d = 2$ [38]. Note that for $d = 3$, phase-interchange relations are inequalities [15,69,103].

Torquato [38] has observed that the formula

$$\frac{\sigma_e}{\sigma_1} = \frac{1 + 2\phi_2\beta_{21} - 2\phi_1\zeta_2\beta_{21}^2}{1 - \phi_2\beta_{21} - 2\phi_1\zeta_2\beta_{21}^2} \quad (3.17)$$

yields an accurate approximate expression for the effective conductivity of *three-dimensional* dispersions, provided that the mean

cluster size of the dispersed phase (phase 2) is much smaller than the macroscopic length scale. This relation is mentioned here because it is, for $\sigma_2 \geq \sigma_1$, Milton's four-point lower bound, (3.13), with γ_2 set equal to zero. It also can be obtained by truncating the expansion (2.27) after third-order terms.

3.1.2. *Macroscopically anisotropic media*

In the case of macroscopically anisotropic media, correlation function independent extensions of the Hashin–Shtrikman isotropic bounds have been obtained by various workers—see, for example, Murat and Tartar [74–75], Lurie and Cherkaev [76,77], and Milton and Kohn [63]. Since the main concern of this review is improved bounds, that is, correlation function dependent bounds, the reader is referred to the above cite references for further details.

Hori [104,105] developed perturbation expansions and bounds for the effective conductivity tensor $\boldsymbol{\sigma}_e$ in the case of macroscopically anisotropic media. The n-point tensor microstructural parameters involved unfortunately are, in general, conditionally convergent integrals and involve derivatives of the correlation functions rather than the correlation functions themselves. Willis [54] derived two-point bounds on $\boldsymbol{\sigma}_e$ for composites containing aligned, spheroidal inclusions. More recently, Milton [79] employed the elegant and powerful field equation recursion method to obtain an infinite hierarchy of bounds on the effective conductivity tensor $\boldsymbol{\sigma}_e$. His bounds are given in terms of symmetric, positive-semidefinite matrices called "weights" and "normalization factors" that depend upon the microgeometry. However, Milton did not express these matrices explicitly in terms of integrals over the n-point correlation functions. Sen and Torquato [20] subsequently derived a new perturbation expansion for $\boldsymbol{\sigma}_e$ of d-dimensional two-phase media of arbitrary topology which was given earlier by (2.27). The n-point tensors $\mathbf{A}_n^{(i)}$ of that expansion were shown to be related to Milton's weights and normalization factors, and thus the latter quantities have been given in terms of integrals over the $S_n^{(i)}$ for the first time [20]. Sen and Torquato then derived, using the method of Padé approximants and expansion (2.31), new n-point bounds on $\boldsymbol{\sigma}_e$ for d-dimensional media of arbitrary topology that depend upon the n-point parameters $\mathbf{A}_n^{(i)}$ or $\mathbf{a}_n^{(i)}$ [defined by (2.29)] for $n = 2$, 3 and 4, and contain, as special cases, the isotropic Hashin–Shtrikman and Hashin two-point bounds [13,23], isotropic Beran–Silnutzer three-point bounds [45,53], and the isotropic Milton four-point bounds [69].

The Sen-Torquato two-point bounds are given for $\sigma_2 \geq \sigma_1$ by

$$\boldsymbol{\sigma}_L^{(2)} \leq \boldsymbol{\sigma}_e \leq \boldsymbol{\sigma}_U^{(2)}, \tag{3.18}$$

$$\frac{\boldsymbol{\sigma}_L^{(2)}}{\sigma_1} = \left[\mathbf{U} + \left(\phi_2 \mathbf{U} - \frac{1}{\phi_2}\mathbf{a}_2\right)\delta_{21}\right] \cdot \left[\mathbf{U} - \frac{1}{\phi_2}\mathbf{a}_2\delta_{21}\right]^{-1}, \tag{3.19}$$

$$\frac{\boldsymbol{\sigma}_U^{(2)}}{\sigma_2} = \left[\mathbf{U} + (\phi_1 \mathbf{U} - \frac{1}{\phi_1}\mathbf{a}_2)\delta_{12}\right] \cdot \left[\mathbf{U} - \frac{1}{\phi_1}\mathbf{a}_2\delta_{12}\right]^{-1}, \tag{3.20}$$

where

$$\mathbf{a}_2 = \mathbf{a}_2^{(1)} = \mathbf{a}_2^{(2)} = -\phi_1\phi_2\mathbf{A}_2^*, \tag{3.21}$$

$$\mathbf{A}_2^* = \frac{1}{d}\left[\mathbf{U} - \frac{1}{\phi_1\phi_2}\mathbf{A}_2\right], \tag{3.22}$$

$$\mathbf{A}_2 = \mathbf{A}_2^{(1)} = \mathbf{A}_2^{(2)} = \frac{d}{2\pi(d-1)}\int_\epsilon d\mathbf{x}\left[\frac{\mathbf{x}\mathbf{x}d - x^2\mathbf{U}}{x^{d+2}}\right]\left[S_2^{(i)}(\mathbf{x}) - \phi_i^2\right], \tag{3.23}$$

and δ_{ij} is given by (2.28). The subscript ϵ on the integral of (3.23) indicates that it is to be carried out with the exclusion of an infinitesimally small d-dimensional sphere centered at $\mathbf{x}$. The notation of (3.18) signifies that the tensors $(\boldsymbol{\sigma}_U^{(2)} - \boldsymbol{\sigma}_e)$ and $(\boldsymbol{\sigma}_e - \boldsymbol{\sigma}_L^{(2)})$ are positive-semidefinite. It has been shown that the conductivity functions (3.19) and (3.20) are realized for a variety of models [69,74,99,106], one of which is an assemblage of singly-coated, oriented d-dimensional ellipsoids, that is, a generalization of the Hashin–Shtrikman singly-coated sphere assemblage.

The two-point parameters $\mathbf{A}_2$, $\mathbf{a}_2$, and $\mathbf{A}_2^*$ given above have been shown [20] to possess general properties worth noting. First, for macroscopically isotropic media,

$$\mathbf{A}_2 = \mathbf{O},\ \mathbf{a}_2 = \frac{-\phi_1\phi_2\mathbf{U}}{d}, \qquad \mathbf{A}_2^* = \frac{\mathbf{U}}{d}. \tag{3.24}$$

Second, for general anisotropic media,

$$\mathrm{tr}(\mathbf{A}_2) = 0, \qquad \mathrm{tr}(\mathbf{a}_2) = -\phi_1\phi_2, \qquad \mathrm{tr}(\mathbf{A}_2^*) = 1. \tag{3.25}$$

Third, the two-point parameters are bounded from above and below as follows:

$$-(d-1)\phi_1\phi_2 \leq (A_2)_{kk} \leq \phi_1\phi_2, \tag{3.26}$$

$$-\phi_1\phi_2 \leq (a_2)_{kk} \leq 0, \tag{3.27}$$

$$0 \leq (A_2^*)_{kk} \leq 1, \tag{3.28}$$

where X_{kk} $(k = 1, \ldots, d)$ denote the diagonal elements of a tensor $\mathbf{X}$. Note that the correlation-function independent Milton–Kohn bounds [63] are obtained essentially by extremizing over (3.26)–(3.28).

As noted earlier, the two-point parameters are related to Milton's [79] first normalization factor $\mathbf{N}_1$. In terms of the "polarization" $\mathbf{A}_2^*$, this relation is given by

$$\mathbf{A}_2^* = (\mathbf{U} + \mathbf{N}_1)^{-1}. \tag{3.29}$$

Thus, (3.29) along with (3.21)–(3.23) gives $\mathbf{N}_1$ explicitly in terms of $S_2^{(i)}$. Milton [79] gave the general properties of all of the normalization factors and weights.

Explicit representations of the Sen-Torquato three-point and four-point bounds on $\boldsymbol{\sigma}_e$ as well as the general properties of the $\mathbf{A}_n^{(i)}$ are given elsewhere [20,107].

3.2. Elastic moduli

As in the conduction problem, classical variational principles for the effective stiffness tensor $\mathbf{C}_e$ of a two-phase composite are stated here explicitly.

Minimum potential energy:

$$<\boldsymbol{\epsilon}>:\mathbf{C}_e:<\boldsymbol{\epsilon}> \leq <\mathbf{e}:\mathbf{C}:\mathbf{e}>, \qquad \forall \mathbf{e} \in B_U, \tag{3.30}$$

$$B_U = \{\text{stationary } \mathbf{e}(\mathbf{x}),\ \text{satisfying compatibility}; <\mathbf{e}> = <\boldsymbol{\epsilon}>\}. \tag{3.31}$$

The last condition of (3.31) states that the average of the trial strain field $\mathbf{e}(\mathbf{x})$ must equal the average of the actual strain field $\boldsymbol{\epsilon}(\mathbf{x})$ [cf (2.10)]. Thus, (3.30) yields an upper bound on $\mathbf{C}_e$.

Minimum complementary energy:

$$<\boldsymbol{\tau}>:\mathbf{C}_e^{-1}:<\boldsymbol{\tau}> \geq <\mathbf{s}:\mathbf{C}^{-1}:\mathbf{s}>, \quad \forall \mathbf{s} \in B_L, \tag{3.32}$$

$$B_L = \{\text{stationary } \mathbf{s}(\mathbf{x})\ ;\ \nabla\cdot\mathbf{s} = 0, <\mathbf{s}> = <\boldsymbol{\tau}>\}. \tag{3.33}$$

The last condition of (3.33) requires that the increase trial stress field $\mathbf{s}$ equal the average of the actual stress field $\boldsymbol{\tau}$ [cf (2.9)]. Relation (3.32) along with an admissible stress field $\mathbf{s}(\mathbf{x})$ yields a lower bound on $\mathbf{C}_e$. The variational principles, as in the conduction case, are old; see, for example, Ref 2 and references therein. The proofs of these theorems follow in precisely the same manner as that for the conduction problem—see Ref 90, for example.

3.2.1. *Macroscopically isotropic media*

In analogy with the conduction problem, the first and one of the simplest elastic moduli bounds on the effective bulk modulus K_e and effective shear modulus G_e of three-dimensional isotropic media were the weighted arithmetic and harmonic means of the elastic moduli proved respectively by Hill [46] and Paul [47]. These one-point bounds, which have come to be known as the Voight–Reuss bounds, are easily generated from the variational principles (3.30) and (3.32) by taking the admissible strain and stress fields to be constant tensors.

Employing variational principles which involve the polarization fields, Hashin and Shtrikman (HS) [14] for $d = 3$ obtained the best possible bounds on K_e and G_e given only volume fraction information. These bounds were subsequently generalized by Walpole [51]. Hill [22] and Hashin [48] obtained corresponding bounds on the effective transverse bulk modulus k_e and effective transverse shear modulus G_e for transversely isotropic fiber-reinforced two-phase materials in which

$$k_i = K_i + \frac{G_i}{3} \tag{3.34}$$

is the transverse bulk modulus of phase i for transverse compression without axial extension. All of the aforementioned two-point bounds [14,22,48,51] are exact through second order in the difference of the respective phase moduli and are not stated here explicitly since they are special cases of the three-point bounds described below. The bounds on K_e and k_e are achieved for the same composite-sphere and cylinder assemblages described already for the conduction problem. The corresponding shear moduli bounds are, however, not realized by such assemblages. Recently, Milton [108], Norris [109], and Lurie and Cherkaev [110], independently showed that the Hashin–Shtrikman bounds on G_e were attained by hierarchical laminates, thus demonstrating, for the first time, their optimality. In other independent work, Francfort and Murat [78] found a realization of these bounds using laminates of *finite* rank.

Employing the principles (3.30) and (3.32) and admissible fields based upon the first few terms of the perturbation expression of the fields, Beran and Molyneux [50] and McCoy [52] derived three-point bounds on K_e and G_e for $d = 3$. Silnutzer [53] obtained two-dimensional analogs of these bounds on K_e and G_e. Milton [93,96] subsequently simplified each of the above three-point bounds, showing that the bounds on the effective bulk moduli for $d = 2$ or 3 can be expressed in terms of ϕ_2 and the three-point parameter ζ_2 defined by (3.8) and (3.9) and that the bounds on the effective shear moduli for $d = 2$ or 3 can be expressed in terms of ϕ_2, ζ_2, and another three-point parameter η_2. The microstructural parameter η_2 for $d = 2$ and $d = 3$ is respectively given by

$$\eta_2 = \frac{16}{\pi\phi_1\phi_2}\int_0^\infty \frac{dr}{r}\int_0^\infty \frac{ds}{s} \times \int_0^\pi d\theta\, \cos(4\theta)\left[S_3^{(2)}(r,s,t) - \frac{S_2^{(2)}(r)S_2^{(2)}(s)}{\phi_2}\right] \tag{3.35}$$

and

$$\eta_2 = \frac{5\zeta_2}{21} + \frac{150}{7\phi_1\phi_2}\int_0^\infty \frac{dr}{r}\int_0^\infty \frac{ds}{s}\int_{-1}^1 d(\cos\theta) \times P_4(\cos\theta)\left[S_3^{(2)}(r,s,t) - \frac{S_2^{(2)}(r)S_2^{(2)}(s)}{\phi_2}\right], \tag{3.36}$$

where P_4 is the Legendre polynomial of order 4. The parameter η_2 lies in the closed interval [0,1], as does ζ_2. Milton and Phan-Thien [56] obtained three-point bounds on the shear modulus G_e for $d = 3$ with the same microstructural information but which are sharper than the McCoy bounds.

Before presenting the three-point bounds, it is useful to introduce some shorthand notation for any arbitrary property b:

$$< b > = b_1\phi_1 + b_2\phi_2, \tag{3.37}$$

$$< \tilde{b} > = b_1\phi_2 + b_2\phi_1, \tag{3.38}$$

$$< b >_\zeta = b_1\zeta_1 + b_2\zeta_2, \tag{3.39}$$

$$< b >_\eta = b_1\eta_1 + b_2\eta_2, \tag{3.40}$$

where, as before,

$$\zeta_1 = 1 - \zeta_2 \tag{3.41}$$

and

$$\eta_1 = 1 - \eta_2. \tag{3.42}$$

The simplified forms of the Silnutzer three-point bounds on the effective transverse bulk and shear moduli are respectively given by

$$k_L^{(3)} \le k_e \le k_U^{(3)}, \tag{3.43}$$

$$k_L^{(3)} = \left[< 1/k > - \frac{\phi_1\phi_2(1/k_2 - 1/k_1)^2}{< 1/\tilde{k} > + < 1/G >_\zeta}\right]^{-1}, \tag{3.44}$$

$$k_U^{(3)} = \left[< k > - \frac{\phi_1\phi_2(k_2 - k_1)^2}{< \tilde{k} > + < G >_\zeta}\right], \tag{3.45}$$

and

$$G_L^{(3)} \le G_e \le G_U^{(3)}, \tag{3.46}$$

$$G_L^{(3)} = \left[< 1/G > - \frac{\phi_1\phi_2(1/G_2 - 1/G_1)^2}{< 1/\tilde{G} > + \Xi}\right], \tag{3.47}$$

$$G_U^{(3)} = \left[< G > - \frac{\phi_1\phi_2(G_2 - G_1)^2}{< \tilde{G} > + \Theta}\right], \tag{3.48}$$

$$\Theta = \frac{[2 < k >_\zeta < G >^2 + < k >^2 < G >_\eta]}{< k + 2G >^2}, \tag{3.49}$$

$$\Xi = 2 < 1/k >_\zeta + < 1/G >_\eta. \tag{3.50}$$

As noted in section 2.2, the effective axial shear modulus μ_e is equivalent to determining the effective transverse conductivity σ_e. Thus, the bounds described above for σ_e are also bounds on μ_e.

The simplified form of the three-point Beran–Molyneux bounds on the effective bulk modulus K_e for $d = 3$ are given by

$$K_L^{(3)} \le K_e \le K_U^{(3)}, \tag{3.51}$$

$$K_L^{(3)} = \left[< 1/K > - \frac{4\phi_1\phi_2(1/K_2 - 1/K_1)^2}{4 < 1/\tilde{K} > + 3 < 1/G >_\zeta}\right]^{-1}, \tag{3.52}$$

$$K_U^{(3)} = \left[< K > - \frac{3\phi_1\phi_2(K_2 - K_1)^2}{3 < \tilde{K} > + 4 < G >_\zeta}\right]. \tag{3.53}$$

The three-point Milton–Phan-Thien bounds on the effective shear modulus G_e for $d = 3$ are given by

$$G_L^{(3)} \le G_e \le G_U^{(3)} \tag{3.54}$$

$$G_L^{(3)} = \left(< G > - \frac{6\phi_1\phi_2(G_2 - G_1)^2}{6 < \tilde{G} > + \Xi^{-1}}\right), \tag{3.55}$$

$$G_U^{(3)} = \left(< G > - \frac{6\phi_1\phi_2(G_2 - G_1)^2}{6 < \tilde{G} > + \Theta}\right), \tag{3.56}$$

where

$$\Xi = \frac{5\left\langle \frac{1}{G}\right\rangle_\zeta \left\langle \frac{6}{K} - \frac{1}{G}\right\rangle_\zeta + \left\langle \frac{1}{G}\right\rangle_\eta \left\langle \frac{2}{K} + \frac{21}{G}\right\rangle_\zeta}{\left\langle \frac{128}{K} + \frac{99}{G}\right\rangle_\zeta + 45\left\langle \frac{1}{G}\right\rangle_\eta}, \tag{3.57}$$

$$\Theta = \frac{3 < G >_\eta < 6K + 7G >_\zeta - 5 < G >_\zeta^2}{2 < K - G >_\zeta + 5 < G >_\eta}. \tag{3.58}$$

Note that the effective shear modulus for $d = 2$ and $d = 3$ are both denoted by G_* [cf (3.46) and (3.54)].

Milton and Phan-Thien [56] also derived four-point bounds on the elastic moduli of three-dimensional two-phase composites. These results are not explicitly given here, however.

3.2.2. *Macroscopically anisotropic media*

Correlation function independent extensions of the Hashin–Shtrikman elasticity bounds to anisotropic composites were first obtained by Kantor and Bergman [67] using the analytic-function method and by Francfort and Murat [78] via the translation method. Milton and Kohn [63] obtained such elasticity bounds that improve upon these earlier results and are shown to be attained by sequentially layered laminate materials.

Willis [8,54] derived two-point bounds on $\mathbf{C}_*$ for n-phase composites using anisotropic generalizations of the Hashin–Shtrikman variational principles. These bounds are dependent upon the two-point probability function $S_2^{(i)}$ and, for two-phase materials, are the elasticity analogs of the Sen–Torquato two-point bounds on the effective conductivity tensor given by (3.18)–(3.20). The bounds of Willis are considerably more involved then the former bounds and hence are not given here. The reader is referred to Willis [8,54] for explicit representations of these two-point bounds.

3.3. Trapping constant

Reck and Prager [83] and Doi [85] were the first to employ variational principles to derive bounds on the diffusion-controlled trapping constant γ. Subsequently, Rubinstein and Torquato [26] derived general variational principles from which one can derive all previous bounds and generate new classes of bounds. Their variational principles, based upon minimizing energy functionals, are now summarized.

Variational upper bound:

$$\gamma \le \frac{< \nabla v \cdot \nabla v I >}{< vI >^2}, \qquad \forall v \in D_U, \tag{3.59}$$

$$D_U = \{\text{stationary } v(\mathbf{x});\ v = 0 \text{ on } \partial\mathcal{V},\ < vI > = < uI >\}. \tag{3.60}$$

The last condition of (3.10) states that the average scaled trial concentration field v in $\mathcal{V}_1$ must equal the average of the actual scaled concentration field u in $\mathcal{V}_1$ given by (2.16).

Variational lower bound:

$$\gamma \ge < \nabla v \cdot \nabla v I >^{-1}, \qquad \forall v \in D_L, \tag{3.61}$$

$$D_L = \{\text{stationary } v(\mathbf{x}); \Delta v = -1 \quad \text{in} \quad \mathcal{V}_1\}. \tag{3.62}$$

Rubinstein and Torquato also gave volume-average versions of these bounds. The proofs of (3.59) and (3.61) were given by them.

Rubinstein and Torquato [26] and Torquato and Rubinstein [88], using the principles (3.59) and (3.61), derived four different classes of rigorous bounds on the diffusion-controlled trapping constant γ: (i) two-point *interfacial-surface* lower bound; (ii) three-point *multiple-scattering* lower bound; (iii) two-point *void* lower bound; and (iv) two-point *security-spheres* upper bound. These bounds are given in terms of relatively simple functionals of the correlation functions involved and therefore are worth stating explicitly.

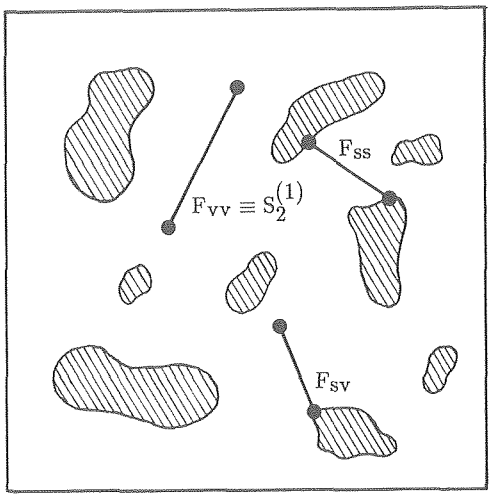

FIG 2. Schematic representation of the two-point correlation functions $S_2^{(1)}(\mathbf{x}_1, \mathbf{x}_2) \equiv F_{vv}(\mathbf{x}_1, \mathbf{x}_2)$, $F_{sv}(\mathbf{x}_1, \mathbf{x}_2)$ and $F_{ss}(\mathbf{x}_1, \mathbf{x}_2)$ defined in the text. For isotropic media they depend upon the relative distance between the two points. These functions are general, applying to particulate media (as shown here) as well as to nonparticulate media.

Interfacial-surface lower bound:

$$\gamma \ge \left\{ \int \frac{1}{4\pi r} \left[\frac{\phi_1^2}{s^2} F_{ss}(\mathbf{r}) - \frac{2\phi_1}{s} F_{sv}(\mathbf{r}) + F_{vv}(\mathbf{r}) \right] d\mathbf{r} \right\}^{-1} \tag{3.63}$$

Here F_{ss}, F_{sv}, and $F_{vv} = S_2^{(1)}$ are the surface-surface, surface-void, and void-void correlation functions defined more precisely in section 4 and depicted in Fig 2. ϕ_1 is the volume fraction of the trap-free region (porosity) and s is the specific surface (interfacial surface area per unit volume). For large r, $F_{ss} \to s^2$, $F_{sv} \to s\phi_1$, and $F_{vv} \to \phi_1^2$. The bound (3.63) is valid for general statistically homogeneous but anisotropic media and was first derived by Doi [85] using a different procedure than Rubinstein and Torquato [26].

Multiple-scattering lower bound:

$$\gamma \ge \left[\frac{1}{\rho^2} \int G_2(\mathbf{y}_1) |\nabla \mathcal{G}(\mathbf{y}_1)|^2 \, d\mathbf{y}_1 + \frac{1}{\rho^2} \int \int Q_3(\mathbf{y}_1, \mathbf{y}_2) \nabla \mathcal{G}(\mathbf{y}_1) \cdot \nabla \mathcal{G}(\mathbf{y}_2) \, d\mathbf{y}_1 \, d\mathbf{y}_2 \right]^{-1}, \tag{3.64}$$

where

$$Q_3(\mathbf{y}_1, \mathbf{y}_2) = G_3(\mathbf{x}; \mathbf{r}_1, \mathbf{r}_2) - \rho G_2(\mathbf{x}; \mathbf{r}_1) - \rho G_2(\mathbf{x}; \mathbf{r}_2) + \rho^2 \phi_1, \tag{3.65}$$

$$\mathbf{y}_i = \mathbf{x} - \mathbf{r}_i, \tag{3.66}$$

and

$$\mathcal{G}(\mathbf{r}) = \frac{1}{4\pi r} \tag{3.67}$$

is the Green's function of the Laplacian operator. This three-point bound applies to media composed of random distributions of equisized, possibly overlapping, spherical traps at number density ρ and volume fraction ϕ_2. The $G_n(\mathbf{x}; \mathbf{r}^q)$ are the point/q-particle distribution functions described briefly in (3.10) and in detail in section 4. The two-point quantity G_2 is schematically given in Fig 3. This bound is the analog of the multiple-scattering (or cluster) conductivity bound derived by Torquato [58].

Void lower bound:

$$\gamma \ge \left\{ \frac{1}{\phi_2^2} \int \frac{1}{4\pi r} [S_2^{(1)}(\mathbf{r}) - \phi_1^2] \, d\mathbf{r} \right\}^{-1} \tag{3.68}$$

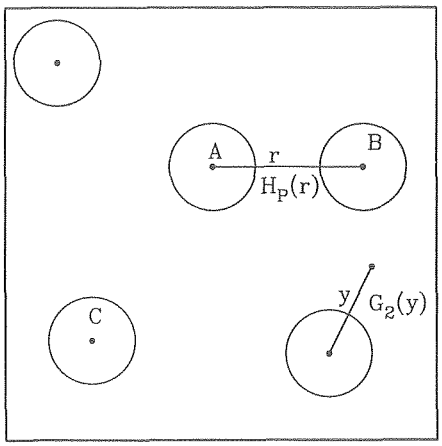

FIG 3. Schematic representation of the two-point functions, $H_P(r)$, the nearest-neighbor distribution, and $G_2(y)$, the point/particle function ($y = |\mathbf{x} - \mathbf{r}_1|$), for an isotropic distribution of disks defined in the text. Particle B is nearest to particle A at the radial distance r. The remaining particles lie outside this radial distance.

This two-point bound, derived by Torquato and Rubinstein [88], is weaker than the interfacial-surface bound (3.63) but has the advantage that it depends only on the simpler two-point probability function $S_2^{(1)}$ for the void phase or, equivalently, the void-void correlation function $F_{vv}(\mathbf{r})$. It is valid for any statistically anisotropic medium with porosity ϕ_1 and trap volume fraction ϕ_2.

Security-spheres upper bound:

$$\frac{\gamma}{\gamma_0} \geq \frac{c_1 c_2 + 9\phi_2^2 c_1^2 c_3}{c_2^2 + 18\phi_2^2 c_1 c_2 c_3 + 81\phi_2^4 c_1^2 c_3^2}, \tag{3.69}$$

where

$$c_1 = 2R \int_1^\infty e(\beta) H_P(\beta)\, d\beta, \tag{3.70}$$

$$c_2 = \left[1 - R\phi_2 \int_1^\infty f(\beta) H_P(\beta)\, d\beta\right]^2, \tag{3.71}$$

$$c_3 = \frac{R}{90} \int_1^\infty g(\beta) H_P(\beta)\, d\beta, \tag{3.72}$$

$$e(x) = \frac{x}{x-1}, \tag{3.73}$$

$$f(x) = x(x+1), \tag{3.74}$$

$$g(x) = 4x^2 - 5x^4 - 5x^3 + 5x^2 + 5x - 4, \tag{3.75}$$

$$\gamma_0 = \frac{3\phi_2}{R^2}. \tag{3.76}$$

This security-spheres upper bound [88] improves upon an earlier security-spheres upper bound [26], all of which are valid for equisized, impenetrable spherical traps of radius R at number density ρ. (Note that in each of these references the integrals involving H_P should have been multiplied by a factor of 2.) Thus, the trap volume fraction is $\phi_2 = \rho 4\pi R^3/3$. The quantity γ_0, (3.76), is the Smoluchowski dilute-limit trapping constant for spheres. Here $H_P(r)$ is the probability density associated with finding a nearest neighbor at a radial distance r from a particle located at the origin and is described fully in section 4. In relations (3.70)–(3.72), β is the dimensionless distance $r/2R$. Figure 3 gives a schematic representation of H_P. Note that it should not be confused with the well-known radial distribution function which is proportional to the probability density associated with finding *any* particle at a radial distance r from a particle at the origin.

Observe also that $e(\beta)$, (3.73), has a simple pole at $\beta = 1$ and therefore the integral c_1 of (3.70) generally diverges, yielding the trivial upper bound $\gamma \leq \infty$. However, if $H_P(\beta)$ vanishes as $(\beta - 1)^\epsilon$ at $\beta = 1$, where $\epsilon > 0$, the integral (3.70) converges and (3.69) gives a finite, positive upper bound on γ.

3.4. Fluid permeability

Prager [82] and Weissberg and Prager [84] were the first to employ variational principles to derive *upper* bounds on the isotropic fluid permeability. Doi [85] derived a different upper bound on the permeability using what he thought was a different variational principle; in actuality, he used a minimum energy principle as did Prager et al. Berryman and Milton [86] subsequently, using a *volume-average* approach, corrected a normalization constraint in the Prager variational principle. Torquato and Beasley [87] rederived the Weissberg–Prager upper bound on the permeability using an ensemble-average approach. More recently, Rubinstein and Torquato [28] derived new variational principles for upper and lower bounds on the isotropic permeability ($\mathbf{k} = k\mathbf{U}$) from which one can derive all previous bounds and generate new classes of bounds. Their ensemble-averaged bounds are given by

Variational upper bound:

$$k \geq < \nabla \mathbf{q} : \nabla \mathbf{q} I >, \qquad \forall \mathbf{q} \in E_U, \tag{3.77}$$

$$E_U = \{\text{stationary } \mathbf{q}(\mathbf{x}); \nabla \times (\Delta \mathbf{q} + \hat{\mathbf{e}}) = 0 \text{ in } \mathcal{V}_1\}. \tag{3.78}$$

Variational lower bound:

$$k \leq \frac{< \mathbf{w} \cdot \hat{\mathbf{e}} I >^2}{< \nabla \mathbf{q} : \nabla \mathbf{q} I >}, \qquad \forall \mathbf{q} \in E_L, \tag{3.79}$$

$$E_L = \{\text{stationary } \mathbf{q}(\mathbf{x}); \mathbf{q} = 0 \text{ on } \partial\mathcal{V}, \ \nabla \cdot \mathbf{q} = 0 \text{ in } \mathcal{V}_1, \text{ and } < \mathbf{q} \cdot \hat{\mathbf{e}} I > = < \mathbf{w} \cdot \hat{\mathbf{e}} I >\}. \tag{3.80}$$

Here $\hat{\mathbf{e}}$ is an arbitrary unit vector and $\mathbf{w}$ is the actual velocity field that satisfies (2.20)–(2.22). Rubinstein and Torquato also derived volume-average bounds. Note that these variational principles for the upper and lower bounds on k share a close resemblance to the lower and upper bounds, (3.61) and (3.59), respectively, on the trapping constant γ. The proofs of (3.77) and (3.79) are given in Ref 28.

Rubinstein and Torquato [28], via the principles (3.77) and (3.79), derived four different classes of rigorous bounds on the fluid permeability k: (i) two-point *interfacial-surface* upper bound; (ii) three-point *multiple-scattering* upper bound; (iii) two-point *void* upper bound; and (iv) two-point *security-spheres* upper bound. These are now explicitly stated.

Interfacial-surface upper bound:

$$k \leq \frac{2}{3} \int_0^\infty r \left[\frac{\phi_1^2}{s^2} F_{ss}(r) - \frac{2\phi_1}{s} F_{sv}(r) + F_{vv}(r)\right] dr. \tag{3.81}$$

The correlation functions involved here are the same as those described below relation (3.63). Doi [85] derived (3.81) using a different procedure.

Multiple-scattering upper bound:

$$k \leq \frac{1}{2\rho^2} \int G_2(\mathbf{y}_1) \mathbf{t}(\mathbf{y}_1) : \mathbf{t}(\mathbf{y}_1)\, d\mathbf{y}_1 + \frac{1}{2\rho^2} \int \int Q_3(\mathbf{y}_1, \mathbf{y}_2) \mathbf{t}(\mathbf{y}_1) : \mathbf{t}(\mathbf{y}_2)\, d\mathbf{y}_1\, d\mathbf{y}_2, \tag{3.82}$$

where

$$\mathbf{t} = \nabla(\mathbf{S} \cdot \hat{\mathbf{e}}) + \nabla(\mathbf{S} \cdot \hat{\mathbf{e}})^T. \tag{3.83}$$

$$S(\mathbf{r}) = (1 + \tfrac{1}{6}\Delta)\psi(\mathbf{r}), \tag{3.84}$$

$$\psi(r) = \frac{1}{8\pi}\left(\frac{\mathbf{U}}{r} + \frac{\mathbf{rr}}{r^3}\right). \tag{3.85}$$

This three-point bound, first derived by Torquato and Beasley [87] in a slightly different form, applies to porous media in which the impermeable solid phase is composed of random distributions of equisized, possibly overlapping spheres of unit radius at number density ρ. The distribution functions involved are identical to those that arise in (3.10) and (3.64).

Recently, Beasley and Torquato [89] derived an optimized three-point multiple-scattering upper bound (not stated here) which improves upon bound (3.82).

Void upper bound:

$$k \le \frac{2}{3\phi_2^2}\int_0^\infty r\left[S_2^{(1)}(r) - \phi_1^2\right]\,dr. \tag{3.86}$$

Here $\phi_1 = 1 - \phi_2$ is the porosity and $S_2^{(1)}$ is the two-point probability function for the fluid phase. This bound was first given by Prager [82] and subsequently corrected by Berryman and Milton [86] whose result agrees with (3.86).

Security-spheres lower bound:

$$\frac{k}{k_0} \ge \left[2R\int_1^\infty h(\beta^{-1})H_P(\beta)\,d\beta\right]^{-1}, \tag{3.87}$$

where

$$h(x) = (1 - x^5)\left(1 - \frac{9x}{4} + \frac{5x^3}{2} - \frac{9x^5}{4} + x^6\right)^{-1}, \tag{3.88}$$

$$k_0 = \frac{2R^2}{9\phi_2}. \tag{3.89}$$

This is valid for random beds of equisized, impenetrable spheres of radius R at number density ρ so that the sphere volume fraction is $\phi_2 = \rho 4\pi R^3/3$. The quantity k_0 of (3.89) is the Stokes dilute-limit permeability for spheres. $H_P(r)$ is the nearest-neighbor distribution function defined below (3.76). Note that this security-spheres bound is identical to one derived by Rubinstein and Keller [111] for the related inverse drag problem. (Note that the integrals of Refs 28 and 111 which involve H_P should have been multiplied by a factor of 2.)

Observe from (3.88) that $h(\beta^{-1})$ has a pole of order three at $\beta = 1$. Therefore, the integral (3.87) generally diverges and yields the trivial lower bound $k \ge 0$. However, if $H_P(\beta)$ vanishes faster than $(\beta - 1)^2$ at $\beta = 1$, the integral converges and (3.87) gives a positive lower bound on k.

3.5. Remarks

It is useful to comment on the utility of lower-order bounds, such as two-, three-, and four-point bounds, when the bounds diverge from one another. To fix ideas, consider the isotropic conduction problem. Similar arguments will apply to the elasticity problem and, in a generalized sense, to the trapping and flow problems. Moreover, the same arguments are easily extended to the corresponding anisotropic bounds in the cases of $\boldsymbol{\sigma}_e$, $\mathbf{C}_e$, and $\mathbf{k}$.

The fact that upper and lower bounds on σ_e diverge from one another in cases where the phase conductivities σ_1 and σ_2 are drastically different does not mean the bounds have no value in such instances. It has been observed by Torquato [38] that, because of the correspondence between n-point bounds on σ_e and certain realizable geometries, lower-order *lower* bounds are expected to yield good estimates of σ_e/σ_1 for $\sigma_2 \gg \sigma_1$, provided that the volume fraction of the highly conducting phase $\phi_2 < \phi_2^c$ (where ϕ_2^c is the percolation-threshold value) and the characteristic *cluster* size of phase 2, Λ_2, is much smaller than the macroscopic length scale L. (The percolation threshold ϕ_i^c of phase i is the volume fraction at which the first sample-spanning cluster of phase i appears. A cluster of phase i is defined as that part of phase i which can be reached from a point in phase i without touching any part of phase j, $i \ne j$.) For heterogeneous media composed of distributions of particles, Λ_2 can be roughly estimated from the well-defined *mean cluster size* [112] or *mean number of clusters* [113], which have been studied in continuum percolation theory (see section 4.7). Note that the condition $\Lambda_2 \ll L$ alone implies $\phi_2 < \phi_2^c$. For spatially periodic arrays of impenetrable d-dimensional spheres or for equilibrium distributions of impenetrable d-dimensional spheres, the condition $\Lambda_2 \ll L$ is satisfied for all ϕ_2 except very near the close packing value which corresponds to ϕ_2^c for such systems. In summary, for general media, even though the upper bounds on σ_e are much larger than the lower bounds for $\sigma_2 \gg \sigma_1$ (and, in fact, goes to infinity in the limit $\sigma_2/\sigma_1 \to \infty$), the lower-order lower bounds should give good estimates of σ_e/σ_1 provided that $\Lambda_2 \ll L$. Of course the accuracy of the lower-order lower bounds increases as n increases. Similarly, lower-order *upper* bounds are expected to yield useful estimates of σ_e/σ_1 for $\sigma_2 \gg \sigma_1$ given that $\phi_2 > \phi_2^c$ and $\Lambda_1 \ll L$. Above the threshold of phase 2, the last condition $\Lambda_1 \ll L$ is actually not necessary and can be relaxed without comprising the accuracy of the estimate on σ_e. Note that very similar arguments apply to lower-order elastic moduli bounds when one phase is much stiffer than the other [114] and to the corresponding anisotropic bounds [107].

Although such statements regarding the utility of lower-order bounds on the trapping constant γ and fluid permeability tensor $\mathbf{k}$ have heretofore not been made explicitly, it is clear that similar arguments can be put forth. For simplicity, consider the isotropic permeability k (the same comments will apply to the principal components of $\mathbf{k}$ in the direction of the principal axes, respectively). The true permeability k will lie much closer to the lower-order *upper* bounds (rather than the lower bounds) provided that $\Lambda_2 \ll L$, where phase 2 is the impermeable solid phase. The *lower* bounds should yield good estimates of k whenever $\Lambda_1 \ll L$ is obeyed since in such situations $k = 0$. Here Λ_1 is the characteristic cluster size of the fluid or void phase. Similarly, the true trapping constant will lie much closer to the lower-order *lower* bounds when $\Lambda_2 \ll L$ and lower-order *upper* bounds when $\Lambda_1 \ll L$.

The general claim that one of the improved bounds can provide relatively sharp estimates of the effective property for a wide range of conditions is corroborated by specific calculations given in section 5.

In the study of random media it is not only useful to seek the range of possible values that the effective property can take given limited morphological information (ie, rigorous bounds) but to identify the microstructures that correspond to the extreme values, that is, to determine whether the bounds are optimal. Such investigations have important implications for structural optimization [115,116]. This topic was touched upon in this section but an in-depth discussion is beyond the scope of the present review. It is useful to make a few comments, however. First, results concerning the realizability and optimality of bounds exist only for the effective conductivity tensor σ_e and effective stiffness tensor $\mathbf{C}_e$ [13,14,23,48,59–69, 73–81,100,106,108–110]. Microgeometries which realize the aforementioned bounds on the trapping constant γ and fluid permeability k have not been identified. Second, an extensive literature has developed which describes the realizability of bounds on σ_e and $\mathbf{C}_e$ by laminates [60–64,75,100,108–110], indicating the importance of laminates in modeling composites. Third, in addition to the bounds corresponding to the aforementioned coated-sphere assemblages and laminates, certain bounds are achieved by hierarchical coated assemblages of ellipsoids (ellipses) [66,69,74–77,106].

4. ADVANCES IN MICROSTRUCTURE CHARACTERIZATION

The previous section described the various types of statistical correlation functions ($S_n, G_n, F_{sv}, F_{ss}, H_p$) that have arisen in rigorous bounds on the effective conductivity tensor σ_e, effective stiffness tensor $\mathbf{C}_e$, diffusion-controlled trapping constant γ, and the fluid permeability tensor $\mathbf{k}$. $S_n^{(i)}(\mathbf{x}^n)$ gives the probability of simultaneously finding n points with positions $\mathbf{x}^n \equiv \{\mathbf{x}_1, \ldots, \mathbf{x}_n\}$ in phase i for statistically *inhomogeneous* media. Now since the $S_n^{(2)}$ are easily obtained from the $S_n^{(1)}$ [117], only the latter quantity, denoted by S_n, will be referred to in much of the subsequent discussion. The n-point probability functions S_n arise in conductivity [20,45,53,57,69,79,98,106], elastic moduli [50,52,54,56], trapping constant, and fluid permeability [28,82,85,86] bounds. For example, see bounds (3.5), (3.11), (3.12), (3.18), (3.43), (3.46), (3.51), (3.54), (3.63), (3.68), (3.81), and (3.86). For inhomogeneous particulate media, the point/q-particle distribution function $G_n(\mathbf{x}_1; \mathbf{r}^q)$ ($n = 1 + q$) gives the correlation associated with finding a point with position $\mathbf{x}_1$ in the space exterior to the particles (phase 1) and any q particles with coordinates (center of mass and orientation) $\mathbf{r}^q$. This function arises in the conductivity [58] bounds (3.10), trapping constant [26] bound (3.64), and fluid permeability [28] bounds (3.82) and the ones of Refs 87 and 89. The surface-void, $F_{sv}(\mathbf{x}_1, \mathbf{x}_2)$, and surface-surface, $F_{ss}(\mathbf{x}_1, \mathbf{x}_2)$, correlation functions arise in the trapping constant [26,85] bound (3.63) and fluid permeability [28,85] bound (3.81). $F_{ss}(\mathbf{x}_1, \mathbf{x}_2)$, for example, gives the correlation associated with finding a point at $\mathbf{x}_1$ on the two-phase interface and another point $\mathbf{x}_2$ on the interface. Yet another statistical quantity, the nearest-neighbor distribution function $H_p(r)$, arises in the trapping constant [88] bound (3.69) and the fluid permeability [28] bounds (3.87). Given a random suspension of identical d-dimensional spheres, $H_p(r)\,dr$ gives the probability of finding a nearest neighbor at a radial distance r from a sphere located at the origin.

For statistically homogeneous media, each type of n-point correlation function described above depends upon the relative positions of the n points. Thus, for example, $S_n(\mathbf{x}^n) = S_n(\mathbf{x}_{12}, \ldots, \mathbf{x}_{1n})$, where $\mathbf{x}_{1j} = \mathbf{x}_j - \mathbf{x}_1$. Furthermore, if the medium is statistically isotropic, then the n-point functions depend upon the relative distances, e.g., $F_{ss}(\mathbf{x}_1, \mathbf{x}_2) = F_{ss}(x_{12})$ where $x_{12} = |\mathbf{x}_{12}|$.

There are several comments that need to be made here. First, until recently, application of the aforementioned bounds was virtually impossible because of the difficulty involved in ascertaining the statistical correlation functions, both theoretically and experimentally. Second, Torquato and Stell [117–121] were the first to offer a systematic means of computing and representing the n-point probabilities $S_n^{(i)}$. However, such a formalism for the other types of correlation functions had been lacking. Third, are these different types of correlation functions related to one another? Fourth, can one write down a single expression which contains complete statistical information? As shall be demonstrated, the answers to the last two queries are in the affirmative.

4.1. Unified theoretical approach

For simplicity, consider first a statistical distribution of N identical d-dimensional spheres of radius R (phase 2) in volume V distributed throughout a "matrix" (phase 1). (More complicated models are described below.) Such a model is not as restrictive as one might initially surmise, especially since the particles may be allowed to overlap in varying degrees, thereby allowing interparticle clustering and thus the generation of interesting microstructures with long winding chains or large clusters with voids such as shown in Fig 4. Thus, the *matrix* need not be continuous. The case $d = 1$ (rods) is a useful model of certain laminates. The instance $d = 2$ (disks) can be employed to model a general class of fiber-reinforced materials and thin films. The case $d = 3$ (spheres) can be used to model unconsolidated media (eg, suspensions) as well as consolidated media (eg, sandstones, sintered materials, cermets, etc). See Fig 5 for a two-dimensional example of the former.

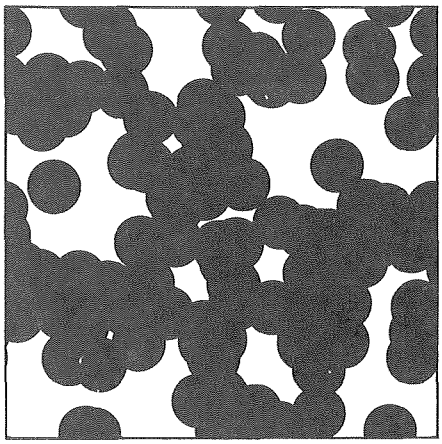

FIG 4. A distribution of identical, fully penetrable cylinders (disks) at a cylinder volume fraction $\phi_2 \approx 0.7$ which is slightly higher than the percolation-threshold value of $\phi_2^c \approx 0.68$ [126,127]. This model generally goes by many names, including "overlapping particles," "randomly centered" particles, "penetrable" particles, and the "Swiss-cheese" model.

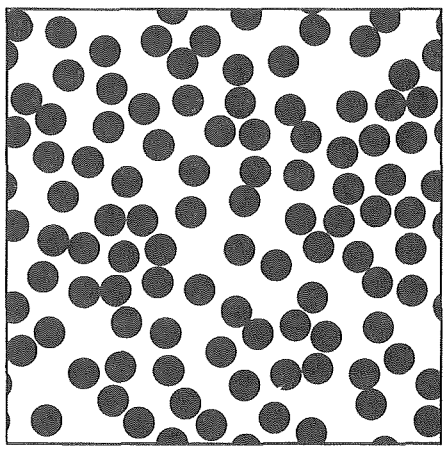

FIG 5. A distribution of identical, totally impenetrable cylinders (disks) at $\phi_2 \approx 0.35$. This model is generally also referred to as "impenetrable" or "hard" particles.

The d-dimensional spheres are spatially distributed according to the *specific* N-particle probability density $P_N(\mathbf{r}^N)$ which normalizes to unity. The ensemble average of any many-body function $F(\mathbf{r}^N)$ is then given by

$$< F(\mathbf{r}^N) >= \int F(\mathbf{r}^N) P_N(\mathbf{r}^N) d\mathbf{r}^N.$$

The reduced n-particle *generic* probability density is defined by

$$\rho_n(\mathbf{r}^n) = \frac{N!}{(N-n)!} \int P_N(\mathbf{r}^N)\, d\mathbf{r}_{n+1} \ldots d\mathbf{r}_N. \qquad (4.1)$$

Thus, $\rho_n(\mathbf{r}^n)$ characterizes the probability of finding any n spheres with positions $\mathbf{r}^n$. If the medium is statistically homogeneous, the $\rho_n(\mathbf{r}^n)$ will depend upon the relative displacements $\mathbf{r}_{12}, \ldots, \mathbf{r}_{1n}$, where $\mathbf{r}_{1i} = \mathbf{r}_i - \mathbf{r}_1$. In such instances, it is understood that the "thermodynamic limit" has been taken, that is, $N \to \infty$, such that the number density $\rho = N/V = \rho_1(\mathbf{r}_1)$ is some finite constant.

Torquato [122] has introduced the general n-point distribution function $H_n(\mathbf{x}^m; \mathbf{x}^{p-m}; \mathbf{r}^q)$, which is defined to be the correlation associated with finding m points with positions $\mathbf{x}^m$ on certain surfaces within the medium, $p-m$ with positions $\mathbf{x}^{p-m}$ in certain spaces exterior to the spheres, and q sphere centers with positions $\mathbf{r}^q$, $n = p+q$, in a statistically *inhomogeneous* medium of N identical d-dimensional spheres. Torquato found a series representation of H_n for such media which enables one to compute it; namely, he found that

$$H_n(\mathbf{x}^m; \mathbf{x}^{p-m}; \mathbf{r}^q) = (-1)^m \frac{\partial}{\partial a_1} \cdots \frac{\partial}{\partial a_m} G_n(\mathbf{x}^p; \mathbf{r}^q), \tag{4.2}$$

where

$$G_n(\mathbf{x}^p; \mathbf{r}^q) = \sum_{s=0}^{\infty} (-1)^s G_n^{(s)}(\mathbf{x}^p; \mathbf{r}^q), \tag{4.3}$$

$$G_n^{(s)}(\mathbf{x}^p; \mathbf{r}^q) = \frac{1}{s!} \prod_{i=1}^{q} \prod_{k=1}^{p} e(y_{ik}; a_k) \int \rho_{q+s}(\mathbf{r}^{q+s}) \times \prod_{j=q+1}^{q+s} m^{(p)}(\mathbf{x}^p; \mathbf{r}_j)\, d\mathbf{r}_j, \tag{4.4}$$

$$m^{(p)}(\mathbf{x}^p; \mathbf{r}_j) = 1 - \prod_{i=1}^{p} [1 - m(y_{ij}; a_i)], \tag{4.5}$$

$$m(y_{ij}; a) = \begin{cases} 1, & y_{ij} < a, \\ 0, & \text{otherwise}, \end{cases} \tag{4.6}$$

$$e(y_{ij}; a) = 1 - m(y_{ij}; a), \tag{4.7}$$

$$y_{ij} = |\mathbf{x}_i - \mathbf{r}_j|. \tag{4.8}$$

The key idea in arriving at (4.2) is the consideration of adding p "test" particles of radii $b_1, \ldots, b_p$ in the system of N spherical inclusions of radius R, with $p \ll N$. Since the ith test particle is capable of excluding the centers of the actual inclusions from spheres of radius a_i (where, for $b_i > 0$, $a_i = R + b_i$ and, for $b_i = 0$, $a_i = R - c_i$, $0 \le c_i \le R$), then it is natural to associate with each test particle a subdivision of space into two regions: D_i, the space available to the ith test particle (ie, the space outside N spheres of radius a_i centered at $\mathbf{r}^N$) and the complement space D_i^*. Let $\mathcal{S}_i$ denote the surface between D_i and D_i^*. Then, more specifically, $H_n(\mathbf{x}^m; \mathbf{x}^{p-m}; \mathbf{r}^q)$ gives the correlation associated with finding the center of a test particle of radius b_1 at $\mathbf{x}_1$ on $\mathcal{S}_1, \ldots$, and the center of a test particle of radius b_m at $\mathbf{x}_m$ on $\mathcal{S}_m$, and the center of a test particle of radius b_{m+1} at $\mathbf{x}_{m+1}, \ldots$, and the center of a test particle of radius b_p at $\mathbf{x}_p$ in D_p, and of finding any q inclusions with configuration, $\mathbf{r}^q$, where $\mathbf{x}^{p-m} \equiv \{\mathbf{x}_{m+1}, \ldots, \mathbf{x}_p\}$ and $n = p + q$. Note that it is only in the limit $b_i \to 0$ or $a_i \to R$ that D_i is the space exterior to the actual inclusions, ie, the matrix phase.

Note that the factor multiplying the integral of (4.4) is by definition equal to unity when $q = 0$. Given the $\rho_n(\mathbf{r}^n)$ for the ensemble one can, in principle, compute H_n for distributions of identical spheres of variable interpenetrability. According to relations (4.2)–(4.4), one needs to know the n-particle probability densities ρ_n in order to compute the general n-point distribution function H_n. The ρ_n have been extensively investigated in the context of the statistical mechanics of liquids and solids [123]. Here of course the microscopic scale refers to the arrangement and motion of molecules. Thus, the powerful machinery and results of statistical mechanics can be brought to bear on the problem of characterizing the microstructure of random heterogeneous media. One first specifies the Hamiltonian (energy) of the system of particles; for example, it may be assumed that the total potential energy is a sum of pairwise additive potentials incorporating attractive as well as repulsive interactions. The ρ_n, however, are not uniquely given from the Hamiltonian, since one must specify whether the system is in "equilibrium" (ie, characterized by macrosopic equilibrium properties, such as the pressure) or in the infinitely many possible nonequilibrium states.

From the general quantity H_n one can obtain all of the aforementioned correlation functions as follows:

$$S_n(\mathbf{x}^n) \equiv S_n^{(1)}(\mathbf{x}^n) = \lim_{a_i \to R, \forall i} H_n(\emptyset; \mathbf{x}^n; \emptyset), \tag{4.9}$$

$$G_n(\mathbf{x}_1; \mathbf{r}^q) = \lim_{a_1 \to R} H_n(\emptyset; \mathbf{x}_1; \mathbf{r}^q), \tag{4.10}$$

$$F_{sv}(\mathbf{x}_1, \mathbf{x}_2) = \lim_{a_i \to R, \forall i} H_2(\mathbf{x}_1; \mathbf{x}_2; \emptyset), \tag{4.11}$$

$$F_{ss}(\mathbf{x}_1, \mathbf{x}_2) = \lim_{a_i \to R, \forall i} H_2(\mathbf{x}_1, \mathbf{x}_2; \emptyset; \emptyset), \tag{4.12}$$

and

$$H_P(r) = \lim_{a_1 \to 0} \frac{\partial}{\partial a_1} \lim_{|\mathbf{x}_1 - \mathbf{r}_1| \to 0} H_2(\emptyset; \mathbf{x}_1; \mathbf{r}_1). \tag{4.13}$$

Here $\emptyset$ denotes the empty set. For particulate media the S_n are termed the n-point *matrix* probability functions. Note that the series for S_n obtained in this way is identical to the one derived by Torquato and Stell [117]. Representations of the remaining quantities (point/n-particle quantities, surface correlation functions, and the nearest-neighbor distribution functions) were obtained for the first time from (4.2).

Note that Torquato [122] has also given the asymptotic properties of the general H_n for cases in which a subset of the n points are far from one another and has given successive upper and lower bounds on the H_n. The reader is referred to this reference for further details on these topics.

The concept of a distribution of particles is very general if it is not restricted to impenetrable particles (see Fig 4). The intersection of particles need not have any physical meaning, but is simply a device for generating complex shapes from simple elements. An example of an interpenetrable-sphere model is the so-called penetrable-concentric-shell (PCS) model or "cherry-pit" model [42,58,124]. Here each D-dimensional sphere of diameter $2R$ is composed of an impenetrable core of diameter $2\lambda R$, encompassed by a perfectly penetrable shell of thickness $(1-\lambda)R$ (cf Fig 6). The extreme limits $\lambda = 0$ and 1 correspond, respectively, to cases of fully penetrable and totally impenetrable spheres (see Figs 4 and 5). In some instances these limits shall be simply referred to as overlapping and impenetrable (hard) spheres, respectively. This is a versatile model in that it enables one to vary the degree of "connectedness" of the particle phase by varying the impenetrability index λ.

If the overlapping spheres have a distribution of sizes, even more interesting microstructures are possible (see Fig 7). This microstructure most qualitatively resembles ones found in certain ceramic-metal (cermet) composites. An example of a silver-magnesium fluoride cermet is depicted in Fig 8 [125].

For fully penetrable spheres ($\lambda = 0$) at number density ρ (ie, number of particles per unit volume), there is a complete absence of spatial correlation between the particles and thus one has the exact simple relation valid for all n:

$$\rho_n(\mathbf{r}^n) = \rho^n, \qquad \forall n. \tag{4.14}$$

For $d = 2$ and $d = 3$, the particle phase percolates at $\phi_2^c \simeq 0.68$ [126,127] and $\phi_2^c \simeq 0.3$ [126,128], respectively. For $d = 3$, the medium is actually bicontinuous for the range $0.3 \le \phi_2 \le 0.97$, where $\phi_2 = 0.97$ or $\phi_1 = 0.03$ corresponds to the percolation threshold of the matrix [128,129], ie, for $\phi_1 < 0.03$ the matrix is disconnected. Thus, three-dimensional overlapping spheres may serve as a

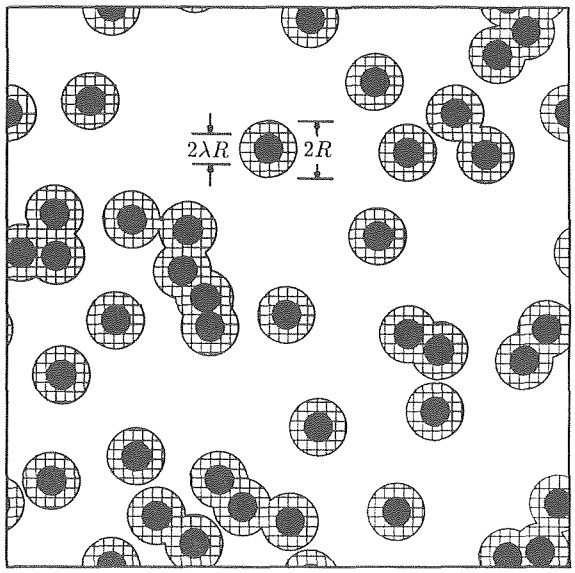

FIG 6. A distribution of identical disks of radius R in the penetrable-concentric-shell model [42,58]. Each disk is composed of an inner impenetrable core of diameter $2\lambda R$ (indicated by the black circular region, encompassed by a perfectly penetrable concentric shell of thickness $(1 - \lambda)R$, $0 \leq \lambda \leq 1$. This system is also referred to as the "cherry-pit" model.

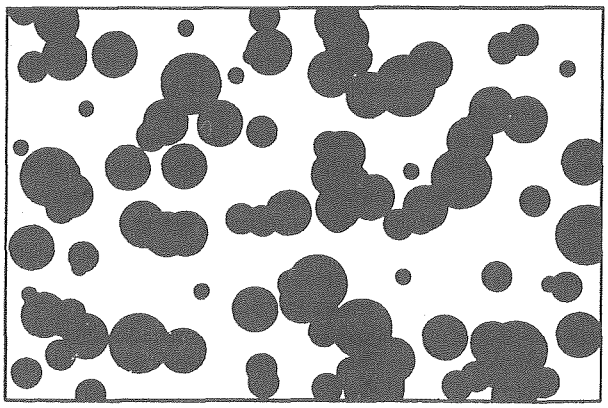

FIG 7. A distribution of overlapping disks with a polydispersivity in size.

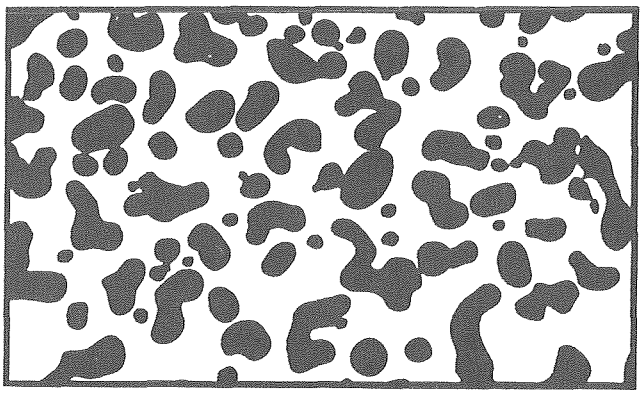

FIG 8. Reproduction of a micrograph of a silver-magnesium fluoride cermet [125]. The inclusions are metallic and form a variety of shapes from simple globules to long filaments.

useful model of bicontinuous media such as sandstones. Note that unlike general three-dimensional *random* media, two-dimensional random media can never be bicontinuous.

For totally impenetrable spheres ($\lambda = 1$) at number density ρ, the impenetrability condition alone does not uniquely determine the ensemble. To fix the ensemble, one must specify further information about the process of manufacture. For example, stating that the hard-sphere system is also in *thermal equilibrium* (which, roughly speaking, may be regarded as the most random distribution of spheres subject to the impenetrability constraint) completely specifies the distribution. Vastly more is known about the equilibrium ρ_n than about the infinitely many nonequilibrium ρ_n [123]. In light of this knowledge and because the former is a reasonable model of heterogeneous media, many of the results for the H_n (about to be described) were obtained for equilibrium ensembles.

The most important of the n-particle densities is the two-particle quantity $\rho_2(\mathbf{r}_1, \mathbf{r}_2)$; for isotropic, equilibrium distributions of spheres, which interact with an *arbitrary interparticle potential*, it exactly obeys the Ornstein–Zernike integral equation [123]:

$$h(r_{12}) = c(r_{12}) + \rho \int c(|\mathbf{r}_{23} - \mathbf{r}_{12}|)h(r_{23})\, d\mathbf{r}_3, \tag{4.15}$$

where the "total" correlation function

$$h(r) = \frac{\rho_2(r)}{\rho^2} - 1, \tag{4.16}$$

$$\mathbf{r}_{ij} \equiv \mathbf{r}_j - \mathbf{r}_i, \qquad r_{ij} \equiv |\mathbf{r}_{ij}|, \tag{4.17}$$

and $c(r)$ is the "direct" correlation function. Relation (4.15) may be regarded as the definition of $c(r_{12})$ which measures the direct effect of particle 1 on particle 2. The total correlation function $h(r_{12})$ (which goes to zero for large separation distances) measures the total effect (direct and indirect) of particle 1 on particle 2. Figure 9 shows $h(r)$ for hard spheres in equilibrium at the sphere volume fractions $\phi_2 = 0.3$ and 0.5. Although it is clear that $c(r) = 0$ for $r \to \infty$, the behavior for small r is not obvious. Thus, (4.15) in practice is solved by employing approximate expressions for $c(r)$. For hard spheres ($\lambda = 1$) a widely employed and accurate expression is the Percus–Yevick approximation, which has been solved analytically (see Ref 124 and references therein). Note that $\rho_2(r; \lambda)$ for the penetrable-concentric-shell model for an arbitrary impenetrability index λ is easily obtained from the totally impenetrable result $\rho_2(r; \lambda = 1)$ using a simple scaling of its arguments [42].

Integral equations for the three-particle and higher-order equilibrium probability densities ($n \geq 3$) have been obtained [123], but they become increasingly difficult to solve as n increases for general interparticle potentials. Often approximations for the ρ_n for $n \geq 3$ are given in terms of the two-particle densities. For example, the superposition approximation

$$\rho_3(r_{12}, r_{13}, r_{23}) \approx \frac{\rho_2(r_{12})\rho_2(r_{13})\rho_2(r_{23})}{\rho^3} \tag{4.18}$$

is commonly employed [123]. Relation (4.18) is known to be accurate for low densities and for equilateral triangular configurations, especially at high densities. For more sophisticated approximations to ρ_3 the reader is referred to Stell [130]. Note that exact low-density expansions are available for the ρ_n [123]; see, for example, relations (4.19) and (4.20) below.

For subsequent discussions, it is useful to review some properties of totally impenetrable sphere systems ($\lambda = 1$) under equilibrium. For $d = 3$ and $d = 2$, the distributions undergo a fluid-solid phase transition at $\phi_2 \simeq 0.5$ and $\phi_1 \simeq 0.7$, respectively [123,131], between a state which is characterized by no long-range order (fluid phase) and a distinctly different state, which is characterized by some degree of long-range order (solid phase). (Here ϕ_2 is the

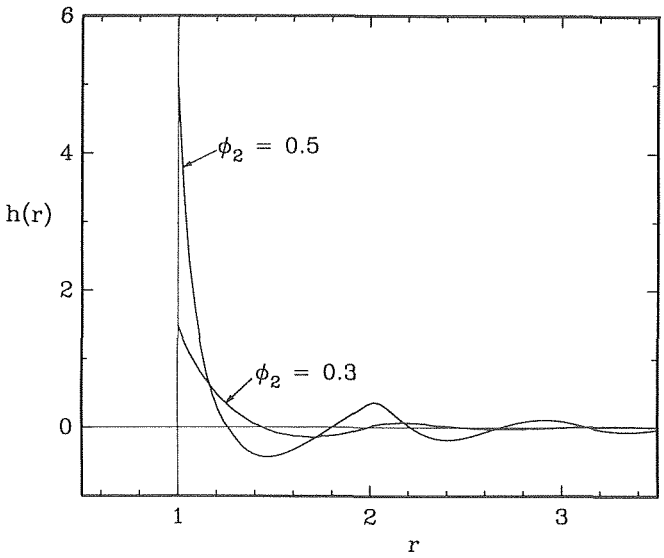

FIG 9. The total correlation function $h(r)$ for isotropic hard spheres of unit diameter in equilibrium at $\phi_2 = 0.3$ and 0.5 generated from Monte Carlo simulations. For $r < 1$, $h(r) = -1$ and in the limit $r \to \infty$, $h(r) \to 0$. Note that $g(r) \equiv h(r)+1$ is the well-known radial distribution function.

particle volume fraction.) For $d = 3$, for example, the solid branch ends at $\phi_2 = \pi\sqrt{2}/6 \simeq 0.74$, which corresponds to closest packing for a face-centered-cubic lattice. Above the fluid-solid transition, the disordered metastable branch ends in the random close-packing state, which for $d = 3$ and $d = 2$ are given by $\phi_2 \simeq 0.63$ and $\phi_2 \simeq 0.81$, respectively [132,133].

An important and useful *nonequilibrium* distribution of arbitrary-shaped particles is one known as *random sequential addition* [134–137]. For the moment consider mutually impenetrable particles. Random sequential addition is an irreversible process which consists of placing particles, one by one, into a d-dimensional volume V under the following conditions: (i) Once a particle has been placed, its position and orientation is permanently fixed, and (ii) no two particles overlap. The process continues until there is no remaining space for additional particles, satisfying the impenetrability condition. The final state is known as the "jamming" limit. For hard disks, the jamming limit corresponds to $\phi_2 \simeq 0.55$ [136]. This model for $d = 1$ (known also as the "parking" problem) has a fairly long history and exact results are available for all quantities of interest (see, eg, Widom [134,135]). Higher dimensions have no analytical solutions for the coverage at the jamming limit and thus random sequential addition for $d = 2$ and $d = 3$ has been studied mainly by computer simulations [136,137]. Interpenetrable-sphere models can be generated under a random sequential addition process [138]. For example, for the penetrable-concentric-shell model, overlaps of the inner impenetrable cores of radius λR are prohibited. For $\lambda = 0$ (fully penetrable spheres), the random sequential addition and equilibrium ensembles are obviously identical. For totally impenetrable spheres ($\lambda = 1$) of radius R these two ensembles are the same through third-order in ρ [134]: the two-particle and three-particle densities given by

$$\rho_2(r_{12}) = \rho^2\Theta(r_{12} - 2R)[1 + \rho v_2^*(r_{12}; 2R)] + \mathcal{O}(\rho^4), \qquad (4.19)$$

$$\rho_3(r_{12}, r_{13}, r_{23}) = \rho^3\Theta(r_{12} - 2R)\Theta(r_{13} - 2R)\Theta(r_{23} - 2R) + \mathcal{O}(\rho^4), \qquad (4.20)$$

where

$$\Theta(r) = \begin{cases} 1\ , & r > 0 \\ 0\ , & r < 0, \end{cases} \qquad (4.21)$$

$$v_2^*(r; a, a) = (2a - r)\Theta(2a - r) \qquad (d = 1) \qquad (4.22)$$

$$v_2^*(r; a, a) = 2a^2\left[\cos^{-1}\frac{r}{2a} - \frac{r}{2a}\left(1 - \frac{r^2}{4a^2}\right)^{1/2}\right]\Theta(2a - r) \qquad (d = 2) \qquad (4.23)$$

$$v_2^*(r; a, a) = \frac{4\pi a^3}{3}\left(1 - \frac{3}{4}\frac{r}{a} + \frac{1}{16}\frac{r^3}{a^3}\right)\Theta(2a - r) \qquad (d = 3) \qquad (4.24)$$

are identical for these ensembles. Here $v_2^*(r; a, a)$ represents the intersection volume of two identical d-dimensional spheres of radius a whose centers are separated by the distance r. At fourth order in ρ, the random sequential addition and equilibrium ensembles are known to be different [134].

In summary, relation (4.2) provides a means of representing and computing the general n-point distribution function H_n for d-dimensional interpenetrable spheres. Lower-order S_n have been computed for various distributions of identical d-dimensional spheres [119–121,138–145]. For the same class of models, lower-order G_n [58,146], surface correlation functions, F_{sv} and F_{ss} [147,148], and H_P [133,149,150] have been calculated. Recently, the formalism of Torquato leading to the expression (4.2) for the H_n has been extended to treat spheres with a *polydispersivity* in size [151]. Lower-order correlation functions have been evaluated for such polydispersed systems [152–155]. Generalizations to *anisotropic* distributions of particles have been given [106] and, as a result, lower-order functions have been calculated for random arrays of oriented cylinders [106] and ellipsoids [156]. More recently, series representations of the S_n for certain *cell* models have been given [157]. These and other developments will be described in the subsequent subsections.

4.2. Computer simulation techniques

In the last five years, considerable progress has been made on the determination of statistical correlation functions from computer simulations [138,142,145,148,150,157]. From a theoretician's point of view, simulations may be regarded as "experiments," against which theories for specific models of heterogeneous media may be tested. Computer simulations also offer a means of studying model systems which may be too difficult to treat theoretically. Obtaining statistical measures such as H_n from simulations is a two-step process. First, one must generate realizations of the disordered medium. Second, one samples each realization for the desired quantity and then averages over a sufficiently large number of realizations.

Haile, Massobrio, and Torquato [142] appear to have been the first to compute correlation functions from simulations. They employed the molecular dynamics method [123]. Since this initial work, the preponderance of simulation investigations made use of the Monte Carlo method introduced by Metropolis et al [158]. This procedure can be used to study the behavior of equilibrium systems of particles that interact with an arbitrary potential. For economy of space, the procedure is briefly outlined for a system of d-dimensional hard spheres at number density ρ in the canonical ensemble (generally, fixed number of particles N, fixed volume V, and fixed temperature T). (Equilibrium hard-sphere configurations are independent of temperature.) Particles are initially placed, with no hard core overlaps in a cubical cell of volume $V = L^d$ on the sites of a regular lattice (eg, body-centered cubic for $d = 3$). The cell is surrounded by periodic images of itself. Each particle is then moved randomly (by some small amount) to a new position which is accepted or rejected according to whether or not hard cores overlap. *Periodic boundary conditions* are employed, that is, anytime a particle exists, the face of the central cell, its periodic image from a replicated cell, enters the opposing face of the central cell. Periodic boundary conditions are imposed to simulate an infinite, random system (ie, a statistically homogeneous medium) while employing a small number of particles ($50 \leq N \leq 1000$) in the central cell.

Equilibrium is achieved after moving each of the particles a sufficient number of times. The equilibrium distribution is a unique state. Each equilibrium configuration or realization is then sampled for the desired statistical measure. For example, a crude method to determine the one-point probability function $S_1 = \phi_1$ (the matrix or void volume fraction) is to randomly throw many points into the sample and record the ratio of the total number of successes (points in the matrix) to the total number of attempts [145]. Generally, periodic boundary conditions must be used when sampling for quantities such as H_n.

The following is a summary of the problems that have been studied using computer simulations. The one-point probability function ϕ_1 (porosity) has been determined for the d-dimensional penetrable-concentric-shell or cherry-pit model for $d = 2$ and $d = 3$ and selected values of the impenetrability index λ [145]. The two-point probability function $S_2(r)$ has been computed for totally impenetrable spheres ($d = 3$ and $\lambda = 1$) [148] and for the cherry-pit model ($d = 2$) for various λ [138]. The surface correlation functions, $F_{sv}(r)$ and $F_{ss}(r)$, have been computed for totally impenetrable spheres ($d = 3$ and $\lambda = 1$) [148]. Certain functionals of the three-point quantities S_3 and G_3 have been calculated for distributions of disks in the cherry-pit model [159] and for totally impenetrable spheres [160], respectively. A statistical measure analogous to the two-point correlation functions described above which reflects topological information about clustering and percolation in particle systems (described in section 4.1.7) has recently been obtained using simulations [161]. Some of the aforementioned findings will be compared to theoretical results in the ensuing subsections.

4.3. Identical d-dimensional spheres:

Theoretical and computer-simulation determinations of the n-point distribution function H_n for isotropic distributions of identical d-dimensional spheres are described. Virtually all of the results reported will be either for fully penetrable particles, totally impenetrable particles, or spheres in the penetrable-concentric-shell model.

For this discussion and subsequent discussions, it is convenient to introduce, for systems of identical particles of *arbitrary* shape at number density ρ, the dimensionless density

$$\eta = \rho v_1, \tag{4.25}$$

where v_1 is the volume of a particle and for d-dimensional spheres of radius R is given by

$$v_1(R) = 2R \qquad (d = 1), \tag{4.26}$$

$$v_1(R) = \pi R^2 \qquad (d = 2), \tag{4.27}$$

$$v_1(r) = \frac{4\pi}{3} R^3 \qquad (d = 3). \tag{4.28}$$

For totally impenetrable particles, the reduced density η is exactly the particle volume fraction ϕ_2, that is,

$$\eta = \phi_2 = 1 - \phi_1. \tag{4.29}$$

This equality is not obeyed if the particles can overlap and, in particular, for the penetrable-concentric-shell or cherry-pit model with impenetrability index λ, one generally has the inequality

$$\eta(\lambda) \geq \phi_2(\lambda), \tag{4.30}$$

with equality applying when $\lambda = 1$ (totally impenetrable particles). For the special limit of fully penetrable particles ($\lambda = 0$), it is well known that the matrix volume fraction is

$$\phi_1 = 1 - \phi_2 = \exp[-\eta]. \tag{4.31}$$

Relation (4.31), proved below for spheres, actually applies to objects of general shape.

4.3.1. *Fully penetrable spheres*

The H_n are particularly easy to determine for fully penetrable spheres by virtue of the simplicity of relation (4.14) for the ρ_n. Substitution of (4.14) into (4.2) yields the exact relation [122]

$$\begin{aligned} H_n(\mathbf{x}^m; \mathbf{x}^{p-m}; \mathbf{r}^q) &= (-1)^m \rho^q \exp[-\rho v_p(\mathbf{x}^p)] \frac{\partial}{\partial a_1} \cdots \frac{\partial}{\partial a_m} \prod_{\ell=1}^{q} \prod_{k=1}^{p} e(y_{k\ell}; a_k) \\ &+ (-1)^m \rho^q \left[\prod_{\ell=1}^{q} \prod_{k=1}^{p} e(y_{k\ell}; a_k) \right] \frac{\partial}{\partial a_1} \cdots \frac{\partial}{\partial a_m} \exp[-\rho v_p(\mathbf{x}^p)] \end{aligned} \tag{4.32}$$

Here $v_p(\mathbf{x}^p; a_1, \ldots, a_p)$ is the union volume of p d-dimensional spheres of radii $a_1, \ldots, a_p$, centered at $\mathbf{x}_1, \ldots, \mathbf{x}_p$, respectively. (The reader is referred to Ref 58 for an explicit expression of $v_2(\mathbf{x}_1, \mathbf{x}_2; a_1, a_2)$ for the case $d = 3$.) To summarize, H_n for fully penetrable spheres is expressible in terms of the purely geometrical quantity v_p.

Letting $m = q = 0$ in relation (4.32) yields

$$H_n(\mathbf{x}^n) = \exp[-\rho v_n(\mathbf{x}^n; a_1, \ldots, a_n)], \tag{4.33}$$

which is the probability of inserting n spheres of radii $a_1, \ldots, a_n$ into a system of N spheres of radius R at positions $\mathbf{x}_1, \ldots, \mathbf{x}_n$, respectively (ie, into the available space or the region exterior to the excluded space). Taking the limit $a_i \to R$, $\forall i$ in (4.33) enables one to recover the n-point matrix probability function derived by Torquato and Stell [119], that is,

$$S_n(\mathbf{x}^n) = \exp[-\rho v_n(\mathbf{x}^n; a_1 = R, \ldots, a_n = R)]. \tag{4.34}$$

The union volume of two identical spheres of radius a is given by

$$v_2(r; a, a) = 2v_1 - v_2^*(r; a, a), \tag{4.35}$$

where the intersection volume v_2^* for one-, two-, and three-dimensional spheres is given by (4.22)–(4.24), respectively. The union volume of three identical spheres of radius a, $v_3(x, y, z; a, a, a)$, has been given, among others, by Rowlinson [162] for $d = 2$ and by Powell [163] for $d = 3$. Note that letting $n = 1$ in (4.34) gives that $S_1 = \phi_1 = \exp[-\eta]$, which proves relation (4.31). Figure 10 shows $S_2(r)$ for $d = 3$ for particles of unit diameter at $\phi_2 = 0.6$.

Letting $m = 0$ and $p = 1$ in (4.32) and taking the limit $a_1 \to R$ yields the point/q-particle function as first given by Torquato [58]:

$$G_n(\mathbf{x}_1; \mathbf{r}^q) = \rho^q \phi_1 \prod_{\ell=1}^{q} e(y_{1\ell}; R), \tag{4.36}$$

where (4.31) has been used and $y_{1\ell}$ is defined by (4.8).

The surface correlation functions s, F_{sv}, and F_{ss} and their generalizations for fully penetrable spheres can be obtained from (4.34). For example, the prescription (4.12) gives the specific surface as

$$s = \rho \phi_1 \frac{\partial}{\partial R} v_1(R), \tag{4.37}$$

where ϕ_1 is given by (4.31) and the surface area of a d-dimensional sphere is $\partial v_1(R)/\partial R$, where $v_1(R)$ is given by relations (4.26)–(4.28). Note that, for *impenetrable* spheres, one has the relation

$$s = \rho \frac{\partial}{\partial R} v_1(R). \tag{4.38}$$

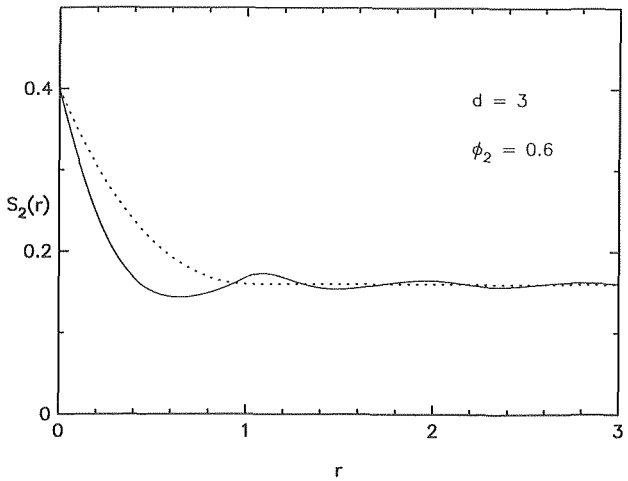

FIG 10. The two-point matrix probability function $S_2(r)$ versus the r, the distance between the two points, for isotropic distributions of spheres of unit *diameter* at a sphere volume $\phi_2 = 0.6$ as compared by Torquato and Stell [121]. The solid and dashed curves represent hard and overlapping spheres, respectively.

For the penetrable-concentric-shell model, the inequality

$$s(\lambda) \leq s(1) \tag{4.39}$$

holds for fixed reduced density η. Letting $m = 1$, $p = 2$ and $q = 0$ in (4.34) leads to

$$F_{sv}(\mathbf{x}_1, \mathbf{x}_2) = -\lim_{a_1 \to R} \frac{\partial}{\partial a_1} \exp[-v_2(\mathbf{x}_1, \mathbf{x}_2; a_1, R)]. \tag{4.40}$$

Letting $m = 2$, $p = 2$ and $q = 0$ in (4.34) yields

$$F_{ss}(\mathbf{x}_1, \mathbf{x}_2) = -\lim_{a_i \to R, \forall i} \frac{\partial}{\partial a_1} \frac{\partial}{\partial a_2} \exp[-v_2(\mathbf{x}_1, \mathbf{x}_2; a_1, a_2)]. \tag{4.41}$$

Relations (4.40) and (4.41) were first given by Doi [85]. Three-point and higher-order surface correlation functions are easily obtained from (4.34); for example, letting $m = 2$, $p = 3$ and $q = 0$ gives

$$F_{ssv}(\mathbf{x}_1, \mathbf{x}_2, \mathbf{x}_3) = \lim_{a_i \to R, \forall i} \frac{\partial}{\partial a_1} \frac{\partial}{\partial a_2} \exp[-v_3(\mathbf{x}_1, \mathbf{x}_2, \mathbf{x}_3; a_1, a_2, R)]. \tag{4.42}$$

For general statistically homogeneous distributions of spheres, Torquato, Lu, and Rubinstein [133], among other things, found an exact series representation of the nearest-neighbor distribution function $H_P(r)$:

$$H_P(r) = \sum_{k=1}^{\infty} \frac{(-1)^{k+1}}{k!} \frac{\partial}{\partial r} \int \frac{\rho_{k+1}(\mathbf{r}^{k+1})}{\rho} \prod_{i=2}^{k+1} m(|\mathbf{r}_1 - \mathbf{r}_i|; r)\, d\mathbf{r}_i \tag{4.43}$$

They also found exact relations for the associated cumulative and conditional-pair distributions. These were termed "particle" quantities and this explains the subscript P. Torquato et al [133] also investigated related "void" nearest-neighbor functions. Substitution of (4.14) into (4.43) yields the exact relation

$$H_P(r) = \rho \frac{\partial v_1(r)}{\partial r} \exp[-\rho v_1(r))], \tag{4.44}$$

where $v_1(r)$ is given by (4.26)–(4.27). Hertz [164] apparently was the first to consider the evaluation of H_P for a three-dimensional system of "point" particles, that is, particles whose centers are Poisson distributed. For spheres with hard cores, an exact evaluation of (4.43) is not possible (see the ensuing discussion regarding totally impenetrable spheres).

4.3.2. *Totally impenetrable spheres*

For distributions of totally impenetrable particles (not necessarily spherical in shape), many of the series representations of the aforementioned n-point correlation functions truncate exactly after n-body terms (ie, terms which involve correlations between n bodies) [122]. For example, at the *two-point* level for isotropic arrays of totally impenetrable spheres one has exactly from (4.2) that

$$S_2(r) = 1 - 2\phi_2 + \rho m \otimes m + \rho_2 \otimes m \otimes m, \tag{4.45}$$

$$G_2(r) = e(r; R)[\rho - \rho_2 \otimes m], \tag{4.46}$$

$$F_{sv}(r) = s - \rho\delta \otimes m - \rho_2 \otimes \delta \otimes m, \tag{4.47}$$

$$F_{ss}(r) = \rho\delta \otimes \delta + \rho_2 \otimes \delta \otimes \delta, \tag{4.48}$$

where ρ is the number density, ϕ_2 is the sphere volume fraction, s is the specific surface given by (4.38), $\rho_2(r)$ is the two-particle probability density, $m(r; R)$ is the step function given by (4.6) with $a = R$, $\delta(r - R)$ is the Dirac delta function, and the symbol $\otimes$ denotes a convolution integral, that is, for any pair of functions $f_1(r)$ and $f_2(r)$

$$f_1 \otimes f_2 \equiv \int f_1(r) f_2(|\mathbf{r} - \mathbf{r}'|) d\mathbf{r}'. \tag{4.49}$$

It is useful to employ the general relationship between the two-point probability functions for phase 2 (particle phase) $S_2^{(2)}$ and for phase 1 (matrix phase) $S_2^{(1)} \equiv S_2$ [117] for any two-phase isotropic medium,

$$S_2^{(2)} = 1 - 2\phi_1 + S_2^{(1)}, \tag{4.50}$$

in conjunction with (4.29) and (4.45) to yield

$$S_2^{(2)}(r) = \rho v_2^*(r; R; R) + \rho_2 \otimes m \otimes m. \tag{4.51}$$

Here

$$v_2^*(r; R; R) = m \otimes m \tag{4.52}$$

is the intersection volume of two identical spheres of radius R as general given by (4.22)–(4.24). The terms of (4.51) have simple probabilistic interpretations: (i) ρv_2^* is the probability that both points fall in a single sphere, and (ii) $\rho_2 \otimes m \otimes m$ is the probability that each point falls in two different spheres. The terms involved in the other two-point correlation functions have similar interpretations. For particles which can interpenetrate one another, however, such simple interpretations are generally invalid because of the allowability of overlap. Examination of (4.45)–(4.48) reveals that the different two-point correlation functions are related to one another [122].

For $d = 1$ the convolution integrals of (4.45)–(4.48) can be solved analytically [140,147]. The one-body convolutions are easily evaluated analytically for any d. The two-body convolution integrals for $d = 2$ and $d = 3$ have been evaluated numerically for equilibrium distributions at arbitrary density ρ or particle volume fraction ϕ_2 using Fourier transform techniques and Percus–Yevick and related approximations to ρ_2 [121]. Thus, theoretical determinations of S_2, G_2, F_{sv}, and F_s have been obtained for such models [121,140,146,147]. Moreover, $S_2(r)$ has been calculated from computer simulations for equilibrium [142] and nonequilibrium [138] distributions of totally impenetrable spheres.

Figure 10 compares $S_2(r)$ for totally impenetrable (hard) and fully penetrable (overlapping) spheres (d = 3) of unit *diameter* at

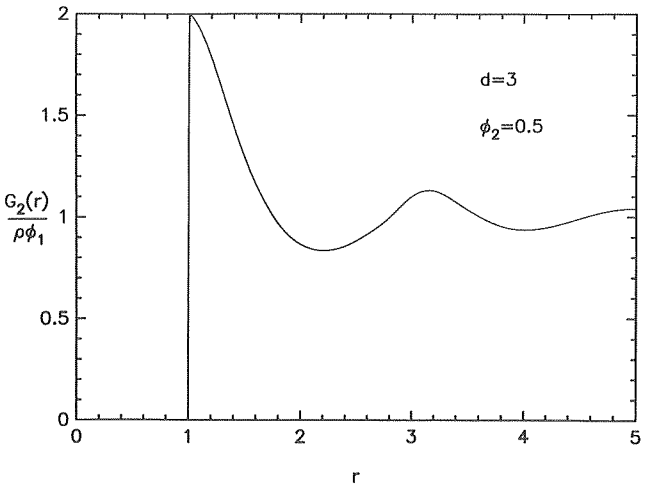

FIG 11. The point/particle distribution function $G_2(r)$, scaled by its long-range value of $\rho\phi_1$, for system of hard spheres of unit *radius* at $\phi_2 = 0.5$ as computed by Torquato [147].

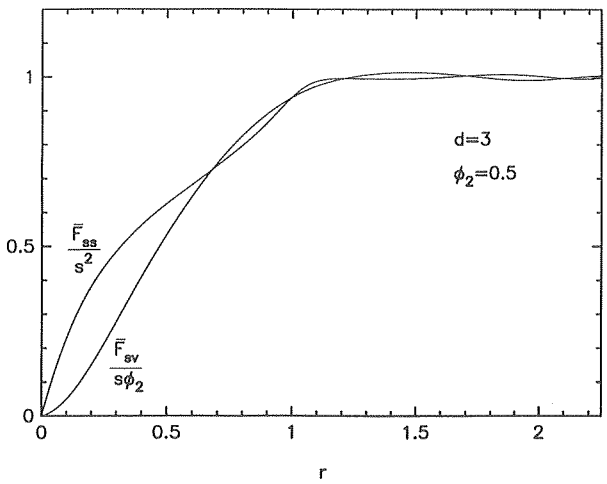

FIG 12. The scaled two-body contributions to the surface correlation functions $F_{sv}(r)$ and $F_{ss}(r)$ for hard spheres of unit *diameter* at $\phi_2 = 0.5$ as calculated by Torquato [122,147]. Here $\overline{F}_{sv} = \rho_2 \otimes \delta \otimes m$ and $\overline{F}_{ss} = \rho_2 \otimes \delta \otimes \delta$.

a sphere volume fraction $\phi_2 = 0.6$ [121]. The function $S_2(r)$ for fully penetrable spheres decays exponentially until it achieves its long-range value of ϕ_1^2 at $r = 2R = 1$; but the corresponding function for impenetrable particles oscillates about its long-range value for small r, indicating short-range order due to exclusion-volume effects that are completely absent in the overlapping case. Increasing the dimensionality from unity, for small r, decreases S_2 [140]. For large r, increasing d decreases the amplitude of the oscillations [140]. Figure 11 shows the point/particle quantity $G_2(r)$ for impenetrable spheres (d = 3) of unit *radius* at $\phi_2 = 0.5$ [146]. Figure 12 depicts the *scaled* two-body contributions to F_{sv} and F_{ss} for the same model [122,147]. These theoretical calculations of the surface functions obtained by Torquato were found to be in excellent agreement with the simulations of Seaton and Glandt [148].

Corresponding three-point and high-order correlation functions for such models have been also studied theoretically [118,122]. The reader is referred to these references for further details.

Unlike the aforementioned functions, the nearest-neighbor distribution function $H_p(r)$ is not a truncated series for totally impenetrable spheres. The general expression is an infinite series given by (4.43). For the case of hard rods ($d = 1$), the ρ_n, for all n, are known exactly for equilibrium distributions. Torquato, Lu, and Rubinstein [133] then found the exact relation for rods of unit length

$$H_p(r) = \frac{2\eta}{1-\eta} \exp\left[\frac{-2\eta(r-1)}{1-\eta}\right] \qquad r \geq 1, \tag{4.53}$$

where η is the reduced density given by (4.25). For $r < 1$, $H_p(r) = 0$ in any dimension. For d-dimensional hard sphere with $d \geq 2$, an exact evaluation of series (4.43) is impossible because the ρ_n for $n \geq 3$ are not known exactly. Thus, for $d = 2$ and 3, Torquato et al [133] devised several schemes to approximately sum the series. The most accurate scheme yielded

$$H_p(r) = \frac{4\eta(2r-\eta)}{(1-\eta)^2} \exp\left[\frac{-4\eta}{(1-\eta)^2}[r^2-1)+\eta(r-1)]\right], \qquad r > 1, \tag{4.54}$$

for hard disks ($d = 2$) and

$$H_p(r) = 24\eta(f_1 + f_2 r + f_3 r^3)\exp\{-\eta[24f_1(r-1) + 12f_2(r^2-1) + 8f_3(r^3-1)]\} \tag{4.55}$$

for hard spheres ($d = 3$), where

$$f_1 = \frac{\eta^2}{2(1-\eta)^3}, \tag{4.56}$$

$$f_2 = \frac{-\eta(3+\eta)}{2(1-\eta)^3}, \tag{4.57}$$

and

$$f_3 = \frac{1+\eta}{(1-\eta)^3}. \tag{4.58}$$

This represents the first time that analytical expressions for the nearest-neighbor distribution function $H_p(r)$ have been given for finite-sized hard particles.

Figure 13 compares the nearest-neighbor distribution function $H_p(r)$ for fully penetrable disks (ie, Poisson distributed "point" particles) and hard disks of unit diameter as calculated from (4.44) and (4.54) at $\phi_2 = 0.3$. Exclusion-volume effects associated with the hard cores of the latter model considerably changes the behavior of $H_p(r)$ relative to the idealized case of point particles. Figure 14 compares $H_p(r)$ for hard spheres ($d = 3$) of unit diameter at $\phi_2 = 0.3$ and 0.5 to the corresponding Monte Carlo simulation data of Torquato and Lee [150]. Observe the excellent agreement of the theory with the simulation data.

It should be mentioned that from $H_p(r)$ one can compute other quantities of fundamental interest such as: (i) the exclusion probability, $E_p(r)$, the probability of finding no particle centers within a sphere of radius r surrounding a particle at the origin; and (ii) the mean nearest-neighbor distance, ℓ; and (iii) the random close-packing density. The first of these quantities is given by

$$E_p(r) = 1 - \int_0^r H_p(r)\,dr, \tag{4.59}$$

whereas the second quantity is given by

$$\ell = \int_0^\infty r H_p(r)\,dr = \int_0^\infty E_p(r)\,dr. \tag{4.60}$$

The random close-packing density, for hard-sphere systems, can be computed from the mean nearest-neighbor distance by determining the density at which ℓ becomes σ. Torquato et al have studied these as well as other related quantities. Finally, we note that Lu and Torquato [151] have generalized these results to spheres with a polydispersivity in size.

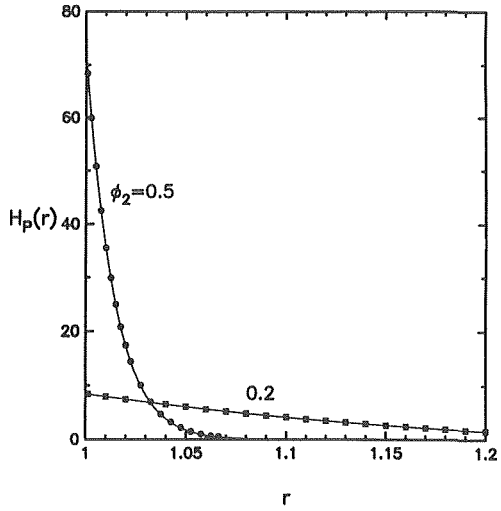

FIG 13. Comparison of the nearest-neighbor distribution function for penetrable disks (*i.e., Poisson distributed "point" particles*) and impenetrable disks of unit diameter as calculated from (4.44) and (4.54), respectively, at $\phi_2 = 0.3$ [133,149].

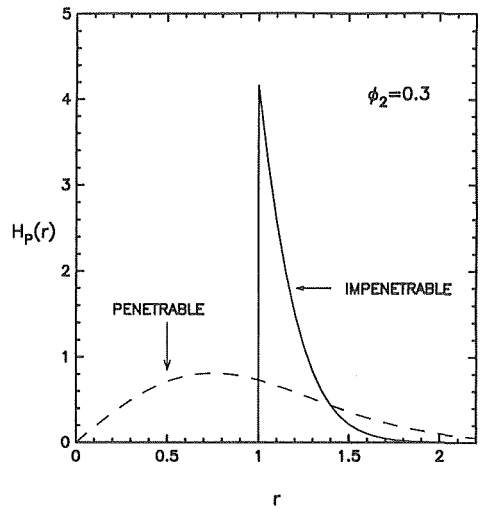

FIG 14. The nearest-neighbor distribution function $H_p(r)$ for hard spheres ($d = 3$) of unit diameter at $\phi_2 = 0.2$ and 0.5 as calculated by Torquato et al [133,149] from (4.55). The black circles and squares are simulation data due to Torquato and Lee [150].

4.3.3. *Interpenetrable-sphere models*

Torquato and Stell [120] and Chiew and Glandt [139] obtained analytical approximations for the porosity ϕ_1 and specific surface in the "permeable-sphere" model. Subsequently, Rikvold and Stell [141] obtained *scaled-particle* approximations of the same quantities in the "cherry-pit" model [42]. For example, their results for $\phi_1(\eta, \lambda)$ in d dimensions are given by

$$\phi_1(\eta, \lambda) = (1 - \lambda^d \eta) \exp\left[-\frac{(1 - \lambda^d)\eta}{1 - \lambda^d \eta}\right] F_d(\eta, \lambda), \tag{4.61}$$

where

$$F_1(\eta, \lambda) = 1, \tag{4.62}$$

$$F_2(\eta, \lambda) = \exp\left[-\frac{\lambda^2 \eta^2 (1 - \lambda)^2}{(1 - \lambda^2 \eta)^2}\right], \tag{4.63}$$

$$F_3(\eta, \lambda) = \exp\left\{\frac{-3\lambda^3 \eta^2}{2(1 - \lambda^3 \eta)^3}[2 - 3\lambda + \lambda^3 - (3\lambda - 6\lambda^2 + 3\lambda^3)\lambda^3 \eta]\right\}. \tag{4.64}$$

In the extreme limits, $\lambda = 1$ and $\lambda = 0$, relation (4.61) yields the exact results (4.29) and (4.31). Lee and Torquato [145] obtained ϕ_1 as a function of the reduced density η and impenetrability index λ in the cherry-pit model for $d = 2$ and $d = 3$. The aforementioned theoretical results were shown to be in excellent agreement with simulations.

The two-point probability function $S_2(r)$ has been determined from computer simulations by Smith and Torquato for distributions of disks in the cherry-pit model [138]. It was found that, for the range $0 < \lambda < 0.5$, S_2 was negligibly different than S_2 for fully penetrable disks ($\lambda = 0$) at the same ϕ_2. For $0.5 \leq \lambda < 1$, the amplitude of the oscillations in S_2, for fixed ϕ_2, increases as λ increases. The specific surface for this two-dimensional model was also evaluated in this study.

4.4. Polydispersed d-dimensional spheres

Determination of the correlation functions for isotropic distributions of d-dimensional spheres with a *polydispersivity* in size are described. Specifically, the spheres possess a continuous distribution in radius R characterized by a (normalized) probability density $f(R)$. The average of any function $A(R)$ is defined by

$$\overline{A(R)} = \int_0^\infty A(R) f(R)\, dR. \tag{4.65}$$

Some results for overlapping as well as hard particles are now given.

4.4.1. *Fully penetrable spheres*

Chiew and Glandt [139] have obtained expressions for the porosity ϕ_1 and specific surface s for polydispersed overlapping spheres ($d = 3$) at *total* number density ρ (cf Fig 7). The d-dimensional generalizations of their results are as follows:

$$\phi_1 = \exp[-\rho \overline{v_1(R)}], \tag{4.66}$$

$$s = \rho \overline{\frac{\partial v_1(R)}{\partial R}} \exp[-\rho \overline{v_1(R)}], \tag{4.67}$$

where $v_1(R)$ is given by (4.26)–(4.27). Note that we can obtain corresponding results for overlapping spheres with M different sizes from the results above by letting

$$f(R) = \sum_{i=1}^{M} \frac{\rho_i}{\rho} \delta(R - R_i), \tag{4.68}$$

where ρ_i and R_i are number density and radius of type-i particles, respectively. For example, use relations (4.65)–(4.69) with $M = 1$ gives the *monodisperse* results (4.31) and (4.37).

Stell and Rikvold [152] and Joslin and Stell [153] found S_n for such a model:

$$S_n(\mathbf{x}^n) = \exp[-\rho\, \overline{v_n(\mathbf{x}^n; R, \ldots, R)}], \tag{4.69}$$

where v_n is the union volume of n spheres of radius R defined earlier.

Miller and Torquato [154] obtained the surface correlation functions, F_{sv} and F_{ss}, for binary mixtures of overlapping spheres by extending the general formalism of Torquato [122] given for

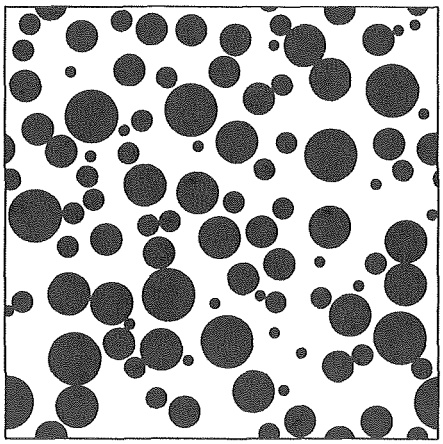

FIG 15. A distribution of hard disks (cylinders) with a polydispersivity in size.

monodispersed spheres. These results were subsequently generalized to the continuous case by Torquato and Lu [155] and for d = 3 are explicitly given by

$$F_{sv}(r) = 4\pi\rho\overline{\left[R^2 - \left(\frac{R^2}{2} - \frac{rR}{4}\right)\Theta(2R - r)\right]}S_2(r) \tag{4.70}$$

and

$$F_{ss}(r) = \left\{16\pi^2\rho^2\overline{\left[R^2 - \left(\frac{R^2}{2} - \frac{rR}{4}\right)\Theta(2R - r)\right]}^2 + \frac{2\pi\rho}{r}\overline{R^2\Theta(2R - r)}\right\}S_2(r), \tag{4.71}$$

From the above discussion it is seen that the polydispersed results are simple generalizations of the monodispersed results. For completeness, therefore, it is useful to state the polydispersed generalization of the monodispersed result for the point/particle function $G_2(r)$ [relation (4.36) with $q = 1$]:

$$G_2(r) = \rho\phi_1\overline{\Theta(R - r)}. \tag{4.72}$$

4.4.2. Totally impenetrable spheres

For hard-sphere systems with a polydispersivity in size (see Fig 15) the porosity and specific surface are respectively given by

$$\phi_1 = 1 - \rho\overline{v_1(R)} \tag{4.73}$$

and

$$s = \rho\overline{\frac{\partial v_1(R)}{\partial R}}. \tag{4.74}$$

In the process of computing conductivity and elasticity bounds for polydispersed systems of hard spheres, Thovert, Kim, Torquato, and Acrivos [165] determined the associated two- and three-point probabilities S_2 and S_3. They did not, however, state these results for S_2 and S_3 explicitly. It is useful to give the explicit result for the two-point function here:

$$S_2(r) = 1 - \rho\overline{v_2(r; R, R)} + \int dR_1 f(R_1)\int dR_2 f(R_2)\int d\mathbf{r}_1\int d\mathbf{r}_2\rho_2(r_{12}; R_1, R_2) \times m(|\mathbf{x}_1 - \mathbf{r}_1|; R_1)\, m(|\mathbf{x}_2 - \mathbf{r}_2|; R_2), \tag{4.75}$$

where $r \equiv |\mathbf{x}_1 - \mathbf{x}_2|$, $m(r; a)$ is the step function defined by (4.6), and $f(R_1)f(R_2)\rho_2(r_{12}; R_1, R_2)$ is the probability density associated with finding a particle with radius R_1 at $\mathbf{r}_1$ and another particle with radius R_2 at $\mathbf{r}_2$, $r_{12} = |\mathbf{r}_2 - \mathbf{r}_1|$. Blum and Stell [166,167] were the first to obtain ρ_2 analytically in terms of $f(R)$ in the Percus–Yevick approximation (see also Salacuse and Stell [168]).

4.4.3. Remarks

Very recently, the formalism of Torquato [122] initially employed to obtain series representations of the general n-point distribution function H_n for monodispersed spheres of variable penetrability has been generalized to the polydispersed case by Lu and Torquato [151]. One arrives at this generalization by still considering the addition of p "test" particles into a system of N particles but one in which N_1 of the particles have radius R_1, N_2 for the particles have radius $R_2, \ldots$, and N_M of the particles have radius R_M so that $\sum_{k=1}^{M} N_k = N$. The ρ_n for this system of N particles with a discrete size distribution generalize accordingly. One easily passes to the *continuous-size limit* by replacing sums over components with integrals. Thus, this procedure is relatively straightforward given the monodisperse result (4.2) and, not surprisingly, the resulting polydispersed expression for H_n is functionally very similar to (4.2). For this reason it is not given here explicitly. The polydispersed expression therefore contains all of the results of section 4.3.

New results immediately follow from this relation. For example, in the special case of polydispersed hard spheres (4.12) yields the appropriate surface-surface function:

$$F_{ss}(\mathbf{x}_1, \mathbf{x}_2) = \int dR_1\rho_1(r_1; R_1)f(R_1) \times \int d\mathbf{r}_1\delta(|\mathbf{x}_1 - \mathbf{r}_1| - R_1)\delta(|\mathbf{x}_2 - \mathbf{r}_1| - R_1) + \int dR_1 f(R_1)\int dR_2 f(R_2) \times \int d\mathbf{r}_1\int d\mathbf{r}_2\rho_2(\mathbf{r}_1, \mathbf{r}_2; R_1, R_2) \times \delta(|\mathbf{x}_1 - \mathbf{r}_1| - R_1)\delta(|\mathbf{x}_2 - \mathbf{r}_2| - R_2). \tag{4.76}$$

Comparison of this relation to the monodisperse counterpart, (4.48), reveals that there is a simple prescription to map the monodisperse result to the polydisperse result. Therefore, the polydispersed equivalent of the surface-void function (4.47) is not written here.

It is instructive to comment on useful choices for the size distribution $f(R)$. Commonly employed probability densities are the Schulz [169] and log-normal [170] distributions. The Schulz distribution is defined as

$$f(R) = \frac{1}{\Gamma(z+1)}\left(\frac{z+1}{\overline{R}}\right)^{z+1}R^z\exp\left[\frac{-(z+1)R}{\overline{R}}\right], \qquad z > -1, \tag{4.77}$$

where $\Gamma(x)$ is the gamma function. The nth moment is given by

$$\overline{R^n} = \overline{R}^n\frac{(z+1)^{-n}}{z}\prod_{i=0}^{n}(z+i). \tag{4.78}$$

Therefore, by increasing n, the variance decreases, that is, the distribution becomes sharper. In the monodisperse limit, $z \to \infty$, $f(R) \to \delta(R - \overline{R})$.

The log-normal distribution is defined as

$$f(R) = \frac{1}{R\sqrt{2\pi\beta^2}}\exp\left\{-\frac{[\ell n(R/R_o)]^2}{2\beta^2}\right\} \tag{4.79}$$

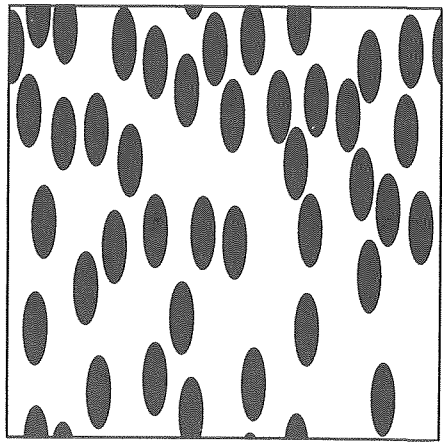

FIG 16. A distribution of hard, oriented ellipses (elliptical cylinders).

and therefore the nth moments are

$$< R^n >= R_0^n \exp(n^2\beta^2/2) . \tag{4.80}$$

As $\beta^2 \to 0$, $f(R) \to \delta(R - R_0)$.

4.5. Anisotropic particulate media

Here correlation function results are given for statistically anisotropic media composed of a distribution of identical, oriented particles of *arbitrary shape*. Torquato and Sen [107] obtained series representatives of the S_n for this microgeometry by a simple reinterpretation of the relations developed by Torquato and Stell [117] for spheres, namely, the latter results are not only applicable to spheres but [after an appropriate generalization of the *inclusion indicator function* $m(r)$, Eq (4.6)] to inclusions in which each configurational coordinate is fully specified by its center-of-mass position. This class of materials includes oriented rectangles, ellipses, and so on for $d = 2$ and oriented rectangular parallelipipeds, ellipsoids, cylinders, and so on, for $d = 3$ (see Fig 16). For this class of microstructures the inclusion indicator function generalizes as

$$m(\mathbf{x}) = \begin{cases} 1 , & \mathbf{x} \in D_I, \\ 0 , & \text{otherwise}, \end{cases} \tag{4.81}$$

where D_I is the inclusion region and $\mathbf{x}$ a position vector measured with respect to the inclusion centroid.

For d-dimensional spheres, it is of course given by (4.6). For nonspherical shapes, $m(\mathbf{x})$ is more complicated. For example, letting $x_i (i = 1, \ldots, d)$ denote the components of $\mathbf{x}$ in the principal axes coordinate frame, one has for a rectangle with sides of lengths $2a$ and $2b$

$$m(\mathbf{x}) = \begin{cases} 1 , & |x_1| \le a \text{ and } |x_2| \le b, \\ 0, & \text{otherwise}. \end{cases} \tag{4.82}$$

For an ellipse with axes of lengths $2a$ and $2b$, respectively,

$$m(\mathbf{x}) = \begin{cases} 1 , & x_1^2/a^2 + x_2^2/b^2 \le 1, \\ 0, & \text{otherwise}. \end{cases} \tag{4.83}$$

The inclusion indicator function for a rectangular parallelepiped having sides of length $2a$, $2b$, and $2c$ is given by

$$m(\mathbf{x}) = \begin{cases} 1, & |x_1| \le a \text{ and } |x_2| \le b \text{ and } |x_3| \le c, \\ 0 & \text{otherwise}. \end{cases} \tag{4.84}$$

For an ellipsoidal inclusion with axes of lengths a, b, and c,

$$m(\mathbf{x}) = \begin{cases} 1, & x_1^2/a^2 + x_2^2/b^2 + x_3^2/c^2 \le 1, \\ 0, & \text{otherwise}. \end{cases} \tag{4.85}$$

Finally, as a last example, the inclusion indicator function for a circular cylinder of diameter $2a$ and length $2b$ is

$$m(\mathbf{x}) = \begin{cases} 1, & x_1^2 + x_2^2 \le a^2 \text{ and } |x_3| \le b, \\ 0, & \text{otherwise}. \end{cases} \tag{4.86}$$

The n-point matrix probability functions S_n for fully penetrable particles are again easily given:

$$S_n(\mathbf{x}^n) = \exp[-\rho v_n(\mathbf{x}^n)] . \tag{4.87}$$

Here $v_n(\mathbf{x}^n)$ denotes the union volume of n identical, oriented objects of arbitrary shape centered at $\mathbf{x}^n$. For example, in the case $n = 2$, the union volumes of two inclusion regions for the aforementioned rectangular and circular cylindrical inclusions are given respectively by

$$v_2(\mathbf{x}) = 8ab - (2a - x)(2b - y)\Theta(2a - x)\Theta(2b - y) \tag{4.88}$$

and

$$\begin{aligned} v_2(\mathbf{x}) = {} & 4\pi a^2 b - (2b - |x\cos\theta|)A(|x\sin\theta|) \\ & \Theta(2a - |x\sin\theta|)\Theta(2b - |x\cos\theta|), \end{aligned} \tag{4.89}$$

where

$$A(r) = 2a^2 \left(\cos^{-1} \frac{r}{2a} - \frac{r}{2a}\sqrt{1 - \frac{r^2}{4a^2}} \right) \Theta(2a - r). \tag{4.90}$$

In (4.88), x and y are the distances between the centroids of the two rectangular regions in the x_1 and x_2 directions, respectively. In (4.89), x is the magnitude of the displacement $\mathbf{x}$ and θ is the polar angle that $\mathbf{x}$ makes with the x_3-axis.

Actually, using the above prescription, one can not only obtain the S_n for such anisotropic media but also the general $H_n(\mathbf{x}^m; \mathbf{x}^{p-m}; \mathbf{r}^q)$ with $m = 0$, that is,

$$\lim_{a_i \to R, \forall i} H_n(\emptyset; \mathbf{x}^p; \mathbf{r}^q), \qquad n = p + q.$$

In other words, one can obtain all of the H_n except those involving surface information and hence contains as special cases $S_n(\mathbf{x}^n)$, $G_n(\mathbf{x}; \mathbf{r}^q)$ and their generalizations.

The two-point matrix probability function $S_2(\mathbf{r}) = S_2(r, \theta)$ for *hard*, oriented prolate and oblate spheroids at various spheroid volume fractions ϕ_2 and aspect ratios b/a has been determined recently by Lado and Torquato [156] using the results given above. Here r is the magnitude of $\mathbf{r}$ and θ is the angle that the vector $\mathbf{r}$ makes with the plane perpendicular to the axis which is parallel to the orientation of the spheroids. $2b$ and $2a$ are the length and maximum diameter of the spheroid. Figure 17 shows the effects of anisotropy for $b/a = 5$ and $\phi_2 = 0.6$ in the form of cross sections through $S_2^*(r, \theta) = S_2(r, \theta) - \phi_1^2$ for $\theta = 0^0$, 45°, and 90°, reading from right to left on the main peak of the curves. Note that the distance is in units of the major semiaxis b, so that the curve $\theta = 0$ (the outermost of the three) is identical to the hard-sphere limit.

4.6. Cell models

There is a wide class of two-phase random media characterized by *cellular* microstructure. Cellular systems of practical interest include foams, emulsions, and biologic media, to mention but a few

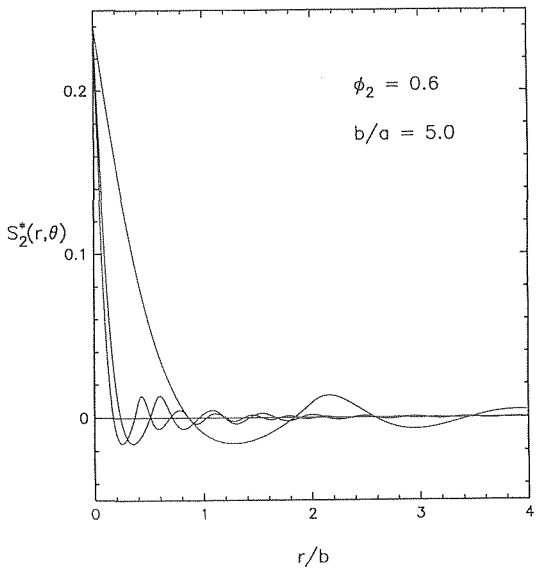

FIG 17. Cross sections through the two-point quantity $S_2^*(r,\theta) \equiv S_2(r,\theta) - \phi_1^2$ for $\theta = 0°, 45°$, and $90°$ (reading from right to left on the main peak of the curves) for oriented, prolate spheroids at an aspect ratio $b/a = 5$ and $\phi_2 = 0.6$ as computed by Lado and Torquato [156].

example. Until recently, knowledge of the correlation functions of cell models has been minimal.

In 1962 Gilbert [171] showed that the two-point probability function $S_2(r)$ is given by a double quadrature for a simple d-dimensional cell model. This medium is constructed in the following matter: (i) a Poisson pattern of points is generated in $\mathcal{R}^d$ with some specified intensity; (ii) the space is partitioned into convex Dirichlet regions of the Poisson points, that is, surrounding a given Poisson point is a region whose interior consists of all points which are nearer to the given Poisson point than to any other Poisson point; and (iii) each Dirichlet region is independently made white (phase 1) or black (phase 2) with probability ϕ_1 or ϕ_2, respectively.

Another interesting and more general model is the symmetric-cell material due to Miller [172]. Such media are constructed by partitioning space into cells of arbitrary shapes and sizes, with cells randomly and independently designated as phase 1 or phase 2 with probabilities ϕ_1 and ϕ_2, respectively. Note that such materials, in contrast to distributions of particles, posses *topological equivalence*, that is, the morphology of the system with volume fraction ϕ_i is identical to another with volume fraction $1 - \phi_i$. Observe also that symmetric-cell materials cannot model dispersions of identical particles since the space couldnot be completely filled by such cells. Recently, Bruno [173] has shown that symmetric-cell materials represent a large class of so-called "infinitely interchangeable" materials. An important feature of cell materials is that one can compute the first few terms of expansion (2.31) for σ_e without explicitly computing the correlation functions [172,173]. Nonetheless, from a microstructural point of view, it is desirable to ascertain the lower-order as well as higher-order correlation functions.

Recently, Lu and Torquato [157] obtained representations of the general S_n, for any n, for the so-called *random lattice* model. This material is contructed by tesselating a d-dimensional cubical subspace into M^d identical d-dimensional cubical cells, with cells randomly and independently designated as phase 1 (white) or phase 2 (black) with probabilities ϕ_1 and ϕ_2, respectively. Figure 18 depicts a two-dimensional realization. Thus, the random lattice model is a special case of the symmetric-cell material and is closely related to the well-known Ising model of a ferromagnet [174]. Every cell has two possible states: occupied (black) or unoccupied (white), corresponding to upward or downward spins in the Ising model in the noninteracting *high-temperature* limit.

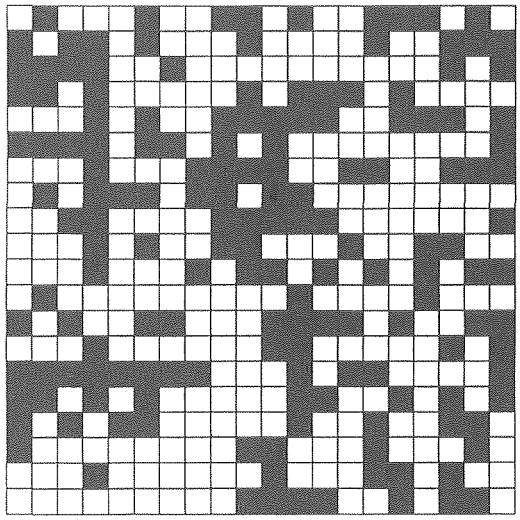

FIG 18. A two-dimensional realization of the *random lattice* model with $\phi_2 = 0.4$. Phase 2 is the black phase.

The S_n for the random lattice model were computed by obtaining the appropriate expressions for the n-particle probability densities ρ_n and using the S_n, ρ_n relations [117] developed for distributions of shperes. The occupied or black cells correspond to "particles" in the continuum description. Let $N \leq M^d$ denote the total number of such hard particles (black cells). Then for a cell of unit length, the volume fraction of the black phase is $\phi_2 = N/M^d$. Lu and Torquato found that

$$\rho_n(\mathbf{r}^n) = \frac{N!}{(N-n)!}\frac{(M^d-n)!}{M^d!}\prod_{i=1}^{n}\left[\sum_{j=1}^{M^d}\delta(\mathbf{r}_i - \mathbf{R}_j)\right]\prod_{i,j}\theta(i,j), \tag{4.91}$$

where

$$\theta(i,j) = \begin{cases} 0, & \mathbf{r}_i = \mathbf{r}_j \\ 1, & \text{otherwise,} \end{cases} \tag{4.92}$$

and $\mathbf{R}_j$ denotes the position of the j the cell. For the random lattice model, the indicator function is given as

$$m(\mathbf{x}) = \begin{cases} 1, & |x_k| \leq \frac{1}{2}(k = 1, \ldots, d), \\ 0, & \text{otherwise.} \end{cases} \tag{4.93}$$

It is important to note that exterior to the generally finite system, ρ_n are identically zero. Substitution of (4.91) into (4.2) in the limit described by (4.9) yields the S_n for this model.

An important finding is that although $S_1(\mathbf{x})$ is equal to the constant $\phi_1 (= 1 - N/M^d)$ within the system, the higher-order quantities (for points within the system) depend upon the absolute positions $\mathbf{r}^n$, that is, the medium is statistically inhomogeneous. This is true even for an infinitely large system. For example, in the cases where $\mathbf{x}_1$ and $\mathbf{x}_2$ lie anywhere in the *same white* cell, the two-point probability function

$$S_2(\mathbf{x}_1, \mathbf{x}_2) = \phi_1. \tag{4.94}$$

In the instances where $\mathbf{x}_1$ and $\mathbf{x}_2$ lie anywhere in *different* white cells,

$$S_2(\mathbf{x}_1, \mathbf{x}_2) = 1 - 2\phi_2 + \phi_2\frac{\phi_2 - 1/M}{1 - 1/M}. \tag{4.95}$$

Using the above formulation, Lu and Torquato derived and computed both translationally invariant and rotationally invariant n-point functions ($n = 2$ and 3). The reader is referred to Ref 157 for those explicit expressions. Figure 19 compares the theoretical

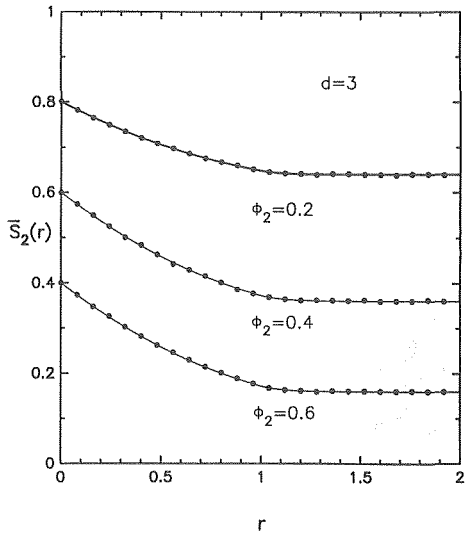

FIG 19. Comparison of the theoretical relation for the rotationally invariant two-point probability function $\bar{S}_2(r)$ for the random lattice model ($d = 3$) derived by Lu and Torquato [157] to computer-simulation data (black circles) for several volume fractions.

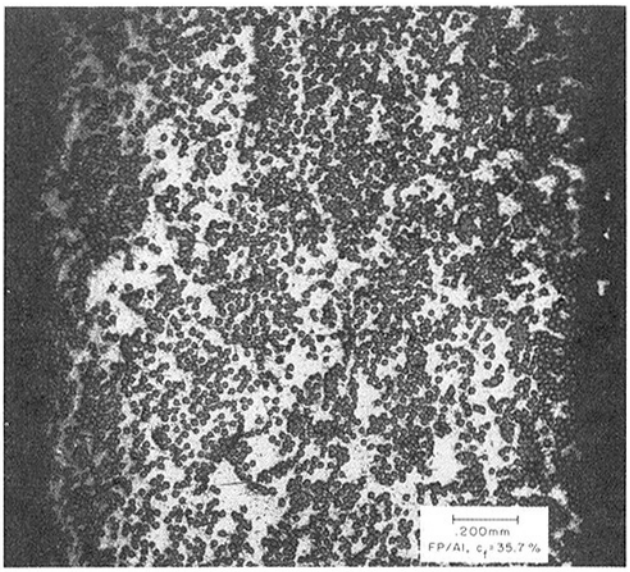

FIG 20. A micrograph of a DuPont FP/Al unidirectional fiber composite. Note the clustering of the ceramic (FP) fibers (black regions). Here c_f corresponds to ϕ_2 of the present article. The micrograph was supplied by Y. Bahei-El-Din of the Department of Civil Engineering at Rensselaer Polytechnic Institute.

FIG 21. Thin film of gold (black regions) on an insulating substrate [177] near but below the gold threshold. Note that the gold clusters are "stringy" or "ramified."

relation for the rotationally invariant two-point function, denoted by $\bar{S}_2(r)$, for several volume fractions in the case $d = 3$, to corresponding Monte Carlo simulation data. The agreement is seen to be excellent.

Note that using (4.91) in conjunction with (4.6) other subsets of the H_n (besides the S_n) can be obtained for the random lattice model. Moreover, the results given above can be generalized to Ising-type models for finite temperatures (ie, with cell-cell interactions).

4.7. Clustering and percolation

The formation of very large clusters can have a dramatic influence on the transport and mechanical properties of random media. Recall that a cluster of phase i is defined as that part of phase i which can be reached from a point in phase i without passing through phase j, $i \neq j$. In particular media, for example, clusters may form as the result of interparticle contacts [175] (eg, see Fig 20 which shows a unidirectional fiber composite). In polymer blends, clustering is determined by the processing conditions and thermodynamics [176]. An important instance is when the cluster spans the entire system. The onset of this is referred to as the *percolation threshold* or *transition*. Figure 21 shows a thin film of gold on an insulating substrate at a metal concentration near but below the threshold [177]. Note that the gold clusters are highly "stringy" or "ramified."

The subject of physical clustering and percolation in "continuum" (off-lattice) models of random media has been receiving considerable attention in recent years [see, eg, 112,113,126–130,161,178–194]. In *lattice* percolation problems one usually consider the clusters fomed by randomly occupying either *sites* or *bonds* on a lattice [195,196]. Continuum-percolation models (ie, distributions of particles), although less tractable than their lattice counterparts, are better able to capture the salient physical features of real systems.

Unfortunately, lower-order H_n do not reflect information about large clusters in the system. It is desired, therefore, to introduce and study quantities analogous to the aforementioned correlation functions for continuum models that reflect information about clustering. Such morphological descriptors may be used to obtain better bounds on effective properties near the percolation threshold.

Torquato, Beasley, and Chiew [190] have introduced the so-called two-point *cluster* function $C_2(\mathbf{x}_1, \mathbf{x}_2)$ defined to be the probability of finding two points at position $\mathbf{x}_1$ and $\mathbf{x}_2$ in the same cluster of phase 2. Thus, C_2 is the analog of $S_2^{(2)}$ or $S_2^{(1)}$ but unlike these predecessors contains topological "connectedness" information. These authors then obtained series representations of C_2 for inhomogeneous distributions of particles (phase 2) by decomposing the known expression for $S_2^{(2)}$ into "connected" and "disconnected" cluster diagrams. For the special case of isotropic distributions of spheres of radius R, their result reduces to

$$C_2(r) = \rho v_2^*(r; R, R) + \rho^2 P_2 \otimes m \otimes m + \text{higher-order diagrams}, \tag{4.96}$$

where v_2^* is the intersection volume of two identical d-dimensional spheres given by (4.22)–(4.24) and $P_2(r)$ is the *pair-connectedness* function such that $\rho^2 P_2(\mathbf{r}_1, \mathbf{r}_2)$ is the probability density associated with finding two particles centered at $\mathbf{r}_1$ and $\mathbf{r}_2$ which are connected ($r \equiv |\mathbf{r}_2 - \mathbf{r}_1|$), that is, which are members of the same cluster of size at least two [112,128,130,182,183,185,188,189,192]. Thus $\rho^2 P_2(r)$ is the connectedness analog of the two-particle density $\rho_2(r)$.

It turns out that one can generally prove that $C_2(r)$ must be

long-ranged (ie, decay to zero slower than r^{-d} for large r) at the percolation threshold in contrast to $S_2(r)$ which is always short-ranged and thus insensitive to physical clustering. Consequently, $C_2(r)$ is a substantially better signature of the microstructure than $S_2(r)$.

For the special case of totally impenetrable spheres of unit diameter (which can only form clusters as the result of interparticle contacts), one has for $d = 3$ that

$$C_2(r) = \eta - \frac{3}{2}\eta r + \frac{\bar{Z}\eta}{4} + \mathcal{O}(r^3), \tag{4.97}$$

where η is the reduced density given by (4.25) and $\bar{Z}$ is the average coordination number (average number of connected nearest neighbors) is, for general sphere distributions, given by

$$\bar{Z} = \rho \int_0^1 4\pi r^2 P_2(r)\, dr. \tag{4.98}$$

Note that for an *equilibrium* distribution of hard spheres, the probability of finding pairs of particles in contact ($r = 1$) is zero and so $\bar{Z} = 0$.

Torquato et al [190] computed the two-point cluster function $C_2(r)$ for "sticky" hard spheres parameterized by a stickiness index τ^{-1}. The limit $\tau \to \infty$ recovers nonsticky hard spheres in equilibrium. In Fig 22 the two-body contribution to the two-point cluster function, $C_2^*(r)$, (divided by ϕ_2^2) is given for several ϕ_2 up to the percolation value for the case $\tau = 0.35$. For fixed r, $C_2^*(r)$ increases with increasing ϕ_2, indicating the presence of increasingly large clusters. At $\phi_2^c = 0.297$, $C_2^*(r)$ becomes long-ranged, as expected.

Subsequently, Lee and Torquato [161] computed $C_2(r)$ for d-dimensional spheres in the penetrable-concentric-shell model for $d = 1$, 2, and 3.

4.8. Experimental techniques

In the late 1950s Debye, Anderson, and Brumberger [196] used the angular distribution of scattered X-rays to measure the two-point probability function $S_2(r)$ and estimate the specific surface s of porous materials. Corson [197] about 15 years later measured the three-point probability function S_3. He took photographs of cross sections of a selected composite material, magnified the photograph, superimposed a sampling grid on the photograph, and then recorded the relevant values for each grid point. Corson's procedure is not automated as it requires that an operator examine each grid point of the photograph, decide what numerical value to assign to that point, and then type that value onto a computer card. This methodology is obviously prohibitively tedious and time-consuming.

With the advent of modern image processing techniques and faster computers, better procedures are available to measure the S_n now than were available to Corson then. Berryman and his colleagues [198–201] have pioneered the use of image processing techniques to accomplish this goal for synthetic and real porous material. Specifically, they have measured S_2 and estimated s of glass-bead samples and of sandstones [198,201]. Moreover, they have devised an efficient means of obtaining and visualizing the three-point probabilty function [200,201]. The reader is referred to the above references for further details regarding the implementation of the technique and its limitations.

5. ADVANCES IN THE CALCULATION OF IMPROVED BOUNDS

The aforementioned advances in the quantitative characterization of microstructure has paved the way to computing improved bounds on the effective conductivity, effective elastic moduli, trapping constant, and fluid permeability for nontrivial models of two-phase random heterogeneous materials. These developments have occurred largely in the last 5 years.

Table 2. The three-point microstructural parameter ζ_2 defined by (3.9) versus the particle volume fraction ϕ_2 for various random distributions of spheres ($d = 3$): symmetric-cell materials with spherical cells [96,172]; identical overlapping spheres [94,119], identical hard spheres [160], and the polydispersion of hard spheres calculated form (5.7) [165][a].

	Three-point parameter ζ_2				
ϕ_2	Symmetric spherical cells	Identical overlapping spheres	Identical hard spheres		Polydispersed hard spheres
0.0	0.0	0.0	0.0	(0.0)	0.0
0.1	0.1	0.056	0.020	(0.021)	0.05
0.2	0.2	0.114	0.041	(0.040)	0.10
0.3	0.3	0.171	0.060	(0.059)	0.15
0.4	0.4	0.230	0.077	(0.077)	0.20
0.5	0.5	0.290	0.094	(0.094)	0.25
0.55	0.55	0.320	0.110	(0.102)	0.275
0.6	0.6	0.351	0.134	(0.110)	0.30
0.7	0.7	0.415			
0.8	0.8	0.483			
0.9	0.9	0.558			
0.95	0.95	0.604			
0.99	0.99	0.658			

[a] The unbracketed and bracketed values given for identical hard spheres correspond to the simulation data of Miller and Torquato [160] and relation (5.4), respectively.

5.1. Conductivity

In the last 5 years, the following conductivity bounds have been computed: (i) three-point bounds (3.7) and (3.11) for distributions of identical overlapping spheres [94,119,124], polydispersed overlapping spheres [152], identical impenetrable spheres [97,114,124,160,202] and polydispersed impenetrable spheres [165]; (ii) three-point bounds (3.10) for distributions of spheres in the penetrable-concentric-shell model [58] (for small ϕ_2) and impenetrable spheres ϕ_2 [97,160]; (iii) three-point bounds (3.5) and four-point bounds (3.12) for transversely isotropic distributions of aligned, identical, overlapping cylinders [143,144], aligned, polydispersed, overlapping cylinders, aligned, identical impenetrable cylinders [203], and aligned, identical cylinders in the penetrable-concentric-shell model [159]; (iv) two-point bounds (3.18) for anisotropic distributions of aligned, overlapping cylinders of finite aspect ratio [107] and of aligned impenetrable prolate and oblate spheroids [204]. Many of these advances are described in some detail below.

5.1.1. Macroscopically isotropic media

In almost all of the aforementioned calculations of bounds on the effective conductivity σ_e, the key microstructural parameter that arises is ζ_2, given by (3.8) for $d = 2$ and (3.9) for $d = 3$. Tables 2 and 3 and Figs 23 and 24 summarize many of the results for ζ_2 for various random distributions of identical and polydispersed d-dimensional spheres.

Until the early 1980s, the only evaluation of ζ_2 was obtained for Miller's symmetric-cell material [172]:

$$\zeta_2 = \phi_2 + \frac{(\phi_1 - \phi_2)(Gd^2 - 1)}{(d - 1)}, \tag{5.1}$$

where G is a parameter which depends only on the shape of the cell and $d = 2$ or 3. This result [96] actually follows from the works

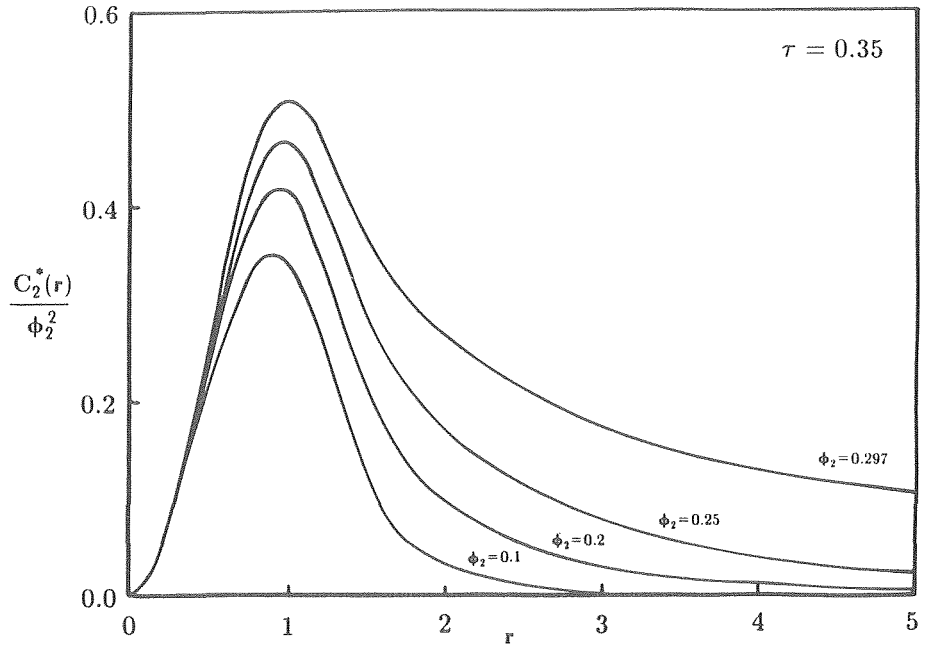

FIG 22. The scaled nontrivial contribution to the two-point cluster function $C_2(r)$ for "sticky" hard spheres for several values of ϕ_2 with a stickiness parameter $\tau = 0.35$. Here $C_2^*(r) = \rho^2 P_2 \otimes m \otimes m$. These results are taken from Torquato et al [190].

Table 3. The three-point parameter ζ_2 defined by (3.8) versus the particle volume fraction ϕ_2 for various random distributions of aligned, infinitely long, circular cylinders: symmetric-cell materials with circular cells [96,205], identical overlapping cylinders [143,144], and identical hard cylinders calculated from (5.5) [203].

	Three-point parameter ζ_2		
ϕ_2	Symmetric spherical cells	Identical overlapping cylinders	Identical hard cylinders
0.0	0.0	0.0	0.0
0.1	0.1	0.062	0.033
0.2	0.2	0.123	0.064
0.3	0.3	0.186	0.095
0.4	0.4	0.249	0.124
0.5	0.5	0.312	0.152
0.6	0.6	0.377	0.179
0.7	0.7	0.444	0.205
0.8	0.8	0.514	
0.9	0.9	0.590	
0.95	0.95	0.635	
0.99	0.99	0.687	

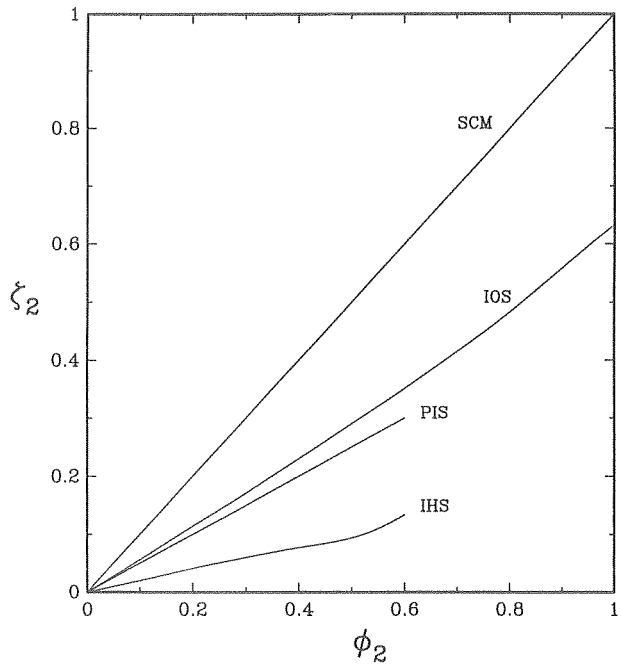

FIG 23. The three-point microstructural parameter ζ_2 defined by (3.9) versus the particle volume fraction ϕ_2 for various random distributions of spheres (d = 3): symmetric-cell materials (SCM) [96,172]; identical overlapping spheres (IOS) [95,119]; identical hard spheres (IHS) [160]; and polydispersed hard spheres (PHS) [165]. The IHS result is obtained from the simulation data of Miller and Torquato [160] and the PHS result is obtained from (5.7).

of Miller [172] and of Silnutzer and Beran [205]. For example, for spherical ($d = 3$) or circular ($d = 2$) cells, $\zeta_2 = \phi_2$. For platelike ($d = 3$) or ribbonlike ($d = 2$) cells, $\zeta_2 = \phi_1$. It should be noted that five-point bounds on σ_c have been computed for the special case of symmetric-cell materials [206,207].

The first comprehensive calculation of ζ_2 for a random model other than the symmetric-cell material was given by Torquato and Stell [92,94,119,124] for distributions of identical overlapping spheres ($d = 3$). Analogous two-dimensional calculations were made by Torquato and Beasley [143] and by Joslin and Stell [144]. Stell and Rikvold [152] and Joslin and Stell [153] showed that ζ_2, for overlapping spheres (cylinders), was insensitive to polydispersivity effects. For overlapping spheres, Berryman [208] and Torquato [114] independently noted that the first term in the volume-fraction (ϕ_2) expansion of ζ_2 was a good approximation to ζ_2 over almost the whole range of ϕ_2. This is also true for $d = 2$ [143,144]. For $d = 3$, for example, Torquato [114] showed that, to first order in ϕ_2, $\zeta_2 = 0.5615\phi_2$, which is accurate to the number of significant figures indicated. The calculation of ζ_2 for overlapping particles is actually relatively straightforward by virtue of the simplicity of S_3 for such models [cf relation (4.34)].

The evaluation of ζ_2 for impenetrable particles, on the other hand, is considerably more complex. For such models, substitution of the appropriate integral relations for S_n [117] into the three-

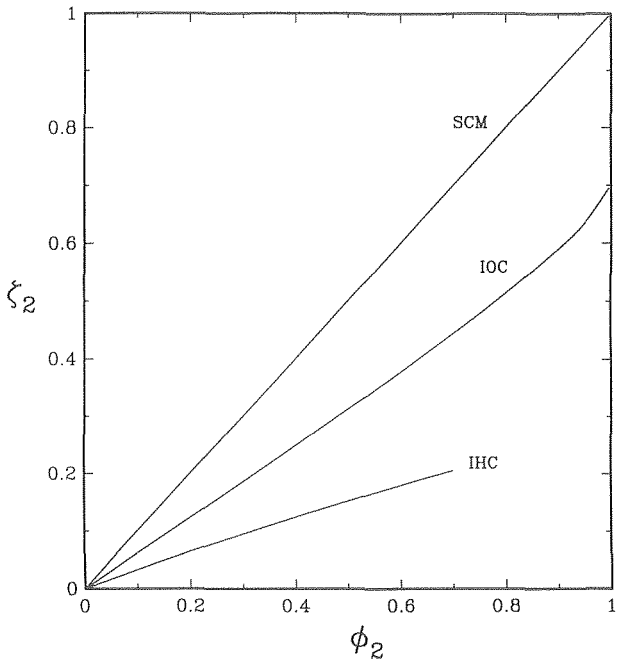

FIG 24. The three-point microstructural parameter ζ_2 defined by (3.8) versus the particle volume fraction ϕ_2 for various random distributions of aligned, infinitely long, circular cylinders: symmetric-cell materials (SCM) [96,205], identical overlapping cylinders (IOC) [143,144] and identical hard cylinders (IHC) [203] as calculated from (5.5).

fold integrals (3.8) and (3.9) result in m-fold integrals with m as large as 12. A general technique has been developed by Lado and Torquato [209] and Torquato and Lado [203] to simplify significantly these multidimensional integrals so that they either could be evaluated analytically or could be reduced to at most a manageable triple quadrature. The basic idea behind this procedure is to expand certain angular-dependent terms of the integrands in orthogonal polynomials and exploit the orthogonality properties of the appropriate basis set. This technique has been applied to the conductivity problem elsewhere [97] and to the problems of determining three-point bounds on the shear modulus [210,211] and fluid permeability [89].

Using a different procedure, Felderhof [202] computed ζ_2 through third order in the sphere volume fraction ϕ_2 in the superposition approximation [cf (4.18)] for an isotropic, equilibrium, distribution of hard spheres. Beasley and Torquato [97] calculated ζ_2 exactly through third order in ϕ_2 for this model and found

$$\zeta_2 = 0.21068\phi_2 - 0.04693\phi_2^2 + 0.00247\phi_2^3. \tag{5.2}$$

Torquato and Lado [114] evaluated ζ_2 to all orders in ϕ_2 up to $\phi_2 = 0.6$ (ie, up to about 94% of the random-close-packing value) in the superposition approximation and noted the approximate linear behavior for $0 \leq \phi_2 \leq 0.4$. Recent work by Stell and his colleagues [130] employing the more sophisticated "ladder" approximation for ρ_3 indicates that, at high values of ϕ_2 ie, $\phi_2 > 0.5$), the superposition approximation significantly overestimates ζ_2. Subsequently, Miller and Torquato [160] carried out Monte Carlo computer simulations to determine ζ_2 very accurately for equilibrium distributions of identical impenetrable spheres for $0 \leq \phi_2 \leq 0.6$. (Note that they actually simulated Torquato's [58] cluster bound (3.10) which, as noted earlier, is isomorphic to the three-point bounds (3.5) for this model but is easier to determine from simulations.) The simulation results for ζ_2 have been compared to the superposition and ladder approximations of ζ_2, and to the linear and quadratic formulas

$$\zeta_2 = 0.21068\phi_2 \tag{5.3}$$

and

$$\zeta_2 = 0.21068\phi_2 - 0.04693\phi_2^2, \tag{5.4}$$

respectively, which are simply Eq (5.2) truncated after one and two terms. Remarkably, the quadratic formula (5.4), exact to second order in ϕ_2, follows the simulation data very closely up to and including $\phi_2 = 0.5$, which is very slightly above the value of the fluid-solid phase transition [123] (see Table 2). This indicates that third- and higher-order terms are negligibly small. Note that the linear term of (5.4) is actually the dominant one as evidenced by the fact that the linear formula (5.3), although not as accurate as the quadratic formula (5.5), is a good approximation to the data for $\phi_2 \leq 0.5$. For $0.5 \leq \phi_2 \leq 0.54$, values in the metastable region, the quadratic formula (5.4) still provides the closest agreement with the data. For $0.54 \leq \phi_2 \leq 0.6$, the linear formula (5.3) is the most accurate, with the quadratic formula (5.4) being the next most accurate calculation. For the range $0 \leq \phi_2 \leq 0.4$, the superposition-approximation results for ζ_2 are more accurate than the ladder approximation. On the other hand, for $\phi_2 \geq 0.5$, the ladder approximation to ζ_2 is superior to the corresponding superposition-approximation results which significantly overestimate ζ_2 in this high-density regime. Note that $\phi_2 = 0.6$ corresponds to about 95% of the random close-packing value $\phi_2^c \approx 0.63$ [132,133].

The significance of the fact that the low-density expansions of ζ_2 for systems of d-dimensional spheres provide very good agreement with simulation data for a wide range of ϕ_2 has been discussed very recently by Miller and Torquato [160]. It suffices to note here that the accuracy of the quadratic formula (5.4) implies that ζ_2 incorporates primarily up to *three-body* effects to *lowest order*, even at high volume fractions: A result consistent with the fact that ζ_2 contains little information about the intrinsically many-body phenomenon of percolation. This is expected to be true for general statistically isotropic two- and three-dimensional distributions of disks and spheres, respectively, with a polydispersivity in size and an arbitrary degree of penetrability. This is a very practically useful conclusion since the exact calculation of ζ_2 through second order in ϕ_2 for distributions of impenetrable particles is much easier to arrive at than the corresponding full density-dependent calculation which necessarily involves the use of some approximation of ρ_3 whose validity is usually questionable at high densities.

It is useful to remark on the behavior of closely related three-point microstructural parameters. First, it was noted by Smith and Torquato [159] that ζ_2 for three-dimensional distributions of particles is qualitatively very similar to corresponding two-dimensional analogs of ζ_2 for transversely isotropic distributions of particles. The results reported in Refs 93,114,124,143,144,152,153,159,160,203,208,212, and 213 certainly confirm this observation. Second, it is also clear that the different microstructural parameter η_2, which arises in three-point bounds on the effective shear modulus of two-phase composites [52,56], also shows the same general trends as ζ_2 for two- and three-dimensional distributions of particles [25,143,165,208,211, 212]. Accordingly, the exact expansions of all the aforementioned three-point parameters through second order in ϕ_2 for such microgeometries should yield accurate estimates of them for a wide range of ϕ_2. In all these cases the linear term should be the dominant one.

Torquato and Lado [203] computed the three-point Silnutzer bounds [53] and the four-point Milton bounds [96] on the effective transverse conductivity σ_t of random distributions of infinitely long, parallel, identical, circular hard cylinders in the superposition approximation. Torquato and Lado [203] had also computed ζ_2 for this two-dimensional model exactly through second order in ϕ_2:

$$\zeta_2 = \frac{\phi_2}{3} - 0.05707\phi_2^2. \tag{5.5}$$

In light of the discussion above, (4.5) should be highly accurate for the range $0 \leq \phi_2 \leq 0.7$, $\phi_2 = 0.7$ corresponding to about 87% of

the random close-packing value for disks ($\phi_2^c \simeq 0.81$) [132,133]. This is also borne out by the general trends of the simulations of Sangani and Yao [214]. The superposition approximation result for ζ_2 [203] is approximately linear for $0 \leq \phi_2 \leq 0.5$ but increasingly overestimates ζ_2 for $\phi_2 \geq 0.5$. Therefore, the superposition result [203] , for $\phi_2 \geq 0.5$, is now superseded by relation (5.5) for this model.

Smith and Torquato [159] computed the same three- and four-point bounds for identical, aligned, infinitely long cylinders in the penetrable-concentric-shell model and hence computed ζ_2 as a function of the impenetrability index λ. Unlike most previous studies, this work considered the nonequilibrium random sequential addition process. Their results are not included in Table 3 or Fig 24, however. For fixed ϕ_2, the effect of increasing λ is to decrease ζ_2, as expected.

Thovert et al [165] computed ζ_2 exactly through first order in ϕ_2 for impenetrable spheres with a polydispersivity in size. For the case of a bidispersed suspension with widely separated particles sizes, they found

$$\zeta_2 = 0.35534\phi_2. \tag{5.6}$$

For the instance of a polydisperse suspension containing n different ($n \to \infty$) and widely separated particle sizes , they found

$$\zeta_2 = 0.5\phi_2. \tag{5.7}$$

This last microgeometry yields the largest effect due to polydispersivity. Note that the bidispersed result (5.6) lies exactly midway between the monodispersed result (5.3) and result (5.7). Miller and Torquato [215] are currently in the process of carrying out analogous two-dimensional calculations. They have found that (5.7) also applies to the corresponding polydispersed two-dimensional geometry. Thus, the effect of polydispersivity is again to increase ζ_2.

Except for the case of polydispersed hard spheres, the physical significance of the results for ζ_2 given in Tables 2 and 3 and Figs 23 and 24 and their interrelationships have been discussed by Torquato and Lado [114,203]. For example, the reasons why ζ_2 for overlapping equisized spheres always lies above the corresponding results for hard equisized spheres have been given by Torquato [114]. Note that the effect of polydispersivity for hard spheres is to increase ζ_2 relative to the monodisperse case. One might initially expect the converse to occur since ζ_2 would then be approaching $\zeta_2 = 0$, the value corresponding to the polydispersed composite-sphere assemblage of Hashin and Shtrikman for $\sigma_2 \geq \sigma_1$. Upon closer inspection it is clear that the average separation distance between the more conducting particles in the composite-sphere assemblage is larger than in the polydispersed hard-sphere geometry. Hence, the latter possesses larger conducting clusters than the former and, for that matter, the monodispersed hard-sphere system. Consequently, ζ_2 for polydispersed hard spheres should increase, rather than decrease, relative to the corresponding monodisperse result.

Torquato and Lado [203] have observed that ζ_2 for cylinders (disks for $d = 2$), be they overlapping, nonoverlapping, possessing polydispersivity in size, and so on, are bounded from above by the symmetric-cell material result of $\zeta_2 = \phi_2$ (see Table 3 and Fig 24). Table 2 and Fig 23 apparently reveals the same conclusion for $d = 3$. A proof of this for a general class of d-dimensional distributions of spheres has not yet been given. This would be a useful result if proven to be rigorously true for a class of sphere distributions since ζ_2 would lie in the generally smaller closed interval $[0,\phi_2]$.

Before presenting calculations for the bounds on σ_e for various conductivity ratios $\alpha = \sigma_2/\sigma_1$, it is useful to discuss the approximation (3.17) of Torquato [38], which will be used to access the accuracy of bounds for three-dimensional dispersions. To test (3.17), Torquato evaluated it for the benchmark model periodic arrays of spheres for the extreme case of superconducting particles ($\alpha = \infty$) using the tabulation of ζ_2 given by McPhedran and Milton

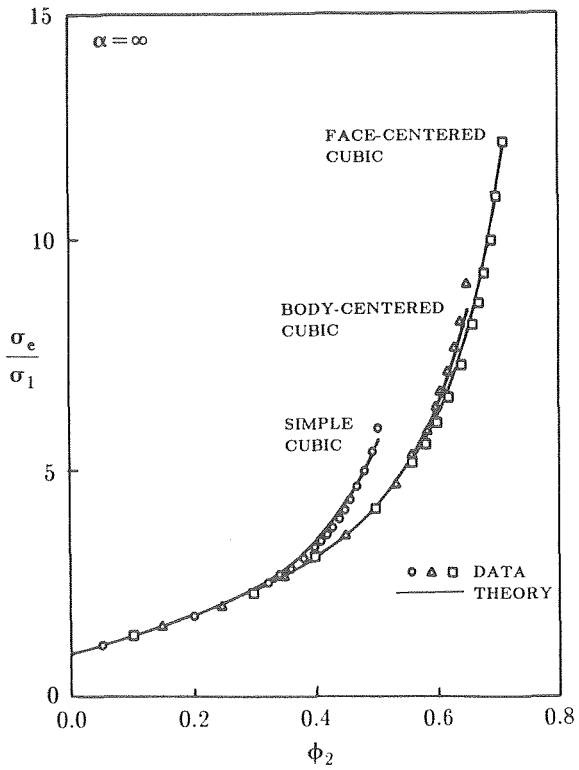

FIG 25. The scaled effective conductivity σ_e/σ_1 for $\alpha = \sigma_2/\sigma_1 = \infty$ versus the sphere volume fraction ϕ_2 for three cubic lattices. Solid lines represent predicted values from relation (3.17) and numerical data is obtained from Refs 217 and 218.

[216] and compared it to exact numerical results for this idealized model [217–221]. These results are summarized in Fig 25, where it is seen that (3.17) provides excellent agreement up to the maximum volume fractions reported, that is, up to about 95% of the respective close-packing volume fractions. Thus, (3.17) does indeed capture the microstructure sensitiveness of σ_e for three-dimensional dispersions.

Improved three- and four-point bounds on σ_e are depicted in Figs 26–29 for distributions of equisized hard cylinders ($d = 2$) and hard spheres ($d = 3$) for various values of α. Included in these figures are corresponding two-point bounds. The figures depicting the cases ($d = 2$) include new and accurate Brownian-motion simulation data for the "exact" effective transverse conductivity σ_e due to Kim and Torquato [222]. (Reference 222 uses first passage time analysis to speed significantly the execution time of the simulations; see also Ref 18.) Figure 29 for $d = 3$ and $\alpha = \infty$ includes the accurate relation (3.17). For $\alpha = 10$, the improved bounds are very sharp and provide significant improvement over two-point bounds (cf Fig 26). For $\alpha = 50$, the bounds widen, as expected, taking into account the possibility of the formation of large conducting clusters in the system. However, the best improved lower bound provides a very accurate estimate of σ_e (cf Fig 27). This is true because there are no large conducting clusters present in d-dimensional, equilibrium hard-sphere distributions for the range of volume fractions considered. For such models, interparticle contacts occur only at the random close-packing densities [see discussion below relation (4.18)]. In the extreme cases of superconducting particles ($\alpha = \infty$), the improved lower bounds still provide good estimates of σ_e for a wide range of ϕ_2 (see Figs 28 and 29). These results confirm the comments made in section 3.5 about the utility of bounds.

Figure 30 compares the three-point bounds on σ_e for the overlapping-sphere model to measurements [223] on the conductivity of air-saturated sandstones with $\alpha = 80$. Here the upper

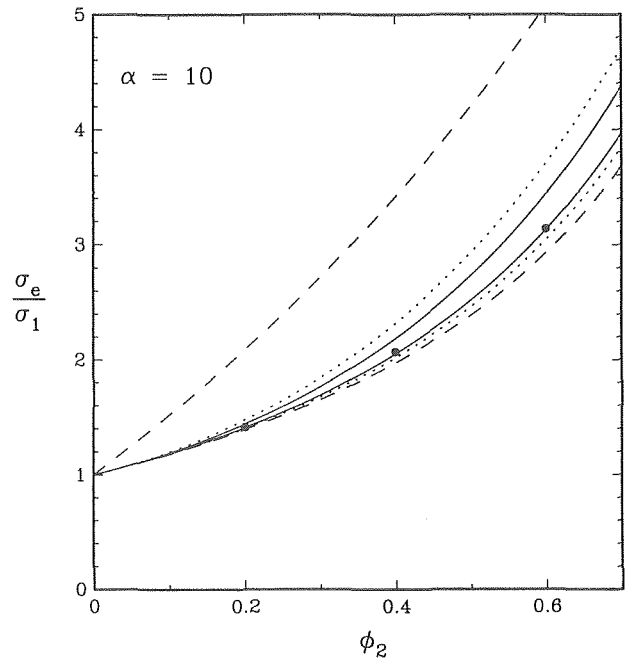

FIG 26. Bounds on σ_e/σ_1 versus ϕ_2 at $\alpha = \sigma_2/\sigma_1 = 10$ for random distributions of oriented, infinitely long, hard cylinders: (– – –) two-point Hashin bounds [23]; (· · ·) three-point Silnutzer bounds [53]; (—) four-point Milton bounds [69]. The black circles are computer simulation determinations of the "exact" scaled conductivity due to Kim and Torquato [222]. The improved bounds were computed using the relation (5.5) derived by Torquato and Lado [203].

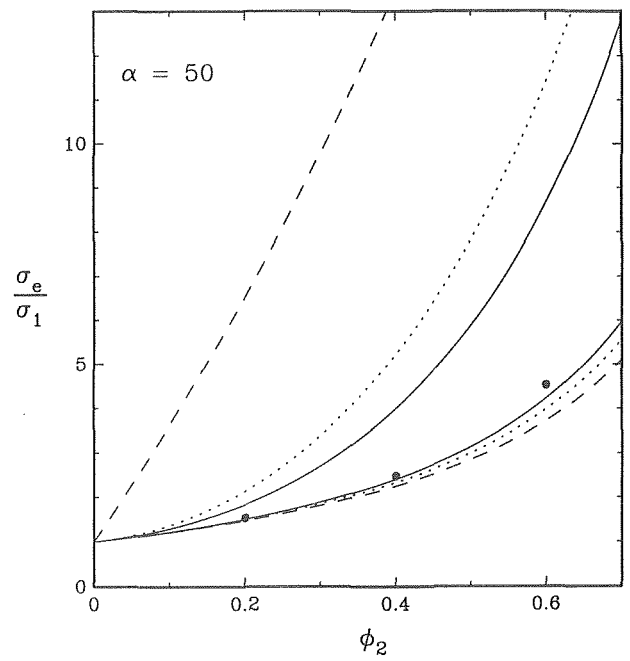

FIG 27. As in Fig 26, with $\alpha = 50$.

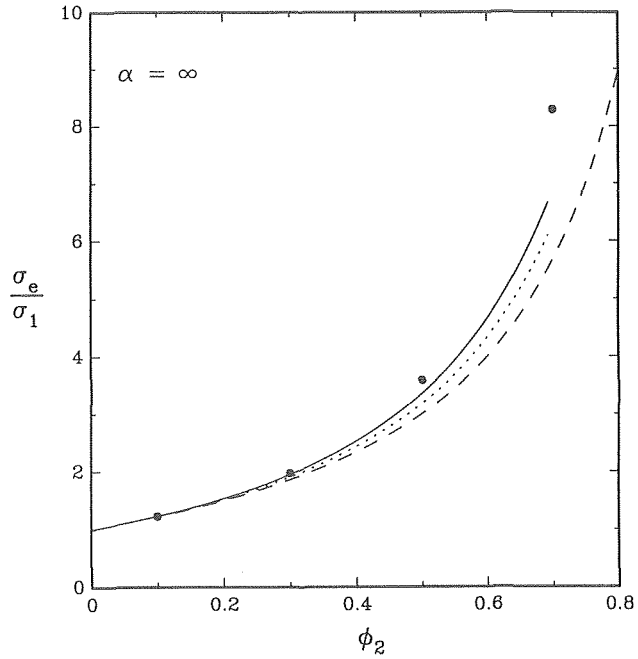

FIG 28. As in Fig 27, with $\alpha = \infty$. Upper bounds do not appear since they diverge to infinity. The four-point lower bound, however, gives a relatively sharp estimate of σ_e/σ_1.

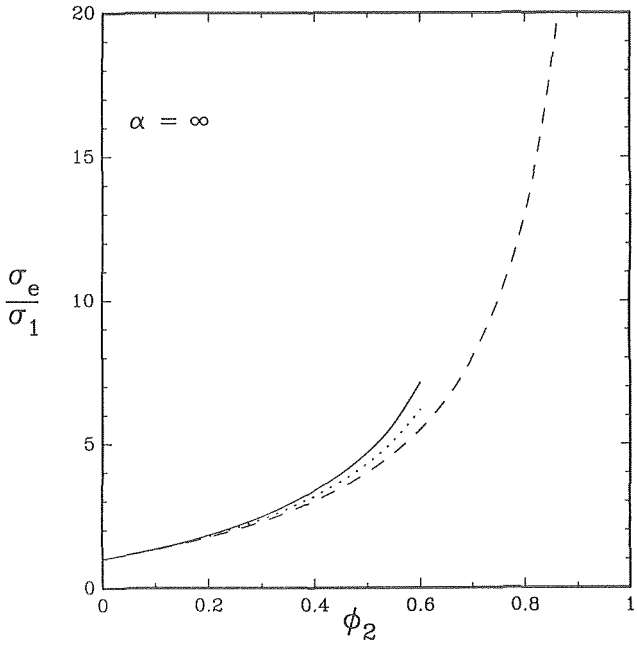

FIG 29. Bounds on σ_e/σ_1 versus ϕ_2 for superconducting hard spheres ($\alpha = \infty$): (– – –) two-point Hashin–Shtrikman lower bound [13]; (· · ·) three-point Milton lower bound [98]. The three-point bound is computed using the simulation data of Miller and Torquato [160] for ζ_2. Included in the figure is the accurate approximation (3.17) denoted by the solid curve.

bound provides an accurate estimate of σ_e since the conducting phase (sandstone) is above its percolation threshold.

Figure 31 compares three-point lower bounds on σ_e for a monodispersion and polydispersion [corresponding to (5.7)] of hard spheres for the case $\alpha = \infty$. Included in the figure is the approximation (3.17) for the polydispersion and the two-point Hashin–Shtrikman lower bound.

5.1.2. *Macroscopically anisotropic media*

Results are given here for the calculation of the two-point anisotropic bounds (3.18) on $\boldsymbol{\sigma}_e$ for three-dimensional distributions of inclusions aligned in the x_3-direction which possess transverse isotropy and azimuthal symmetry (eg, circular cylinders and spheroids). In general, for such media, one has from relations (3.21)–(3.28) that the tensor $\mathbf{a}_2$ arising in the Sen–Torquato [20]

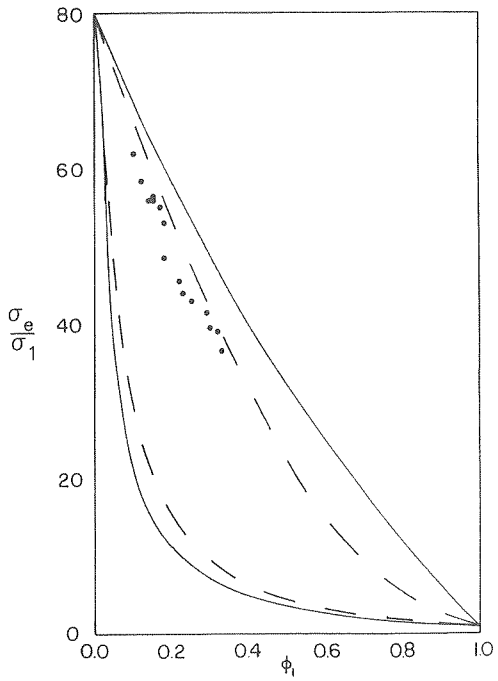

FIG 30. Comparison of measured values of σ_e/σ_1 for air-saturated sandstones (black circles) [223] to the two-point Hashin-Shtrikman [13] bound (—) and to three-point bounds [45,98] (– – –) for equisized overlapping spheres, as a function of porosity ϕ_2. Here $\alpha = \sigma_2/\sigma_1 = 80$, where phase 2 is the solid phase.

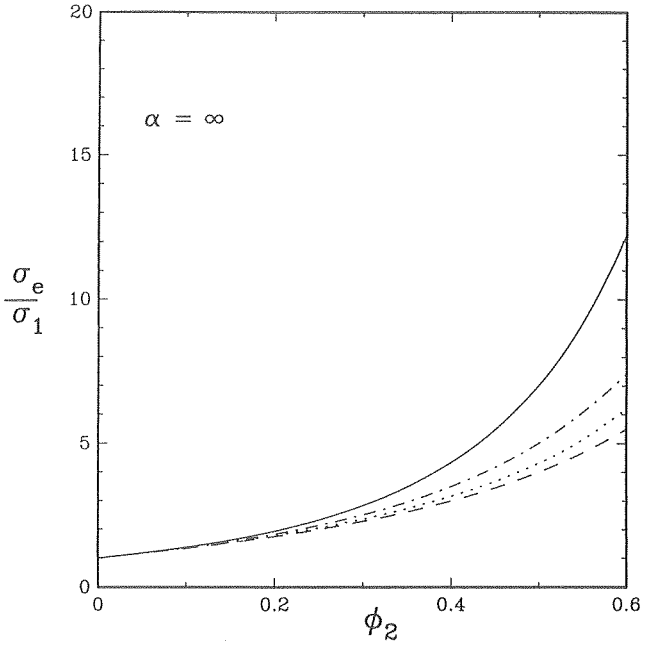

FIG 31. Bounds on σ_e/σ_1 versus ϕ_2 for superconducting monodispersed and polydispersed hard spheres ($\alpha = \infty$): (– – –) two-point Hashin–Shtrikman bound [13]; (· · ·) three-point Milton [98] lower bound for monodispersed spheres; (– · –·) three-point Milton [98] lower bound for polydispersed hard spheres computed using (5.7) as determined by Thovert et al [165]. Included in the figure is approximation (3.17) denoted by a solid curve.

bounds (3.18) is given by

$$\mathbf{a}_2 = -\phi_1\phi_2 \begin{bmatrix} Q & 0 & 0 \\ 0 & Q & 0 \\ 0 & 0 & 1-2Q \end{bmatrix}, \tag{5.8}$$

where

$$Q = \frac{1}{3} - \lim_{\epsilon\to 0} \frac{1}{2\phi_1\phi_2} \int_\epsilon^\infty \frac{dx}{x} \int_0^\pi d(\cos\theta) P_2(\cos\theta)[S_2(\mathbf{x}) - \phi_1^2]. \tag{5.9}$$

It can be shown [204] that for *possibly overlapping* spheroidal inclusions aligned parallel to the x_3-axis with length 2b and maximum diameter 2a, one has

$$Q = \frac{1}{2}\left\{1 + \frac{1}{(b/a)^2 - 1}\left[1 - \frac{1}{2\chi_b}\ln\left(\frac{1+\chi_b}{1-\chi_b}\right)\right]\right\}, \qquad \frac{b}{a} > 1 \tag{5.10}$$

$$Q = \frac{1}{2}\left\{1 + \frac{1}{(b/a)^2 - 1}\left[1 - \frac{1}{\chi_a}\tan^{-1}(\chi_a)\right]\right\}, \qquad \frac{b}{a} < 1 \tag{5.11}$$

where

$$\chi_a^2 = -\chi_b^2 = a^2/b^2 - 1. \tag{5.12}$$

Q depends only on the shape of the inclusion. For example, $Q \longrightarrow 1/3$ for $b/a \longrightarrow 0$, $Q \to 1/2$ for $b/a \to \infty$, and $Q \to 0$ for $b/a \to 0$. Torquato and Lado [204] obtained results (5.10) and (5.11) by employing a scaling relation for S_2 which enables one to map results for possibly overlapping spheres ($b/a = 1$) into equivalent results for possibly overlapping spheroids of aspect ratio b/a. Willis [54] actually was the first to obtain results (5.10) and (5.11). He did so, elegantly, without explicitly evaluating the integral of (5.9) by employing a well-known result due to Eshelby for ellipsoids [224]. Thus, he did not note (or need) the aforementioned scaling relation for S_2 but, because of the nature of the derivation, did not draw an important conclusion, namely, the two-point bounds for spheroids are insensitive to spatial correlations between the spheroids, that is, one gets the same answer whether the spheroids are penetrable or not. This is not true for inclusions of arbitrary shape; the microgeometry of overlapping cylinders described below is a case in point.

Torquato and Sen [107] have recently computed (5.9) and thus the improved bounds (3.18) on σ_e for a distribution of oriented, overlapping, circular cylinders (of length $2b$ and diameter $2a$) in a matrix. The length of each cylinder is directed along the x_3-axis. Figure 32 shows the bounds on the three diagonal components of the effective conductivity $(\sigma_e)_{ii}$ ($i = 1$, 2, and 3) for *conducting, slender rods* ($\alpha = 10$ and $b/a = 10$). Figure 33 depicts the corresponding bounds for the case of *insulating, penny-shaped cracks* ($\alpha = 0.1$ and $b/a = 0.1$).

5.2. Elastic moduli

In the last 5 years, the following elasticity bounds have been computed: (i) three-point bounds (3.51) and (3.54) for distributions of identical overlapping spheres [208,213], identical impenetrable spheres [25,114], identical interpenetrable spheres [225], and polydispersed impenetrable spheres [165]; (ii) three-point bounds (3.43) and (3.46) for distributions of aligned identical [144,212] and polydispersed [153] overlapping, infinitely long, cylinders and of aligned, impenetrable, infinitely long, identical [211] and polydispersed [215] cylinders.

5.2.1. Macroscopically isotropic media

In all of the aforementioned calculations of bounds on the elastic moduli of d-dimensional isotropic media, the key parameters involved are ζ_2, given by (3.8) for $d = 2$ and (3.9) for $d = 3$, and η_2, given by (3.35) for $d = 2$ and (3.36) for $d = 3$. As has been shown, ζ_2 determines improved bounds on the effective bulk modulus K_e (for $d = 3$), transverse bulk modulus k_e (for $d = 2$) and axial shear

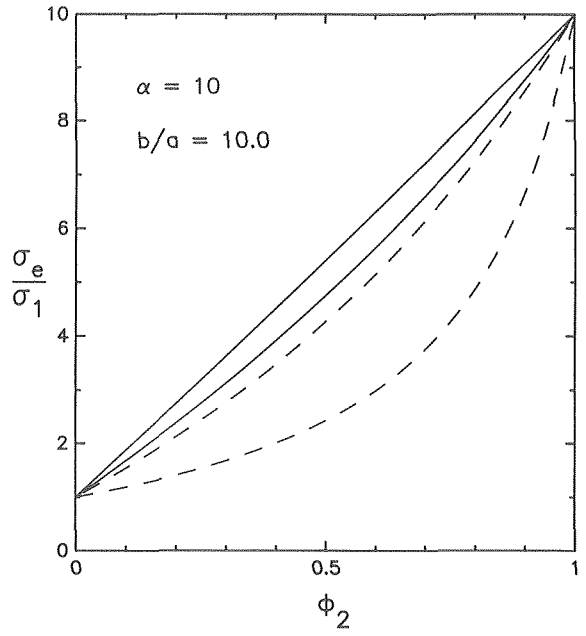

FIG 32. The two-point Sen–Torquato [20] bounds on the scaled effective conductivity diagonal components σ_e/σ_1 [$\sigma_e \equiv (\sigma)_{ii}$] versus ϕ_2 for a composite containing conducting (α = 10), slender (b/a = 10) overlapping cylindrical inclusions [107]. The dashed lines are bounds for $(\sigma_e)_{11} = (\sigma_e)_{22}$ and the solid lines are bounds for $(\sigma_e)_{33}$.

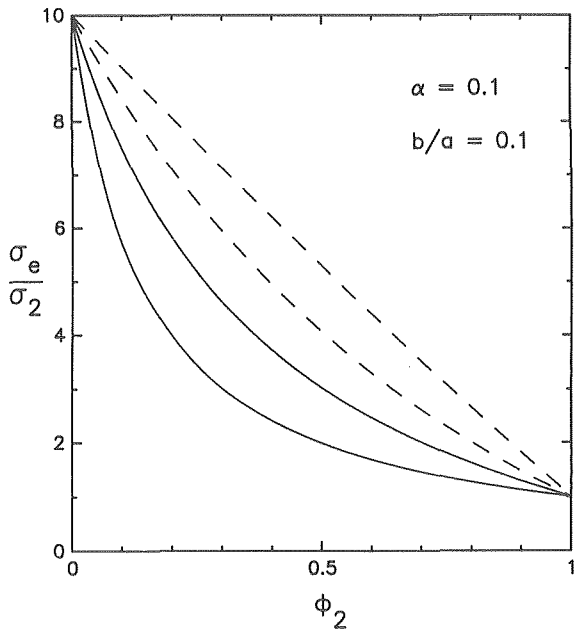

FIG 33. The two-point Sen–Torquato [20] bounds on the scaled effective conductivity diagonal components σ_e/σ_1 [$\sigma_e \equiv (\sigma_e)_{ii}$] versus ϕ_2 for a composite containing nonconducting (α = 0.1), overlapping penny-shaped (b/a = 0.1) cracks [107]. The dashed lines are bounds for $(\sigma_e)_{11} = (\sigma_e)_{22}$ and the solid lines are bounds for $(\sigma_e)_{33}$.

modulus μ_e (for transversely isotropic fiber-reinforced materials). On the other hand, η_2 has been shown to determine bounds on the effective shear modulus G_e for both d = 2 and d = 3. Tables 4 and 5 and Figs 34 and 35 summarize many of the results for η_2 for various random distributions of identical and polydispersed d-dimensional spheres.

Until 1985, the only calculation of η_2 was made for symmetric-

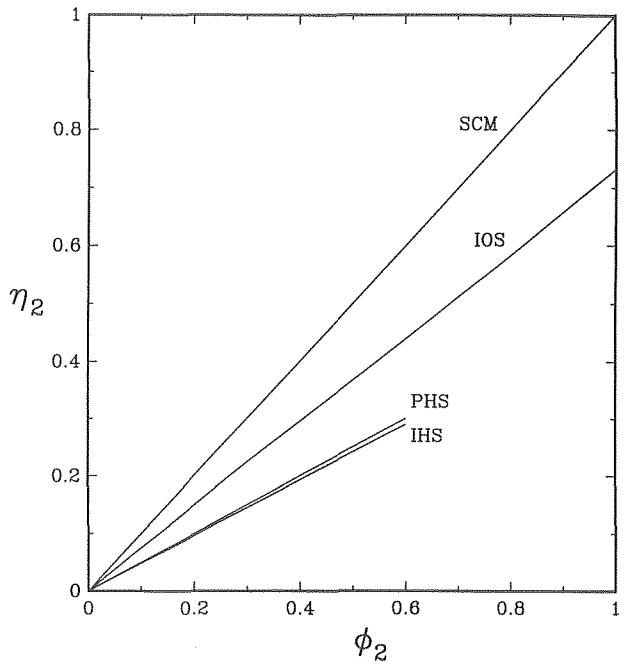

FIG 34. The three-point microstructural parameter η_2 defined by (3.36) versus the particle volume fraction ϕ_2 for various random distributions of spheres (d = 3): symmetric-cell materials (SCM) [53,96]; identical overlapping spheres (IOS) [213]; identical hard spheres (IHS) [225]; and polydispersed hard spheres (PHS) [165]. The IHS and PHS results are obtained from (5.15) and (5.18), respectively.

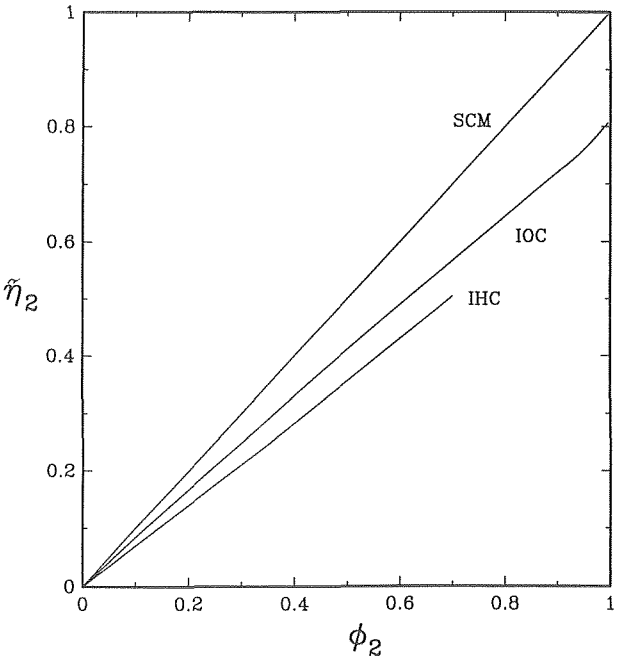

FIG 35. The three-point microstructural parameter η_2 defined by (3.35) versus the particle volume fraction ϕ_2 for various random distributions of aligned, infinitely long, circular cylinders: symmetric-cell materials (SCM) [96,205]; identical overlapping cylinders (IOC) [144,212]; and identical hard cylinders (IHC) [211]. The IHC result is obtained from (5.16).

Table 4. The three-point microstructural parameter η_2 defined by (3.36) versus the particle volume fraction ϕ_2 for various random distributions of spheres ($d = 3$): symmetric-cell materials with spherical cells [53,96]; identical overlapping spheres [213], identical hard spheres calculated from (5.15) [225], and the polydispersion of hard spheres calculated from (5.19) [165].

	Three-point parameter η_2			
ϕ_2	Symmetric spherical cells	Identical overlapping spheres	Identical hard spheres	Polydispersed hard spheres
0.0	0.0	0.0	0.0	0.0
0.1	0.1	0.075	0.048	0.05
0.2	0.2	0.149	0.097	0.10
0.3	0.3	0.224	0.145	0.15
0.4	0.4	0.295	0.193	0.20
0.5	0.5	0.367	0.241	0.25
0.6	0.6	0.439	0.290	0.30
0.7	0.7	0.512		
0.8	0.8	0.583		
0.9	0.9	0.658		
0.95	0.95	0.710		
0.99	0.99	0.742		

Table 5. The three-point parameter η_2, defined by (3.35), versus the particle volume fraction ϕ_2, for various random distributions of aligned, infinitely long, circular cylinders: symmetric-cell materials with circular cells [96,205], identical overlapping cylinders [144,212], and identical hard cylinders calculated from (5.16) [211].

	Three-point parameter η_2		
ϕ_2	Symmetric spherical cells	Identical overlapping cylinders	Identical hard cylinders
0.0	0.0	0.0	0.0
0.1	0.1	0.084	0.070
0.2	0.2	0.167	0.140
0.3	0.3	0.250	0.211
0.4	0.4	0.331	0.283
0.5	0.5	0.411	0.356
0.6	0.6	0.490	0.430
0.7	0.7	0.568	0.505
0.8	0.8	0.644	
0.9	0.9	0.720	
0.95	0.95	0.760	
0.99	0.99	0.801	

cell materials [172]:

$$\eta_2 = \phi_2 + (\phi_1 - \phi_2)[(8H - 3) - 4(4G - 1)], \qquad d = 2, \quad (5.13)$$

$$\eta_2 = \phi_2 + \frac{(\phi_1 - \phi_2)}{6}[4(5E - 1) - 5(9G - 1)], \qquad d = 3, \quad (5.14)$$

where E, G, and H are parameters which depend only on the shape of the cell. These results [96] actually follow from the work of Silnutzer [53] and Silnutzer and Beran [205]. For example, for spherical ($d = 3$) or circular ($d = 2$) cells, $\eta_2 = \phi_2$. For platelike ($d = 3$) and ribbonlike ($d = 2$) cells, $\eta_2 = \phi_1$.

The first thorough evaluation of η_2 for a random model other than the symmetric-cell material was obtained independently by Torquato, Stell, and Beasley [213] and by Berryman [208] for distributions of identical overlapping spheres. Analogous two-dimensional calculations were obtained independently by Torquato and Beasley [212] and by Joslin and Stell [144]. Joslin and Stell [153] demonstrated that η_2, like ζ_2, was insensitive to polydispersivity effects for the special case of overlapping cylinders.

Sen, Lado, and Torquato [25] were the first to compute η_2 to all orders in ϕ_2 for distributions of identical impenetrable spheres in the superposition approximation. They simplified the multidimensional integrals [210] involved using the previously described technique employed for ζ_2 [204,209]. Torquato, Lado, and Smith [225] evaluated η_2 exactly through first order in ϕ_2 for interpenetrable spheres and in the totally impenetrable-sphere limit. They found

$$\eta_2 = 0.48274\phi_2. \quad (5.15)$$

In light of the discussion in section 5.1, the relation (5.15) should serve as an accurate estimate of η_2 for $0 \le \phi_2 \le 0.6$. As in the case of ζ_2, the superposition result for η_2 [25] is approximately linear for $0 \le \phi_2 \le 0.4$ but for $\phi_2 > 0.4$ increasingly overestimates η_2. Again the superposition result [25] is now superseded by (5.15) for large ϕ_2, which is generally more accurate for this model.

Recently, Torquato and Lado [211] computed η_2 for the corresponding two-dimensional model of distributions of impenetrable disks (cylinders). They found for $d = 2$ that the parameter through second order in ϕ_2 is exactly given by

$$\eta_2 = \frac{56}{81}\phi_2 + 0.0428\phi_2^2. \quad (5.16)$$

Thovert et al [165] calculated η_2 exactly through first order in ϕ_2 for impenetrable spheres ($d = 3$) with a polydispersivity in size. For the instance of a bidispersed suspension with widely separated particle sizes, they obtained

$$\eta_2 = 0.49137\phi_2. \quad (5.17)$$

For the case of a polydispersed suspension containing n different ($n \to \infty$) and widely separated particle sizes, they obtained

$$\eta_2 = 0.5\phi_2. \quad (5.18)$$

Again, it is found that the bidispersed result (5.18) lies exactly midway between the monodispersed result (5.15) and the polydispersed result (5.19), which as before corresponds to the geometry which yields the largest polydispersivity effects. Observe that the effect of polydispersivity on η_2 is considerably smaller than the corresponding effect on ζ_2. Miller and Torquato [215] have found that (5.18) also applies to the corresponding polydispersed impenetrable-disk (cylinder) geometry. Thus, the effect of polydispersivity here (unlike three dimensions) is to decrease η_2.

It is noteworthy that, for all of the above reported results for distributions of d-dimensional spheres (symmetric cell materials, overlapping and nonoverlapping spheres with a size distribution, etc), the inequality

$$\eta_2 \ge \zeta_2 \quad (5.19)$$

is obeyed (see Tables 2–5 and Figs 23, 24, 34, and 35). A general rigorous proof of this relation for a class of sphere distributions has not yet been given. Indeed, the observation (5.19) has heretofore not been made.

Observe from the same tables and figures that η_2 for general systems of d-dimensional spheres appear to be bounded from above by the symmetric-cell result $\eta_2 = \phi_2$. As in the case of ζ_2, a proof of this bound for a class of sphere distributions has not yet been given. If this and relation (5.19) are rigorously true, then η_2 will lie in the generally smaller closed interval $[\zeta_2, \phi_2]$ for this class of models.

As noted earlier, for transversely isotropic fiber-reinforced media the effective transverse bulk modulus k_e, transverse shear modulus G_e, and axial shear modulus μ_e will be considered here. Results for the effective transverse conductivity σ_e translate immediately into equivalent results for μ_e [23] by making the following change

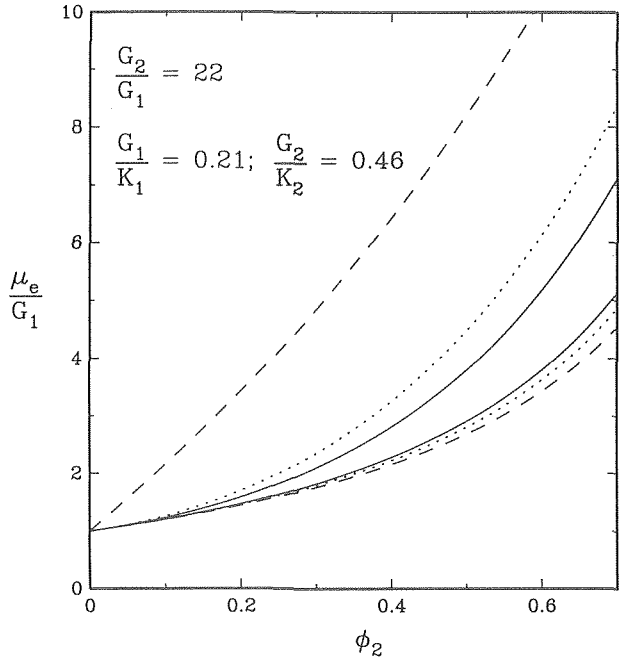

FIG 36. Bounds on the scaled effective axial shear modulus μ_e/G_1 versus ϕ_2 for a glass-epoxy fiber-reinforced composite composed of fibers which are identical, impenetrable cylinders: (– – –) two-point Hashin bounds [23,48]; (···) three-point Silnutzer bounds [53]; (—) four-point Milton bounds [69]. Improved bounds are computed using (5.5) derived by Torquato and Lado [203].

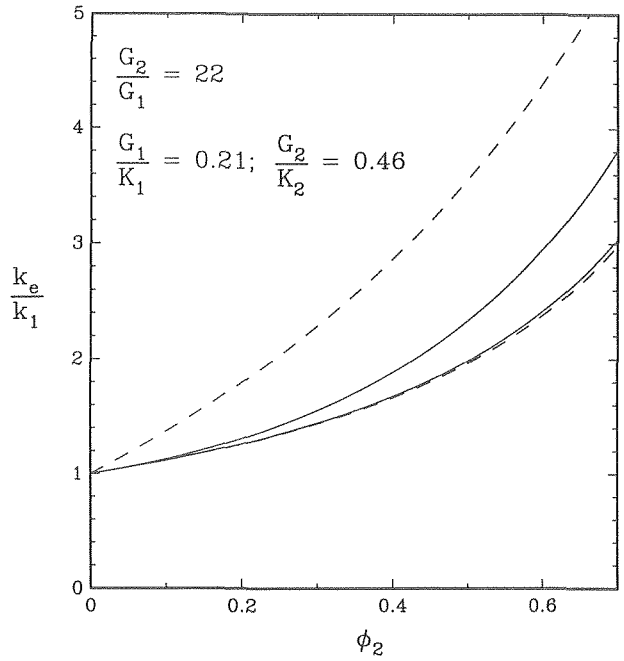

FIG 37. Bounds on the scaled effective transverse bulk modulus k_e/k_1 versus ϕ_2 for a glass-epoxy fiber-reinforced composite composed of fibers which are identical, impenetrable cylinders: (– – –) two-point Hashin bounds [48]; (—) three-point Silnutzer bounds [53]. Improved bounds are computed using (5.5).

of variables: $\sigma_i \to G_i$ and $\sigma_e \to \mu_e$. Thus, (3.5) and (3.12) with $d = 2$ give three- and four-point bounds on μ_e and consequently Figs 26–28 for σ_e/σ_1 also show bounds on μ_e/G_1 for identical impenetrable cylinders which are stiffer than the matrix. The four-point lower bound is seen to provide very good estimates of μ_e/G_1 when compared to the reported simulation data.

Figure 36 shows two-, three-, and four-point bounds on the scaled effective axial shear modulus μ_e/G_1 a distribution of impenetrable cylinders corresponding to a glass-epoxy composite for which $G_2/G_1 = 22$, $G_1/K_1 = 0.21$, and $G_2/K_2 = 0.46$. Here relation (5.5) is used for ζ_2. Based upon the previous observations, the four-point lower bound gives a highly accurate estimate of μ_e for this commonly employed fiber-reinforced material.

Figure 37 depicts the three-point Silnutzer bounds (3.43) on the scaled effective transverse bulk modulus k_e/k_1 for the same model corresponding to a glass-epoxy composite for which $G_2/G_1 = 22$, $G_1/K_1 = 0.21$, and $G_2/K_2 = 0.46$. Relation (5.5) is again used for ζ_2. Included in the figure are two-point bounds. The three-point bounds provide significant improvement over the two-point bounds and are tight enough to yield good estimates of k_e for a wide range of cylinder volume fractions.

Figure 38 shows the two- and three-point bounds on the scaled effective transverse shear modulus G_e/G_1 for the same impenetrable-cylinder model corresponding to a glass-epoxy composite with $G_2/G_1 = 22$, $G_1/K_1 = 0.21$, and $G_2/K_2 = 0.46$. Here relation (5.16) is used for η_2. Again, the three-point lower bound should yield a good estimate of G_e for a wide range of ϕ_2.

In the case of three-dimensional suspensions of impenetrable spheres, the relative improvement of the three-point bounds on the effective bulk modulus K_e and shear modulus G_e over two-point bounds is very similar to the analogous two-dimensional instances just described. Hence, it suffices here to compare the three-point bounds (3.54) on G_e, using (5.15), to the two-point Hashin–Shtrikman bounds [14] and to experimental data for spherical glass beads in an epoxy matrix [226]. It is seen in Fig 39 that the three-point bounds provide significant improvement over the two-point bounds. Moreover, for reasons mentioned earlier, the data lie closer to the three-point lower bound.

Thovert et al [165] have shown that for impenetrable spheres with a size distribution, the effect of polydispersivity in three-point bounds on K_e is quantitatively similar to the one they observed on three-point bounds on the effective conductivity σ_e (cf Fig 31). However, they found the effect of polydispersivity in the case of G_e to be considerably smaller than in the instance of K_e or σ_e.

5.2.2. *Macroscopically anisotropic media*

Willis [8,53] has also found two-point bounds on the effective stiffness tensor $\mathbf{C}_e$ for the special case of oriented ellipsoidal inclusions. Using Eshelby's [224] construction, one can express these two-point bounds in terms of volume fractions and quantities which, as in the anisotropic conductivity problem described in section 5.1.2, depend only on the inclusion shape.

5.3. Trapping constant

In the last 4 years, the following trapping constant bounds have been evaluated: (i) two-point interfacial-surface lower bound (3.63) for distributions of identical impenetrable spherical sinks [227], overlapping spherical sinks with two different sizes [154], and identical spherical sinks in the penetrable-concentric-shell model for small ϕ_2 [26]; (ii) three-point multiple-scattering lower bound (3.64) for distributions of identical overlapping spherical sinks [26] and spheres in the penetrable-concentric-shell model for small ϕ_2 [26]; (iii) two-point void lower bound (3.68) for statistically anisotropic distributions of oriented, impenetrable spheroidal sinks [204]; and (iv) security-spheres upper bound (3.69) for distributions of identical impenetrable spherical sinks [88]. Many of these results are now described more fully using the definition of the trapping constant γ given by (2.18). (Note that other definitions exist which differ by factors involving either the porosity ϕ_1 or diffusion coefficient D or both—see Refs 228 and 229 for further explanation.)

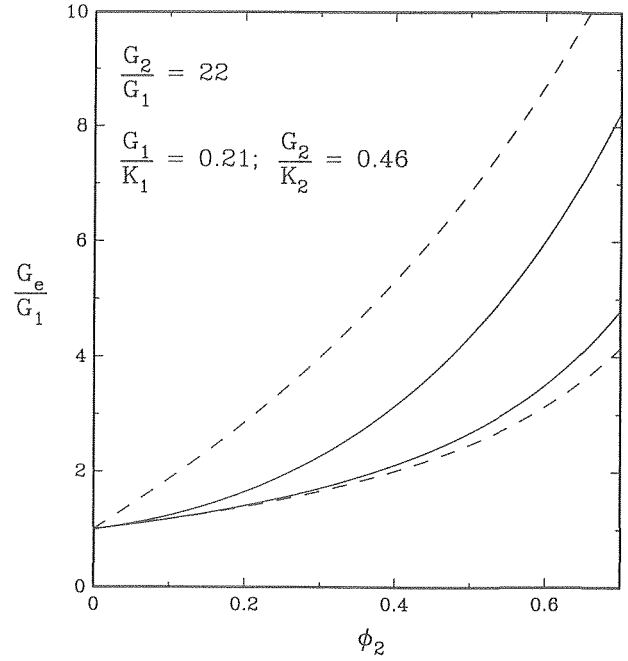

FIG 38. Bounds on the scaled effective transverse shear modulus G_e/G_1 versus ϕ_2 for a glass-epoxy composite composed of fibers which are identical, impenetrable cylinders: (– – –) two-point Hashin bounds [48]; (—) three-point Silnutzer bounds [53]. Improved bounds are computed using (5.16) derived by Torquato and Lado [211].

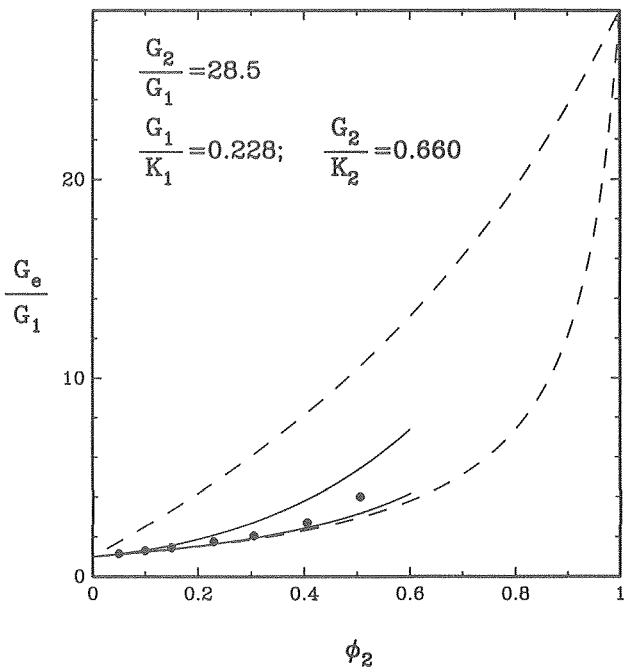

FIG 39. Bounds on the scaled effective shear modulus G_e/G_1 versus ϕ_2 for glass spheres in an epoxy matrix: (– – –) two-point Hashin–Shtrikman bounds [14]; (—) the three-point Milton–Phan-Thien bounds [56]. Included is experimental data due to Smith [226]. The improved bounds are computed using (5.15) derived by Torquato et al [225].

The two-point interfacial-surface lower bound (3.63) has been evaluated by Torquato [227] for identical impenetrable spherical traps. This bound on the scaled trapping constant γ/γ_o is depicted in Fig 40, where it is compared to Brownian-motion simulation data due to Lee et al [229] and to the survival probability theory of Richards [230]. Here

$$\gamma_o = 4\pi\rho R = 3\phi_2/R^2 \tag{5.20}$$

is the infinitely-dilute-limit Smoluchowski result. Two observations are worth noting: (i) even though the bound contains only two-point information it is relatively close to the simulation data, and (ii) Richards' theory violates the bound for $\phi_2 > 0.5$.

The same bound has been computed for identical overlapping spheres [85] and for dilute concentrations of identical spheres in the penetrable-concentric-shell or cherry-pit model [26]. The latter bound is given by

$$\frac{\gamma}{\gamma_o} \geq 1 + \left(\frac{15}{8} + \frac{25}{8}\lambda\right)\phi_2 + \mathcal{O}(\phi_2^2). \tag{5.21}$$

The bound gives the exact Smoluchowski result γ_o. The next term accounts for interactions between pairs of sinks; as the impenetrability parameter λ increases, the second-order coefficient increases, as expected, since the surface area available for reaction increases.

The two-point interfacial surface bound has also been computed for fully penetrable spherical sinks having two different sizes by Miller and Torquato [154]. It was found that the trapping constant γ for the polydisperse case increased or decreased (relative to the monodisperse case), depending upon whether the *relative* interfacial surface area increased or decreased.

For identical fully penetrable sinks, the three-point multiple-scatter lower bound has been evaluated analytically by Rubinstein and Torquato [26]:

$$\frac{\gamma}{\gamma_o} \geq \frac{-\ln\phi_1}{\phi_1\phi_2}. \tag{5.22}$$

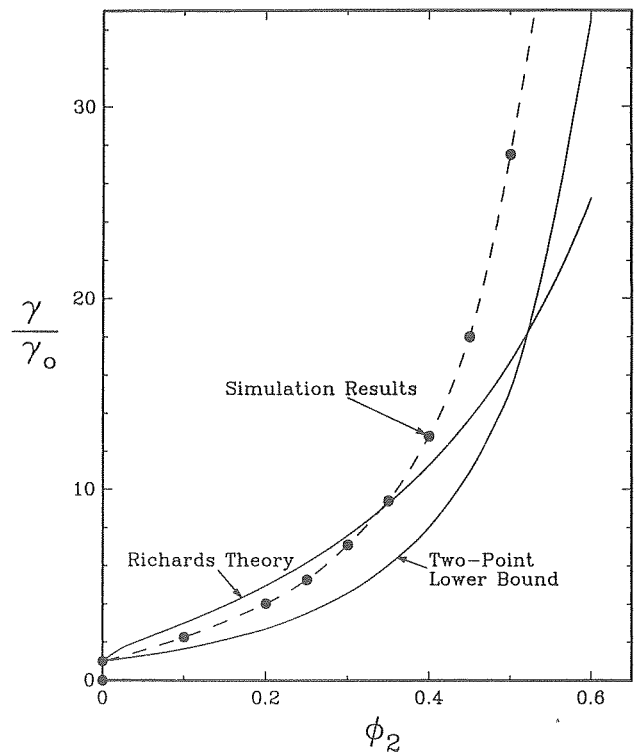

FIG 40. The scaled trapping constant γ/γ_0 for identical, impenetrable spherical traps versus ϕ_2. Included is Richards' theory [230], the two-point interfacial surface bound computed by Torquato [227], and the Brownian-motion simulation data of Lee et al [229].

They also evaluated this bound for dilute spheres in the cherry-pit model and found

$$\frac{\gamma}{\gamma_o} \geq 1+\left[\frac{3}{2}-\lambda^6+3\lambda^4+\frac{9}{8}\lambda+\frac{3}{8}(1-4\lambda^2)\ln(1+2\lambda)\right]\phi_2+\mathcal{O}(\phi_2^2). \tag{5.23}$$

Comparing (5.23) to the corresponding result (5.21) for the two-point interfacial-surface bound reveals that for $0.6 < \lambda \leq 1$, the former is sharper than the latter, but the converse is true for $0 \leq \lambda \leq 0.6$. The reason for this behavior is described in full detail in Ref 26.

Bounds (5.21) and (5.23) do not capture the nonanalytic dependence on ϕ_2 due to screening effects for $\phi_2 << 1$. Under dilute conditions for impenetrable sinks ($\lambda = 1$), one exactly has [33,35]

$$\gamma/\gamma_o = 1 + \sqrt{3\phi_2} + \text{higher order terms} \tag{5.24}$$

It is difficult to construct trial fields in variational principles which incorporate screening and simultaneously satisfy the conditions of (3.62). The fact that current bounds do not yield the correct behavior at small ϕ_2 is not of practical concern since for real materials ϕ_2 is large (or the porosity ϕ_1 is small) and screening effects become important in this regime.

For the statistically anisotropic model of oriented, possibly overlapping, spheroidal traps of length $2b$ and maximum diameter $2a$ at number density ρ, the two-point void lower bound has been determined by Torquato and Lado [204]. They have found that

$$\gamma \geq \frac{\phi_2^2 f(b/a)}{4a^2 K_S}, \tag{5.25}$$

where

$$\phi_2 = \rho\frac{4\pi}{3}a^2 b, \tag{5.26}$$

the density-dependent parameter

$$K_S(\phi_2) = \int_0^\infty x[S_2(x) - \phi_1^2]\,dx \tag{5.27}$$

refers to isotropic distributions of *spheres* of radius $a = R$ (with $x = r/2a$ a dimensionless distance), and

$$f(b/a) = \begin{cases} 2\chi_b/\ln\left(\dfrac{1+\chi_b}{1-\chi_b}\right), & b > a \\ \dfrac{\chi_a}{\tan^{-1}(\chi_a)}, & b < a \end{cases} \tag{5.28}$$

and $\chi_a^2 = -\chi_b^2$ is defined by relation (5.12). Thus, given the evaluation of the void bound for spheres with an arbitrary degree of impenetrability,

$$\gamma \geq (\phi_2^2)/(4a^2 K_S), \tag{5.29}$$

one can obtain corresponding results for oriented, prolate and oblate spheroids by normalizing the former with the shape-dependent factors of (5.28). Note that the same shape factors also arise in the aforementioned two-point conductivity bounds (3.18) for such a model via the dependence on the parameter Q given by (5.10) and (5.11) for prolate and oblate spheroids, respectively. Unlike the bounds (3.18), however, the bound (5.25) also depends on the volume fraction ϕ_2 in a complex fashion through the parameter $K_S(\phi_2)$. Now since $f(b/a) \geq 1$ for $b/a \leq 1$, the void bound for oblate spheroids is always larger than for spheres ($b/a = 1$). Similarly, since $f(b/a) < 1$ for $b/a \geq 1$, the void bound for prolate spheroids is always smaller than for spheres. Thus, the void bound captures the essential physics of the true behavior of the trapping constant for spheroids relative to spheres.

Torquato and Rubinstein [88] have shown that for dilute concentrations of spheres of radius a

$$K_S \sim \phi_2/10 \qquad (\phi_2 << 1) \tag{5.30}$$

and thus (5.25) yields

$$\gamma \geq 5\phi_2/2a^2 \qquad (\phi_2 << 1), \tag{5.31}$$

which implies that, unlike other two-point bounds, it does not give the Smoluchowski result (5.20) in the infinitely dilute limit. Substitution of (5.30) into (5.25) yields the corresponding result for spheroids at the same number density of spheres:

$$\gamma \geq 5\phi_2/2a^2 f(b/a) \qquad (\phi_2 << 1). \tag{5.32}$$

This is to be compared to the exact dilute-limit for spheroids given by

$$\gamma_o = (3\phi_2/a^2)f(b/a). \tag{5.33}$$

Thus, the void bound does give the correct shape dependence on the spheroid and in fact is exact to within a factor of 5/6.

Security-spheres *upper bounds* on γ have been computed for a simple cubic lattice of identical, impenetrable spherical sinks [26,88] to all orders in ϕ_2. For example, bound (3.69) for such a system is given by

$$\gamma/\gamma_o \leq 1 + 1.82\phi_2^{1/3} + \mathcal{O}(\phi_2^{2/3}). \tag{5.34}$$

This upper bound is of the same form as the exact result of Felderhof [231] whose coefficient of $\phi_2^{1/3}$ is 1.76 and therefore (5.34) does indeed give an upper bound. These authors also computed security-spheres upper bounds for random spheres at low concentrations approximately. They are in the process of evaluating such bounds to all orders in ϕ_2 using sophisticated expressions for $H_{l'}(r)$ such as the types described in section 4.

5.4. Fluid permeability

In the last four years, the following fluid permeability bounds have been calculated: (i) two-point interfacial-surface upper bound (3.81) for distributions of identical impenetrable spheres [122], overlapping spheres with a polydispersivity in size [155], and identical spheres in the penetrable-concentric-shell model for small ϕ_2 [87]; (ii) three-point multiple scattering upper bound (3.82) for identical overlapping as well as impenetrable spheres [89] and spheres in the penetrable-concentric-shell model for small ϕ_2 [28,87]; (iii) an *optimized* three-point multiple-scattering upper bound for identical impenetrable spheres [89] and; (iv) security-spheres lower bound (3.87) for arrays of identical impenetrable spheres [28,111]. Many of these results are discussed in detail below.

The two-point upper bound (3.81) on k has been calculated by Torquato [122] for flow around random arrays of identical impenetrable spheres of radius R for a wide range of ϕ_2. The equivalent two-point *lower bound* on the inverse permeability or resistance k^{-1} is plotted in Fig 41 along with other results described below. The same bound has been computed for dilute concentrations of identical spheres of radius R in the cherry-pit model by Torquato and Beasley [87]. This lower bound is given by

$$\frac{k_o}{k} \geq 1 + \left(\frac{15}{8}+\frac{25}{8}\lambda\right) + \mathcal{O}(\phi_2^2), \tag{5.35}$$

where

$$k_o = \frac{2R^2}{9\phi_2} \tag{5.36}$$

is the infinitely-dilute-limit Stokes result. Note that this result for the scaled resistance is identical to (5.21) for the scaled trapping

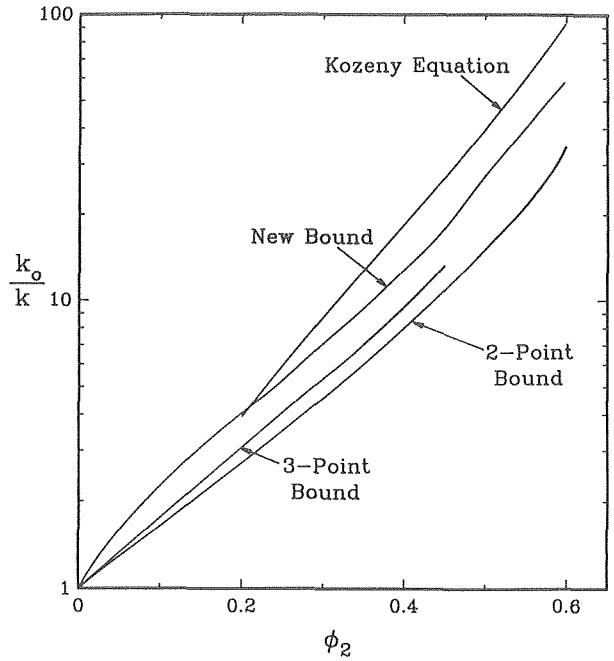

FIG 41. Comparison of improved bounds on the scaled fluid resistance k_o/k for random arrays of identical, hard spheres versus ϕ_2. Included is the two-point interfacial-surface lower bound computed by Torquato [122], optimized three-point multiple-scattering bound derived and computed by Beasley and Torquato [89], the empirical Kozeny–Carman relation (5.40), and a new bound computed from the permeability-trapping constant relation (2.26) and data for γ for this model [229].

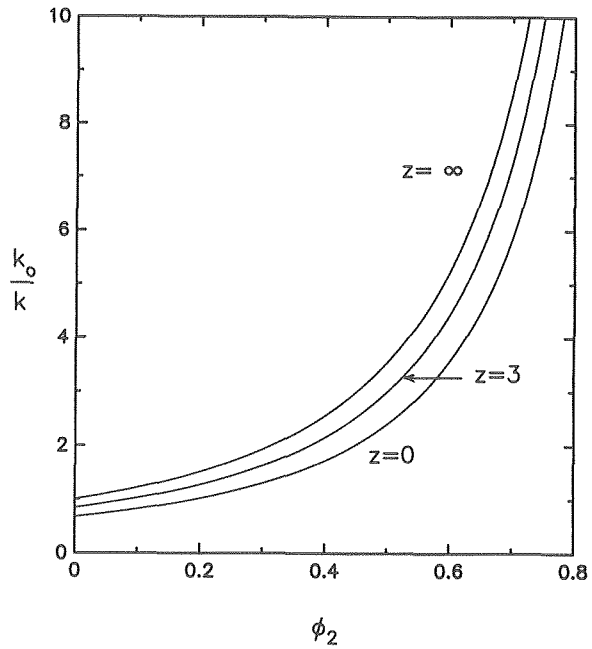

FIG 42. Two-point interfacial surface lower bound on the scaled fluid resistance k_o/k for polydispersed, overlapping spherical grains versus ϕ_2 as computed by Torquato and Lu [155]. The radii are distributed according to the Schulz distribution (4.77). The degree of polydispersivity increases as z increases ($z = \infty$ corresponding to the monodisperse case).

constant. Again, as before, the effect of increasing the impenetrability index λ is to increase the scaled resistance.

Recently, the interfacial-surface bound has been computed for overlapping spherical grains with a continuous size distribution. These results are summarized in Fig 42 where the scaled resistance k_o/k is plotted versus the sphere volume fraction ϕ_2 for the Schulz distribution (4.77). The generalized dilute Stokes result for polydispersed spheres is given by

$$k_o = (2\overline{R^3})/(9\overline{R}\phi_2). \tag{5.37}$$

Increasing the degree of polydispersivity (ie, decreasing z), decreases the specific surface (relative to the monodisperse limit) and thus decreases the fluid resistance. Interestingly, scaling the bound on the resistance k^{-1} by the square of the specific surface (relative to the monodisperse case) gives effectively *universal behavior* at fixed volume fraction, that is, given the monodisperse result, one can compute the bound on k^{-1} for any degree of polydispersivity. Note that for any degree of polydispersivity, the two-point bound on k_o/k is not exact in the limit $\phi_2 \to 0$.

For identical overlapping spheres, the three-point multiple-scattering bound (3.82) yields [28]

$$\frac{k_o}{k} \geq -\frac{\ln \phi_1}{\phi_1 \phi_2}. \tag{5.38}$$

This bound was first derived by Weissberg and Prager [84] using a different procedure. The same bound for dilute random arrays of identical spheres in the cherry-pit model was given by Torquato and Beasley [87]. They found

$$\frac{k_o}{k} = 1 + \left[\frac{3}{2} - \lambda^6 + \frac{11}{4}\lambda^4 + \frac{5}{6}\lambda^2 - \frac{9}{8}\lambda + \frac{3}{4}(1+3\lambda^2)\ln(2\lambda+1) - \frac{\lambda(1+7\lambda)}{16(2\lambda+1)^2} + \frac{\lambda}{16(2\lambda+1)^4}\right]\phi_2 + \mathcal{O}(\phi_2^2). \tag{5.39}$$

Note that (5.23) and (5.29) are not the same for $\lambda > 0$. Comparing the two-point interfacial bound (5.35) on k_o/k to (5.39) reveals that the latter is sharper than the former for $0.52 < \lambda \leq 1$ with the converse holding for $0 \leq \lambda \leq 0.52$.

The variational principle (3.77) was recently employed by Beasley and Torquato [89] to derive an optimized three-point multiple-scattering upper bound on k for possibly overlapping spheres that is sharper than (3.82) for $0 < \lambda \leq 1$. This was evaluated for identical impenetrable spheres in the superposition approximation and is shown in Fig 41. The superposition approximation is accurate for $0 \leq \phi_2 \leq 0.45$ but increasingly overestimates k_o/k for $\phi_2 \geq 0.45$. Included in the figure is the well-known Kozeny–Carman empirical relation

$$\frac{k_o}{k} = \frac{10\phi_2}{(1-\phi_2)^3}. \tag{5.40}$$

Also included in Fig 41 is a "new" bound on k_o/k for this model which was obtained by utilizing "exact" data for the scaled trapping constant γ/γ_o due to Lee et al [229] and the permeability-trapping constant relation (2.26). Thus, the new bound is sharper than the best available variational bound on k_o/k. It also is the closest that any rigorous estimate of k_o/k has come to the Kozeny–Carman empirical relation.

The simulation data of Lee et al [229] for γ/γ_o in the cherry-pit model (at selected values of the impenetrability index λ) and of Miller and Torquato [154] of γ/γ_o for polydispersed spherical traps, in conjunction with (2.26), lead immediately to new lower bounds on k_o/k for these models.

The security-spheres bound (3.87) has been computed exactly (to all orders in ϕ_2) for a simple cubic lattice of identical impenetrable spheres [28,111] and approximately for a dilute random array

of such spheres. In the former case, one finds the upper bound

$$k_o/k \leq 1 + 2.79\phi_2^{1/3} + \mathcal{O}(\phi_2^{2/3}). \quad (5.41)$$

This bound is of the same form as the exact result of Hasimoto [232] whose coefficient of $\phi_2^{1/3}$ is 1.76 and therefore (5.41) is indeed an upper bound. Torquato and Rubinstein are in the process of computing (3.87) to all orders in ϕ_2 for random spheres using accurate expressions for $H_P(r)$ such as the types discussed in section 4.7.

5.5. Remarks

It has been demonstrated that improved bounds, such as three- and four-point bounds, can provide relatively sharp estimates of the effective properties for a wide range of conditions, even when the bounds are not tight. From a practical point of view this conclusion is encouraging since the measurement of five-point and higher-order correlation functions of real heterogeneous materials is beyond presently available technology.

6. CONCLUDING REMARKS

In light of the fact that it is generally impossible to determine exactly the effective properties of random heterogeneous media, any rigorous statements about effective properties must take the form of inequalities, that is, bounds. Although some improved bounds have been in existence for nearly three decades, they have until recently lied dormant and untested because of the difficulty associated with ascertaining the various types of correlation functions involved, even for simple models such as random arrays of nonoverlapping spherical particles. It is largely in the last 5 years that this impasse in microstructure characterization has been broken. In this regard much is now known about simple model microstructures, such as isotropic distributions of identical, possibly overlapping d-dimensional spheres, as well as more complex models, such as isotropic arrays of d-dimensional spheres with a polydispersivity in size and *anisotropic* particulate media. More recently, methods have been developed to describe the microstructure of general nonparticulate media. An important theoretical advance has been the introduction and representation of the general n-point distribution H_n from which one can derive and compute any of the various types of correlation functions that have arisen in the literature and their generalizations. These recent theoretical and experimental advances in the quantitative characterization of the microstructure have enabled investigators to compute improved bounds for nontrivial models and real materials for the first time.

This review has demonstrated that improved bounds are useful because:

1. They rigorously incorporate nontrivial information about the microstructure via statistical correlation functions and consequently serve as a guide in identifying appropriate statistical descriptors.

2. As successively more microstructural information is included, the bounds become progressively narrower.

3. One of the bounds can provide a relatively sharp estimate of the property for a wide range of conditions, even when the reciprocal bound diverges from it.

4. They are usually exact under certain conditions.

5. They can be utilized to test the merits of a theory or computer experiment.

6. They provide a unified framework to study a variety of different effective properties.

Improved bounds have not only been shown to yield accurate estimates of effective properties of simple isotropic morphologies (eg, arrays of spheres), cases in which one may prefer to use a simpler approximation scheme, but also of more complex microstructures such as suspensions of polydispersed particles and anisotropic arrays of inclusions. For these and other complex morphologies (eg, bicontinuous media and inhomogeneous media), the few available approximate formulas are of dubious value since they typically only account for the barest of microstructural information. It is for complex microstructures that bounds make the most significant practical impact.

ACKNOWLEDGMENTS

The author gratefully acknowledges support of the Office of Basic Energy Sciences, U. S. Department of Energy, under Grant No. DEFG05-86ER13482. He is also indebted to his collaborators over the years for the privilege of working with them on the problems discussed herein. The author is thankful to R. V. Kohn and J. Eischen for a careful and critical reading of this manuscript, and to Y. Bahei-El-Din for supplying the micrograph of the FP/Al composite.

REFERENCES

1. Schiedegger A E, *The physics of flow through porous media*, University of Toronto Press, Toronto, 1960.
2. Beran M J, *Statistical continuum theories*, Wiley, New York, 1968.
3. Batchelor G K, Transport properties of two-phase materials with random structure, *Ann Rev Fluid Mech* **6**, 227–255 (1974).
4. Hale D K, The physical properties of composite materials, *J Mater Sci* **11**, 2105–2141 (1974).
5. Watt J P, Davies G F, and O'Connell R J, The elastic properties of composite materials, *Revs Geophys Space Phys* **14**, 541–563 (1976).
6. Dullien F A L., *Porous media: fluid transport and pore structure*, Academic, New York, 1979.
7. Christensen R M, *Mechanics of composite materials*, Wiley, New York, 1979.
8. Willis J R, Variational and related methods for the overall properties of composites, *Adv Appl Mech* **21**, 1–78 (1981).
9. Calef D F and Deutch J M, Diffusion-controlled reactions, *Ann Rev Phys Chem* **34**, 493–524 (1983).
10. Hashin Z, Analysis of composite materials, *J Appl Mech* **50**, 481–505 (1983).
11. Weiss G H, Overview of theoretical models for reaction rates, *J Stat Phys* **42**, 3–36 (1986).
12. Torquato S, Thermal conductivity of disordered heterogeneous media from the microstructure, *Rev Chem Eng* **4**, 151–204 (1987).
13. Hashin Z and Shtrikman S, A variational approach to the theory of the effective magnetic permeability of multiphase materials, *J Appl Phys* **33**, 1514–1517 (1962).
14. Hashin Z and Shtrikman S, A variational approach to the theory of the elastic behavior of multiphase materials, *J Mech Phys Solids* **11**, 127–140 (1963).
15. Avellaneda M, Cherkaev A V, Lurie K A and Milton G W, On the effective conductivity of polycrystals and a three-dimensional phase-interchange inequality, *J Appl Phys* **63**, 4989–5003 (1988).
16. Avellaneda M and Milton G W, Optimal bounds on the effective bulk modulus of polycrystals, *SIAM J. Appl. Math.* **49**, 824–837 (1989).
17. McKenzie D R, McPhedran R C, Savvides N, and Botten L C, Properties and structure of amorphous hydrogenated carbon films, *Philosophical Magazine B* **48**, 341–364 (1983).
18. Torquato S and Kim I C, Efficient simulation technique to compute effective properties of heterogeneous media, *Appl Phys* **55**, 1847–1849 (1989).
19. Papanicolaou G C and Varadan S R S, Boundary value problems with rapidly oscillating random coefficients, *Coll Math Soc Janos Bolyai* **27**, 835–873 (1979).
20. Sen A K and Torquato S, Effective conductivity of anisotropic two-phase composite media, *Phys Rev B* **39**, 4504–4515 (1989).
21. Sanchez-Palencia E, *Nonhomogeneous media and vibration theory*, Lecture Notes in Physics, **127** Springer-Verlag, Berlin, 1980.
22. Hill R, Theory of mechanical properties of fiber-strengthened materials—I. Elastic behavior, *J Mech Phys Solids* **12**, 199–212 (1964).
23. Hashin Z, Theory of composite materials, in *Mechanics of composite materials*, Pergamon Press, New York, 1970.
24. Chen H S and Acrivos A, The effective elastic moduli of composite materials containing spherical inclusions at non-dilute concentrations, *Int J Solids Structures* **14**, 349–364 (1978).
25. Sen A K, Lado F and Torquato S, Bulk properties of composite media. II. Evaluation of bounds on the shear moduli of suspensions of impenetrable spheres, *J Appl Phys* **62**, 4135–4141 (1987).
26. Rubinstein J and Torquato S, Diffusion-controlled reactions: Mathematical for-

mulation, variational principles, and rigorous bounds, *J Chem Phys* **88**, 6372–6380 (1988).
27. Torquato S, Relationship between permeability and diffusion-controlled trapping constant of porous media, *Phys Rev Lett* **64**, 2644–2647 (1990).
28. Rubinstein J and Torquato S, Viscous flow in random porous media: Mathematical formulation, variational principles and rigorous bounds, *J Fluid Mech* **206**, 25–46 (1989).
29. Tartar L, *Nonhomogeneous media and vibration theory*, Appendix 2, Lecture Notes in Physics **127**, Springer-Verlag, Berlin, 1980.
30. Keller J B, Darcy's law for flow in porous media and the two-scale method, in *Nonlinear P.D.E. in engineering and applied sciences*, R. L. Sternberg, A. J. Kalnowski and J. S. Papadakis (eds), Marcel Dekker New York, 1980.
31. Whitaker S, Flow in porous media: A theoretical derivation of Darcy's law, *Trans Porous Media* **1**, 3–25 (1986).
32. Childress S, Viscous flow past a random array of spheres, *J Chem Phys* **56**, 2527–2539 (1972).
33. Felderhof B U and Deutch J M, Concentration dependence of the rate of diffusion-controlled reactions, *J Chem Phys* **64**, 4551–4558 (1976).
34. Hinch E J, An averaged equation approach to particle interactions in a fluid suspension, *J Fluid Mech* **83**, 695–720 (1977).
35. Mattern K and Felderhof B U, Rate of diffusion-controlled reactions in a random array of spherical sinks, *Physica A* **143**, 21–55 (1989).
36. Torquato S, Microstructure and effective properties of random media, *Proceedings of the Summer Seminar on Mathematics of Random Media*, W. Kohler and B. White (eds), American Mathematical Society, Providence, to be published.
37. Brown W F, Solid mixture permittivities, *J Chem Phys* **23** 1514–1517 (1955).
38. Torquato S, Electrical conductivity of two-phase disordered composite media, *J Appl Phys* **58**, 3790–3797 (1985).
39. Maxwell J C, *Treatise on electricity and magnetism*, 1st ed, Clarendon, Oxford, 1873.
40. Jeffrey D J, Conduction through a random suspension of spheres, *Proc Roy Soc London, Ser A* **335**, 355–367 (1973).
41. Felderhof B U, Ford G W, and Cohen E G D., Cluster expansion for the dielectric constant of a polarizable suspension, *J Stat Phys* **28**, 135–164 (1982).
42. Torquato S, Bulk properties of two-phase disordered media. I. Cluster expansion for the effective dielectric constant of dispersions of penetrable spheres, *J Chem Phys* **81**, 5079–5088 (1984).
43. Kröner E, Bounds for the effective elastic moduli of disordered materials, *J Mech Phys Solids* **25**, 137–155 (1977).
44. Prager S, Diffusion and viscous flow in concentrated suspensions, *Physica* **29**, 129–139 (1963).
45. Beran M, Use of the variational approach to determine bounds for the effective permittivity in random media, *Nuovo Cimento* **38**, 771–782 (1965).
46. Hill R, The elastic behavior of a crystalline aggregate, *Proc Roy Soc Lond A* **65**, 349–354 (1952).
47. Paul B, Prediction of elastic constants of multiphase materials, *Trans Metall Soc AIME* **218**, 36–41 (1960).
48. Hashin Z, On elastic behavior of fiber reinforced materials of arbitrary transverse phase geometry, *J Mech Phys Solids* **13**, 119–134 (1965).
49. Weissberg H L, Effective diffusion coefficient in porous media, *J Appl Phys* **34**, 2636–2639 (1963).
50. Beran M J and Molyneux J, Use of classical variational principles to determine bounds for the effective bulk modulus in heterogeneous media, *Q Appl Math* **24**, 107–118 (1966).
51. Walpole L J, On bounds for the overall elastic moduli of inhomogeneous systems I, *J Mech Phys Solids* **14**, 151–162 (1966).
52. McCoy J J, *Recent advances in engineering sciences* 5, Gordon and Breach, New York, 1970.
53. Silnutzer N, Effective constants of statistically homogeneous materials, Ph.D. Thesis, University of Pennsylvania, Philadelphia, 1972.
54. Willis J R, Bounds and self-consistent estimates for the overall moduli of anisotropic composites, *J Mech Phys Solids* **25**, 185–202 (1977).
55. DeVera A L and Strieder W, Upper and lower bounds on the thermal conductivity of a random two-phase material, *J Phys Chem* **81**, 1783–1790 (1977).
56. Milton G W and Phan-Thien N, New bounds on the effective moduli of two-component materials, *Proc Roy Soc Lond A* **380**, 305–331 (1982).
57. Phan-Thien N and Milton G W, New bounds on the effective thermal conductivity of N-phase materials, *Proc Roy Soc Lond A* **380**, 333–348 (1982).
58. Torquato S, Bulk properties of two-phase disordered media. III. New bounds on the effective conductivity of dispersions of penetrable spheres, *J Chem Phys* **84**, 6345–6359 (1986).
59. Kohn R V and Milton G W, On bounding the effective conductivity of anisotropic composites, in *Homogenization and effective moduli of materials and media*, J. L. Eriksen et al (eds), Springer-Verlag, New York 1986.
60. Avellaneda M, Optimal bounds and microgeometries for elastic two-phase composites, *SIAM J Appl Math* **47**, 1216–1228 (1987).
61. Lipton R, On the effective elasticity of a two-dimensional homogenized incompressible elastic composite, *Proc Roy Soc Edinburgh* **110A**, 45–61 (1988).
62. Kohn R V and Lipton R, Optimal bounds for the effective energy of a mixture of isotropic, incompressible elastic materials, *Archive Rational Mech Analysis* **102**, 331–350 (1988).
63. Milton G W and Kohn R V, Variational bounds on the effective moduli of anisotropic composites, *J Mech Phys Solids* **36**, 597–629 (1988).
64. Milton G W, On characterizing the set of possible effective tensors of composites: The variational method and the translation method, *Commun Pure Appl Math* **43**, 63–125 (1990).
65. Bergman D J, The dielectric constant of a composite material: A problem in classical physics, *Phys Rep* **C43**, 377–407 (1978).
66. Bergman D J, Rigorous bounds for the complex dielectric constant of a two-component composite, *Ann Phys* **138**, 78–114 (1978).
67. Kantor Y and Bergman D J, Improved rigorous bounds on the effective elastic moduli of a composite material, *J Mech Phys Solids* **32**, 41–62 (1984).
68. Milton G W, Bounds on the complex Permittivity of a two-component composite material, *J Appl Phys* **52**, 5286–5293 (1981).
69. Milton G W, Bounds on the transport and optical properties of a two-component composite material, *J Appl Phys* **52**, 5294–5304 (1981).
70. Felderhof B U, Bounds on the complex dielectric constant of a two-phase composite, *Physica* **126**, 430–449 (1984).
71. Golden K and Papanicolaou G, Bounds for effective parameters of heterogeneous media by analytic continuation, *Commun Math Phys* **90**, 473–480 (1983).
72. Milton G W, and Golden K, Thermal conduction in composites, in *18th International Thermal Conductivity Conference*, Plenum, New York, 1985.
73. Tartar L, Estimations de coefficients homogénéisés, in *Computing methods in applied sciences and engineering*, **704**, Springer-Verlag, 1979.
74. Tartar L, Estimations fines des coefficients homogénéisés, in *Ennio De Giorgi's Colloquium*, P. Kree (ed), **125**, 1985.
75. Murat F and Tartar, L., Calcul des variations et homogénéisation, in *Les méthodes d' homogénéisation: théorie et applications en physique*, *Coll. de la Dir. des Etudes et Recherches d'Electricité de France*, Eyrolles, Paris, 1985.
76. Lurie K A and Cherkaev A V, Exact estimates of the conductivity of composites formed by two isotropically conducting media taken in prescribed proportion, *Proc Roy Soc Edinburgh* **99A**, 71–87 (1984).
77. Lurie K A and Cherkaev A V, Exact estimates of the conductivity of a binary mixture of isotropic components, *Proc Roy Soc Edinburgh* **104A**, 21–38 (1986).
78. Francfort G A and Murat F, Homogenization and optimal bounds in linear elasticity, *Archives Rat Mech Analysis* **94**, 307–334 (1986).
79. Milton G W, Multicomponent composites, electrical networks and new types of continued fractions I and II, *Commun Math Phys* **111**, 281–372 (1987).
80. Milton G W, A brief review of the translation method for bounding effective elastic tensors of composites, in *Sixth Symposium on Continuum Models and Discrete Systems*, G. A. Maugin (ed), Longman, to be published.
81. Milton G W, The field equation recursion method, in *Proceedings of the Workshop on Composite Media and Homogenization Theory*, Trieste, to be published.
82. Prager S, Viscous flow through porous media, *Phys Fluids* **4**, 1477–1482 (1961).
83. Reck R A and Prager S, Diffusion-controlled quenching at higher quencher concentrations, *J Chem Phys* **42**, 3027–3032 (1965).
84. Weissberg H L and Prager S, Viscous flow through porous media. III. Upper bounds on the permeability for a simple random geometry, *Phys Fluids* **13**, 2958–2965 (1970).
85. Doi M, A new variational approach to the diffusion and flow problem in porous media, *J Phys Soc Japan* **40**, 567–572 (1976).
86. Berryman J G and Milton G W, Normalization constraint for variational bounds on the fluid permeability, *J Chem Phys* **83**, 754–760 (1985).
87. Torquato S and Beasley J D, Bounds on the permeability of a random array of partially penetrable spheres, *Phys Fluids* **30**, 633–641 (1987).
88. Torquato S and Rubinstein J, Diffusion-controlled reactions. II. Further bounds on the rate constant, *J Chem Phys* **90**, 1644–1647 (1989).
89. Beasley J D and Torquato S, New bounds on the permeability of a random array of spheres, *Phys Fluids A* **1**, 199–207 (1989).
90. Milton G W and McPhedran R C, A comparison of two methods for deriving bounds on the effective conductivity of composites, *Lecture Notes in Physics*, R. Burridge, S. Childress, and G. Papanicolaou (eds), Springer-Verlag, New York, 1982.
91. Wiener O, Abhand Math Phys Klasse Konig Sach Ges Wiss **32**, 509 (1912).
92. Torquato S, Microscopic approach to transport in two-phase random media, PhD Thesis, State University of New York, Stony Brook, New York, 1980.
93. Milton G W, Bounds on the electromagnetic, elastic, and other properties of two-component composites, *Phys Rev Lett* **46**, 542–545 (1981).
94. Torquato S and Stell G, Bounds on the effective thermal conductivity of a dispersion of fully penetrable spheres, *Lett Appl Eng Sci* **23**, 375–384 (1985).
95. Schulgasser K, On the conductivity of fiber-reinforced materials, *J Math Phys* **17**, 382–387 (1976).
96. Milton G W, Bounds on the elastic and transport properties of two-component composites, *J Mech Phys Solids* **30**, 177–191 (1982).
97. Beasley J D and Torquato S, Bounds on the conductivity of suspensions of impenetrable spheres, *J Appl Phys* **60**, 3576–3581 (1986).
98. Milton G W, Correlation of the electromagnetic and elastic properties of composites and microgeometries corresponding with effective medium approximations, in *Physics and Chemistry of Porous Media*, D. L. Johnson and P. N. Sen (eds), American Institute of Physics, 1984.
99. Milton G W, A proof that laminates generate all possible effective conductivity functions of two-dimensional, two-phase materials, in *Advances in Multiphase Flow and Related Problems*, G. Papanicolaou (ed), SIAM, Philadelphia, 1986.
100. Keller J B, A theorem on the conductivity of a composite medium, *J Math Phys* **5**, 548–549 (1964).
101. Dykhne A M, Conductivity of a two-dimensional two-phase system, *Soviet Phys JETP* **32**, 63–65 (1971).
102. Mendelson K S, Effective conductivity of two-phase material with cylindrical phase boundaries, *J Appl Phys* **46**, 917–918 (1975).
103. Schulgasser K, On a phase-interchange relationship for composite materials, *J Math Phys* **17**, 378–381 (1976).
104. Hori M, Statistical theory of effective electrical, thermal and magnetic properties of random heterogeneous materials. I. Perturbation expansions for the effective permittivity of cell materials, *J Math Phys* **14**, 514–523 (1973).
105. Hori M, Statistical theory of effective electrical, thermal, and magnetic properties of random heterogeneous materials. II. Bounds for the effective permittivity

of statistically anisotropic materials, *J Math Phys* **14**, 1942–1949 (1973).
106. Bergmann D J, Exactly solvable microscopic geometries and rigorous bounds for the complex dielectric constant of a two-component composite material, *Phys Rev Lett* **44**, 1285–1286 (1980).
107. Torquato S and Sen A K, Conductivity tensor of anisotropic composite media from the microstructure, *J Appl Phys* **67**, 1145–1155 (1990).
108. Milton G W, Modeling the properties of composites by laminates, in *Homogenization and Effective Moduli of Materials and Media*, J L Eriksen et al (eds), Springer-Verlag, New York, 1986.
109. Norris A N, A differential scheme for the effective moduli of composites, *Mech Mat* **4**, 1–16 (1985).
110. Lurie K A and Cherkaev A V, The problem of formation of an optimal multicomponent composite, *J Opt Theor Appl* **46**, 571 (1985).
111. Rubinstein J and Keller J B, Lower bounds on permeability, in *Phys Fluids* **30**, 2919–2921 (1987).
112. Coniglio A, DeAngelis U, and Forlani A, Pair connectedness and cluster size, *J Phys A* **10**, 1123–1139 (1977).
113. Given J A, Kim I C, Torquato S, and Stell G, Comparison of analytic and numerical results for the mean cluster density in continuum percolation, *J Chem Phys* **93** (1990).
114. Torquato S and Lado F, Effective properties of two-phase disordered composite media: II. Evaluation of bounds on the conductivity and bulk modulus of dispersions of impenetrable spheres, *Phys Rev B* **33**, 6428–6434 (1986).
115. Kohn R V, Recent progress in the mathematical modelling of composite materials, in *Composite Material Response: Constitutive Relations and Damage Mechanisms*, G C Sih et al (eds), Elsevier, London, 1988.
116. Kohn R V, Composite materials and structural optimization, in *Smart/Intelligent Materials and Systems*, C Rogers (ed), Technomic, Lancaster, PA, 1989.
117. Torquato S and Stell G, Microstructure of two-phase random media. I. The n-point probability functions, *J Chem Phys* **77**, 2071–2077 (1982).
118. Torquato S and Stell G, Microstructure of two-phase random media. II. The Mayer–Montroll and Kirkwood–Salsburg hierarchies, *J Chem Phys* **78**, 3262–3272 (1983).
119. Torquato S and Stell G, Microstructure of two-phase random media. III. The n-point matrix probability functions for fully penetrable spheres, *J Chem Phys* **79**, 1505–1510 (1983).
120. Torquato S and Stell G, Microstructure of two-phase random media. IV. Expected surface area of a dispersion of penetrable spheres and its characteristic function, *J Chem Phys* **80**, 878–880 (1984).
121. Torquato S and Stell G, Microstructure of two-phase random media. V. The n-point matrix probability functions for impenetrable spheres, *J Chem Phys* **82**, 980–987 (1985).
122. Torquato S, Microstructure characterization and bulk properties of disordered two-phase media, *J Stat Phys* **45**, 843–873 (1986).
123. Hansen J P and McDonald I R, *Theory of simple liquids*, Academic, New York, 1986.
124. Torquato S, Bulk properties of two-phase disordered media. II. Effective conductivity of a dilute dispersion of penetrable spheres, *J Chem Phys* **83**, 4776–4785 (1985).
125. Poladian L, Effective transport and optical properties of composite materials, Ph.D. Dissertation, University of Sydney, Australia, 1990.
126. Haan S W and Zwanzig R, Series expansions in a continuum percolation problem, *J Phys A* **10**, 1547–1555 (1977).
127. Lee S B and Torquato S, Monte Carlo study of correlated continuum percolation: Universality and percolation thresholds, *Phys Rev A* **41**, 5338–5344 (1990).
128. Chiew Y C and Glandt E E, Percolation behavior of permeable and of adhesive spheres, *J Phys A* **16**, 2599–2608 (1983).
129. Kertesz J, Percolation of holes between overlapping spheres: Monte Carlo calculation of the critical volume fraction, *J Physique Lett* **42**, L393-L395 (1981).
130. Stell G, Statistical mechanics applied to random-media problems, in *Proceedings of the summer seminar on mathematics of random media*, W Kohler and B White (eds), American Mathematical Society, Providence, to be published.
131. Wood W W, Monte Carlo calculations for hard disks in the isothermal-isobaric ensemble, *J Chem Phys* **48**, 415–434 (1968).
132. Berryman J G, Random close packing of hard spheres and disks, *Phys Rev A* **27**, 1053–1061 (1983).
133. Torquato S, Lu B, and Rubinstein J, Nearest-neighbor distribution functions in many-body systems, *Phys Rev A* **41**, 2059–2075 (1990).
134. Widom W, Random sequential addition of hard spheres to a volume, *J Chem Phys* **44**, 3888–3894 (1966).
135. Widom W, Random sequential filling of intervals on a line, *J Chem Phys* **58**, 4043–4044 (1973).
136. Feder J, Random sequential adsorption, *J Theor Biol* **87**, 237–254 (1980).
137. Vigil R D and Ziff R M, Random sequential adsorption of unoriented rectangles onto a plane, *J Chem Phys* **91**, 2599–2602 (1989).
138. Smith P A and Torquato S, Computer simulation results for the two-point probability function of composite media, *J Comput Phys* **76**, 176–191 (1988).
139. Chiew Y C and Glandt E D, Interfacial surface area in dispersions and porous media, *J Colloid Interface Sci* **99**, 86–96 (1984).
140. Torquato S and Lado F, Characterization of the microstructure of a distribution of rigid rods and disks in a matrix, *J Phys A* **18**, 141–148 (1985).
141. Rikvold P A and Stell, D-dimensional interpenetrable-sphere models of random two-phase media: Microstructure and an application to chromatography, *J Coll Interface Sci* **108**, 158–173 (1985).
142. Haile J M, Massobrio C, and Torquato S, Two-point matrix probability function for two-phase random media: Computer simulation results for impenetrable spheres, *J Chem Phys* **83**, 4075–4078 (1985).
143. Torquato S and Beasley J D, Effective properties of fiber-reinforced materials. I. Bounds on the thermal conductivity of dispersions of fully penetrable cylinders, *Int J Eng Sci* **24**, 415–434 (1986).
144. Joslin C G and Stell G, Bounds on the properties of fiber-reinforced composites, *J Appl Phys* **60**, 1607–1610 (1986).
145. Lee S B and Torquato S, Porosity for the penetrable-concentric-shell model of two-phase disordered media: Computer simulation results, *J Chem Phys* **89**, 3258–3263 (1988).
146. Torquato S, two-point distribution function for a dispersion of impenetrable spheres in a matrix, *J Chem Phys* **85**, 6248–6249 (1986).
147. Torquato S, Interfacial surface statistics arising in diffusion and flow problems in porous media, *J Chem Phys* **85**, 4622–4628 (1986).
148. Seaton N A and Glandt E D, Spatial correlation functions from computer simulations, *J Chem Phys* **85**, 5262–5268 (1986).
149. Torquato S, Lu B, and Rubinstein J, Nearest-neighbor distribution function for systems of interacting particles, *J Phys A* **23**, L103-L107 (1990).
150. Torquato S and Lee S B, Computer simulations of nearest-neighbor distribution functions and related quantities for hard-sphere systems, *Physica A* **164** (1990)
151. Lu B and Torquato S, General formalism to characterize the microstructure of polydispersed random media, *Phys Rev A*, **43**(4) (1991).
152. Stell G and Rikvold P A, Polydispersivity in fluids and composites: Some theoretical results, *Chem Eng Comm* **51**, 233–260 (1987).
153. Joslin C G, and Stell G, Effective properties of fiber-reinforced composites: Effects of polydispersivity in fiber diameter, *J Appl Phys* **60**, 1610–1615 (1986).
154. Miller C A and Torquato S, Diffusion-controlled reactions among spherical sinks: Effect of polydispersivity in sink size, *Phys Rev B* **39**, 7101–7108 (1989).
155. Torquato S and Lu, B., Rigorous bounds on the fluid permeability: Effect of polydispersivity in grain size, *Phys. Fluids A* **2**, 487–490 (1990).
156. Lado F and Torquato S, Two-point probability function for distributions of oriented ellipsoids, *J Chem Phys* **93** (1990).
157. Lu B and Torquato S, n-Point probability functions for a lattice model of heterogeneous media, *Phys Rev B* **42** (1990).
158. Metropolis N, Rosenbluth A W, Rosenbluth N, Teller A H and Teller E, Equation of state calculations by fast computing machines, *J Chem Phys* **21**, 1087–1092 (1953).
159. Smith P A and Torquato S, Computer simulations results for bounds on the effective conductivity of composite media, *J Appl Phys* **65**, 893–900 (1989).
160. Miller C A and Torquato S, Effective conductivity of hard sphere dispersions, *J Appl Phys* **68**(10), 5486–5493 (1990).
161. Lee S B and Torquato, S., Measure of clustering in continuum percolation: Computer-simulation of the two-point cluster function, *J Chem Phys* **91**, 1173–1178 (1989).
162. Rowlinson J S, The virial expansion in two dimensions, *Mol Phys* **7**, 593–594 (1963).
163. Powell M J D., The volume internal to three intersecting hard spheres, *Mol Phys* **7**, 591–592 (1964).
164. Hertz P, Über den Gegenseitigen Durchschnittlichen Abstand von Punkten die mit Bekannter Mittlever Dichte im Raume Angerodnet Sind, *Math. Ann.* **67**, 387–398 (1909).
165. Thovert J F, Kim I C, Torquato S, and Acrivos A, Bounds on the effective properties of polydispersed suspensions of spheres: An evaluation of two relevant parameters, *J Appl Phys* **67**, 6088–6098 (1990).
166. Blum L and Stell, G., Polydisperse systems. I. Scattering function for polydisperse fluids of hard or permeable spheres, *J Chem Phys* **71**, 42–46 (1979).
167. Blum L and Stell G, Polydisperse systems. I. Scattering function for polydisperse fluids of hard or permeable spheres (Erratum), *J Chem Phys* **72**, 2212 (1980).
168. Salacuse J J and Stell G, Polydisperse systems: Statistical thermodynamics, with applications to several models including hard and permeable spheres, *J Chem Phys* **77**, 3714–3725 (1982).
169. Schulz G V, Über die Kinetik der Kettenpolymerisationen, *Z Phys Chem* **B43**, 25–46 (1939).
170. Cramer H, *Mathematical methods of statistics*, Princeton University Press, Princeton, 1954.
171. Gilbert E N, Random subdivision of space into crystals, *Ann Math Stat* **33**, 958–972 (1962).
172. Miller M, Bounds for effective electrical, thermal, and magnetic properties of heterogeneous materials, *J Math Phys* **10**, 1988–2004 (1969).
173. Bruno O P, The effective conductivity of an infinitely interchangeable mixture, *Commun Pure Appl Math*, in press.
174. Stanley H E, *Introduction to phase transitions and critical phenomena*, Oxford University Press, New York (1971).
175. Gurland J, An estimate of contact and continuity of dispersion in opaque samples, *Trans Met Soc AIME* **236**, 642–646 (1966).
176. Sax J E and Ottino, Influence of morphology on the transport properties of polystyrene/polybutadiene blends. 1. Experimental studies, *Polymer* **26**, 1075–1080 (1985).
177. Voss R F, Laibowitz R B and Alessandri E I, Percolation and fractal properties of thin gold films, in *The mathematics and physics of disordered media*, B. D. Hughes and B. W. Ninham (eds), Springer-Verlag, Berlin, 1983.
178. Winterfeld P H, Scriven L E and Davis H T, Percolation and conductivity of random two-phase two-dimensional composites, *J Phys C* **14**, 2361–2376 (1981).
179. Gawlinski E T and Stanley H E, Continuum percolation in two dimensions: Monte Carlo tests of scaling and universality for non-interacting disks, *J Phys A* **14**, L291-L299 (1981).
180. Elam W T, Kerstein A R and Rehr J J, Critical properties of the void percolation problem for spheres, *Phys Rev Lett* **52**, 1516–1519 (1984).
181. Gawlinski E T and Redner S, Monte-Carlo renormalization group for continuum

percolation with excluded-volume interactions, *J Phys A* **16**, 1063–1071 (1983).
182. Stell G, Exact equation for the pair-connectedness function, *J Phys A* **17**, L855-L858 (1984).
183. Chiew Y C, Glandt E D and Stell G, Clustering and percolation in multicomponent systems of randomly centered and permeable spheres, *J Chem Phys* **83**, 761–772 (1985).
184. Bug A L, Safran S A and Webman I, Continuum percolation of permeable objects, *Phys rev B***33**, 4716–4724 (1986).
185. DiSimone T, Stratt R M and De Moulini S, Continuum percolation in an interacting system: Exact solution of the Percus-Yevick equation for connectivity in liquids, *Phys Rev Let* **56**, 1140–1143 (1986).
186. Post A J and Glandt E D, Cluster concentrations and virial coefficients for adhesive particles, *J Chem Phys* **84**, 4585–4594 (1986).
187. Feng S, Halperin B I and Sen P N, Transport properties of continuum systems near the percolation threshold, *Phys Rev B* **35**, 197–214 (1987).
188. Sevick E M, Monson P E and Ottino J M, Monte Carlo calculations of cluster statistics in continuum models of composite morphology, *J Chem Phys* **88**, 1198–1211 (1988)
189. Xu J and Stell G, An analytic treatment of percolation in simple legends, *J Chem Phys* **89**, 2344–2354 (1988).
190. Torquato S Beasley J D and Chiew Y C, Two-point cluster function for continuum percolation, *J Chem Phys* **88**, 6540–6546 (1988).
191. Sen A K and Torquato S, Series expansions for clustering in continuum percolation models with interactions, *J Chem Phys* **89**, 3799–3807 (1988).
192. Lee S B and Torquato S, Pair connectedness and mean cluster size for continuum-percolation models: Computer simulation results, *J Chem Phys* **89**, 6427–6433 (1988).
193. Xia W and Thorpe M F, Percolation properties of random ellipses, *Phys Rev A* **38**, 2650–2656 (1988).
194. Kirkpatrick S, Percolation and conduction, *Rev Mod Phys* **45**, 574–588 (1973).
195. Stauffer D S, *Introduction to percolation theory*, Taylor and Francis, London (1985).
196. Debye P, Anderson H R and Brumberger H, Scattering by an inhomogeneous solid. II. The correlation function and its applications, *J Appl Phys* **28**, 679–683 (1957).
197. Corson P B, Correlation functions for predicting properties of heterogeneous materials. I. Experimental measurement of spatial correlation functions in multiphase solids, *J Appl Phys* **45**, 3159–3164 (1974).
198. Berryman J G, Measurement of spatial correlation functions using image processing techniques, *J Appl Phys* **57**, 2374–2384 (1985).
199. Berryman J G and Blair S C, Use of digital image analysis to estimate fluid permeability of porous materials: Applications of two-point correlation functions, *J Appl Phys* **60**, 1930–1938 (1986).
200. Berryman J G, Interpolating and integrating three-point correlation functions on a lattice, *J Comput Phys* **75**, 86–102 (1988).
201. Berryman J G, Estimating effective moduli of composites using quantitative image analysis, in *Random media and composites*, R V Kohn and G W Milton (eds), SIAM, Philadelphia, 1989.
202. Felderhof B U, Bounds for the effective dielectric constant of a suspension of uniform spheres, *J Phys C* **15**, 3953–3966 (1982).
203. Torquato S and Lado F, Bounds on the conductivity of a random array of cylinders, *Proc Roy Soc Lond A* **417**, 59–80 (1988).
204. Torquato S and Lado, F., Trapping constant, thermal conductivity and the microstructure of suspensions of oriented spheroids, *J Chem Phys*, to be published.
205. Beran M J and Silnutzer, N., Effective electrical, thermal and magnetic properties of fiber-reinforced materials, *J Comp Mat* **5**, 246–249 (1971).
206. Elsayed M A, Bounds for effective thermal, electrical and magnetic properties of heterogeneous materials using high order statistical information, *J Math Phys* **15**, 2001–2015 (1974).
207. Elsayed M A and McCoy J J, Effect of fiber positioning on the effective physical properties of composite materials, *J Comp Mat* **7**, 466–480 (1973).
208. Berryman J G, Variational bounds on elastic constants for the penetrable sphere model, *J Phys D* **18**, 585–597 (1985).
209. Lado F and Torquato, S., Effective properties of two-phase disordered composite media. I. Simplification of bounds on the conductivity and bulk modulus of dispersions of impenetrable spheres, *Phys Rev B* **33**, 3370–3378 (1986).
210. Sen A K, Lado, F. and Torquato S, Bulk properties of composite media. I. Simplification of bounds on the shear moduli of suspensions of impenetrable spheres, *J Appl Phys* **62**, 3503–3513 (1987).
211. Torquato S and Lado F, Improved bounds on the effective elastic moduli of random arrays of cylinders, *J Appl Mech*, to be published.
212. Torquato S and Beasley J D, Effective properties of fiber-reinforced materials. II. Bounds on the bulk and shear moduli of dispersions of fully penetrable cylinders, *Int J Eng Sci* **24**, 435–447 (1986).
213. Torquato S, Stell G, and Beasley J D, Third-order bounds on the effective bulk and shear modulus of a dispersion of fully penetrable spheres, *Lett Appl Eng Sci* **23**, 385–392 (1985).
214. Sangani A and Yao C, Transport processes in random arrays of cylinders. I. Thermal conduction, *Phys Fluids*, **31**, 2426–2434 (1988).
215. Miller C A and Torquato S, Improved bounds on the transport and elastic properties of arrays of polydispersed cylinders, *J Appl Phys*, to be published.
216. McPhedran R C and Milton G W, bounds and exact theories for the transport properties of inhomogeneous media, *Appl Phys A* **26**, 207–220 (1981).
217. Zuzovsky M and Brenner H, effective conductivities of composite materials composed of cubic arrangements of spherical particles embedded in an isotropic matrix, *J Appl Math Phys (ZAMP)* **28**, 979–992 (1977).
218. McPhedran R C and McKenzie D R, The conductivity of lattices of spheres I. The simple cubic lattice, *Proc Roy Soc London Ser A* **359**, 45–63 (1978).
219. McKenzie D R, McPhedran R C and Derrick G H, The conductivity of lattices of spheres II. The body centered and face centered cubic lattices, *Proc Roy Soc London, Ser A* **362**, 211–232 (1978).
220. Carbonell R G and Whitaker S, Heat and mass transport in porous media, in *NATO Advanced Study Institute on the Mechanics of Fluids in Porous Media*, J. Bear and Y. Corpacioglu (eds), Martinus Nijhoff, 1983.
221. Sangani A S and Acrivos A, The effective conductivity of a periodic array of spheres, *Proc Roy Soc London A* **386**, 263–275 (1983).
222. Kim I C and Torquato S, Determination of the effective conductivity of heterogeneous media by brownian motion simulation, *J Appl Phys* **68** 3892 (1990).
223. Sugawara A and Yoshiezawa, An experimental investigation on thermal conductivity of consolidated porous materials, *J Appl Phys* **33**, 3135–3138 (1962).
224. Eshelby J D, The determination of the elastic field of an ellipsoidal inclusion and related problems, *Proc Roy Soc London A* **241**, 376–396 (1957).
225. Torquato S, Lado F, and Smith P A, Bulk properties of two-phase disordered media. IV. Mechanical properties of suspensions of penetrable spheres at nondilute concentrations, *J Chem Phys* **86**, 6388–6392 (1987).
226. Smith J C, Experimental values for the elastic constants of a particulate-filled glass polymer, *J Res NBS* **80A**, 45–49 (1976).
227. Torquato S, Concentration dependence of diffusion-controlled reactions among static reactive sinks, *J Chem Phys* **85**, 7178–7179 (1986).
228. Richards P M and Torquato S, Upper and lower bounds for the rate of diffusion-controlled reactions, *J Chem Phys* **87**, 4612–4615 (1987).
229. Lee S B, Kim I C, Miller C A and Torquato S, Random-walk simulation of diffusion-controlled processes among static traps, *Phys Rev B* **39**, 11833–11839 (1989).
230. Richards P M, Diffusion to nonoverlapping or spatially correlated traps, *Phys Rev B*, **35**, 248–256 (1987) .
231. Felderhof B U, Wigner solids and diffusion controlled reactions in a regular array of spheres, *Physica A* **130A**, 34–56 (1985).
232. Hasimoto H, On the periodic fundamental solutions of the stokes equations and their application to viscous flow past a cubic array of spheres, *J Fluid Mech* **5**, 317–328 (1959).

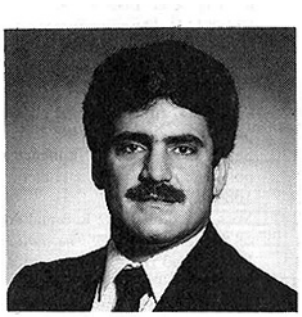

Salvatore Torquato *is an Associate Professor of Mechanical and Aerospace Engineering at North Carolina State University. He has published more than 80 refereed journal articles in the areas of micromechanics of composites, transport in porous media, and statistical thermodynamics. He has given 30 invited lectures on his research work at conferences, research laboratories, and universities within the United States and abroad. He is a member of many professional and honor societies including the American Society of Mechanical Engineers, the American Institute of Chemical Engineers, the Society of Engineering Science, the American Physical Society, the Society of Industrial and Applied Mathematics, Pi Tau Sigma, Tau Beta Pi, and Phi Kappa Phi. He has been the recipient of numerous awards and honors recognizing his research achievements.*